

SYNTHESIS AND SOLUBILITY AND NICKEL AND IRON
"HIDEOUT" REACTION PRODUCTS WITH AQUEOUS
SODIUM AND AMMONIUM PHOSPHATE UNDER
STEAM GENERATOR CONDITIONS

CENTRE FOR NEWFOUNDLAND STUDIES

**TOTAL OF 10 PAGES ONLY
MAY BE XEROXED**

(Without Author's Permission)

ROSEMARIE GAIL HARVEY

五
十
五
五
五



National Library
of Canada

Bibliothèque nationale
du Canada

Acquisitions and
Bibliographic Services

Acquisitions et
services bibliographiques

395 Wellington Street
Ottawa ON K1A 0N4
Canada

395, rue Wellington
Ottawa ON K1A 0N4
Canada

Your file *Votre référence*

ISBN: 0-612-93030-0

Our file *Notre référence*

ISBN: 0-612-93030-0

The author has granted a non-exclusive licence allowing the National Library of Canada to reproduce, loan, distribute or sell copies of this thesis in microform, paper or electronic formats.

L'auteur a accordé une licence non exclusive permettant à la Bibliothèque nationale du Canada de reproduire, prêter, distribuer ou vendre des copies de cette thèse sous la forme de microfiche/film, de reproduction sur papier ou sur format électronique.

The author retains ownership of the copyright in this thesis. Neither the thesis nor substantial extracts from it may be printed or otherwise reproduced without the author's permission.

L'auteur conserve la propriété du droit d'auteur qui protège cette thèse. Ni la thèse ni des extraits substantiels de celle-ci ne doivent être imprimés ou autrement reproduits sans son autorisation.

In compliance with the Canadian Privacy Act some supporting forms may have been removed from this dissertation.

Conformément à la loi canadienne sur la protection de la vie privée, quelques formulaires secondaires ont été enlevés de ce manuscrit.

While these forms may be included in the document page count, their removal does not represent any loss of content from the dissertation.

Bien que ces formulaires aient inclus dans la pagination, il n'y aura aucun contenu manquant.

Canada

SYNTHESIS AND SOLUBILITY OF NICKEL AND IRON “HIDEOUT” REACTION
PRODUCTS WITH AQUEOUS SODIUM AND AMMONIUM PHOSPHATE UNDER
STEAM GENERATOR CONDITIONS

by

© Rosemarie Gail Harvey

A thesis submitted to the
School of Graduate Studies
in partial fulfillment of the
requirements for the degree of
Master of Science

Department of Chemistry
Memorial University of Newfoundland

July 2003

St. John's

Newfoundland

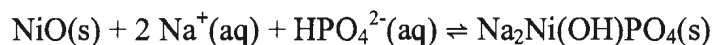
ABSTRACT

Low concentrations of sodium phosphate are added to the boiler water of electric power stations as a means of controlling pH. Hideout is the phenomenon by which sodium phosphate is observed to be retained in the boiler during conditions of high temperature and pressure, only to be released back into the water upon cooling. All-volatile amine treatment is an alternative boiler water pH control method, without the same adverse effects, but it is not known if problems will arise from a changeover from congruent phosphate control to all-volatile treatment. The objective of this research was (i) to develop improved synthetic methods for the known hideout reaction products, maricite, $\text{NaFe}^{\text{II}}\text{PO}_4$, and sodium iron hydroxyl phosphate (SIHP), $\text{Na}_3\text{Fe}^{\text{III}}(\text{PO}_4)_2 \cdot (\text{Na}_{4/3}\text{H}_{2/3}\text{O})$, (ii) identify any ammonium-iron-phosphate reaction products that may form during the changeover, and (iii) measure the solubility of the hideout reaction product sodium-nickel-hydroxy-phosphate (SNHP), $\text{Na}_2\text{Ni}(\text{OH})\text{PO}_4$, so that a thermodynamic database can be derived.

The syntheses of the solid reaction products were carried out in 45 mL Parr 4744 Teflon-lined stainless steel reaction vessels which allowed *in situ* filtration of the products from solution by inversion of the vessel, allowing the remaining solution to drain through a stainless steel mesh. Maricite was synthesized using previous established methods, whereas new methods for synthesizing SIHP from thermal decomposition of iron(III) nitrilotriacetic acid, and chelates, iron oxalate and iron tartrate, have been developed. A new hydrothermal synthesis for $(\text{NH}_4)\text{Fe}^{\text{II}}\text{Fe}^{\text{III}}(\text{PO}_4)_2$ has been developed

by thermally decomposing the chelate, iron tartrate. An additional ammonium reaction product, $(\text{NH}_4)\text{Fe}^{\text{II}}(\text{PO}_4)\cdot\text{H}_2\text{O}$, was synthesized from the iron nitrilotriacetic acid complex. This provided a new synthetic route for this compound and proved that it formed under boiler conditions. The crystal structure of $(\text{NH}_4)\text{Fe}^{\text{II}}(\text{PO}_4)\cdot\text{H}_2\text{O}$ was also confirmed. The major sodium-nickel-phosphate reaction product $\text{Na}_2\text{Ni}(\text{OH})\text{PO}_4$, was synthesized by two separate methods, from nickel oxide and from the thermal decomposition of the nickel nitrilotriacetic acid complex.

Solubility studies of $\text{Na}_2\text{Ni}(\text{OH})\text{PO}_4$, SNHP, were carried out in a modified 450 mL Parr 4562 stirred zirconium reaction vessel, according to the following reaction:



Kinetic experiments were conducted at 250 °C to ensure equilibrium had been reached and solubility data were collected over the temperature range 235-280 °C at a sodium/phosphate mole ratio of 2.5 that had an initial phosphate concentration of 1.5 mol·kg⁻¹. The MULTEQ chemical equilibrium program was used to calculate the composition concentrations of relevant species at each temperature studied, and experimental equilibrium constants were calculated from the activity coefficient model used in MULTEQ. The results were used to create a thermodynamic model for SNHP, consistent with the Helgeson-Kirkham-Flowers model for the standard partial molar properties of aqueous phosphate species.

In conclusion, the maricite synthesis reported by Quinlan (1996) was reproducible and SIHP was synthesized from similar conditions as the maricite synthesis and using the analogous chelate decomposition reaction. Ammonium-iron-phosphate reaction products can form under boiler conditions; those identified in this study were $(\text{NH}_4)\text{Fe}^{\text{II}}\text{Fe}^{\text{III}}(\text{PO}_4)_2$ and $(\text{NH}_4)\text{Fe}^{\text{II}}(\text{PO}_4)\cdot\text{H}_2\text{O}$. The major sodium-nickel-phosphate reaction product synthesized was $\text{Na}_2\text{Ni}(\text{OH})\text{PO}_4$ and the data from this study and that previously reported for this reaction product, were used to create a thermodynamic model for this system, consistent with the database for sodium-iron hideout reactions.

ACKNOWLEDGEMENTS

I would like to thank Dr. Peter Tremaine foremost for the support, guidance, and patience over the last three years. Dr. Tremaine's move to a different province this past year has made things a little more difficult and complicated, but I would like to thank him for sticking with me and believing that I will come through in the end. My thanks also goes out to Dr. Liliana Trevani for all the help she gave me during my first year in the Tremaine group and to Dr. Richard Bartholomew for being there whenever I had problems with my experiments and analysis, and also for being a friend for the past two years. Without the friendship and guidance from my fellow co-workers, my time in the lab would not of been so enjoyable. Thanks to Wanda Aylward, Jenene Roberts, Chris Collins, Kia Zhang and Dr. Rodney Clarke for all the great times.

I would like to thank my supervisory committee, Dr. Graham Bodwell and Dr. Raymond Poirier, for all their help and advice. Being a student at Memorial University during my undergraduate and graduate programs, I've had the pleasure of coming to know many of the faculty and staff in the Chemistry Department and it has greatly helped me throughout my time here. I would especially like to mention Dr. Laurie Thompson for giving me the opportunity to study in his laboratory before moving on into my Masters program. Thanks to Dr. Peter Golding for sparking my interest in chemistry and always showing me friendship whenever we had the chance to meet during the years. You may be retired but you are not forgotten. And I would also like to thank Dr. Brian

Gregory for his kindness and making me feel that he was always available whenever I needed to talk.

I would like to thank a few people who were instrumental in completing my graduate program. ICP-ES analyses were done by Chris Finch of the Newfoundland Department of Mines and Energy, and the single crystal X-ray diffraction structure was solved by Dr. John Bridson and Mr. David Miller. Maggie Piranian provided training and assistance with the powder X-ray diffraction, and Lisa Lee provided training and advice in using the scanning electron microscope. I would like to thank Carl Mulcahy for his help with my electronic equipment and Randy Thorne from the MUN Machine Shop for all his help in any problems that I came across during my experimental runs, for all the great conversations that we've had, and for the friendship that we now share.

My family has been most supportive during my university career even at times when they didn't know exactly what I was studying or how to explain what I was doing to other people. When asked if I was finished university yet, Mom and Dad would say no, but soon I hope. So Mom and Dad, I love you and thanks for everything. You can tell everyone that now, I am finished.

Now for the most important person in my life, my fiancée Jeremy Hughes. I love you and thank you for all the encouragement and for a shoulder to lean on when things were not going so well. You gave me the strength to keep going and not give up. This thesis would not be completed if it wasn't for your love and understanding. I will always be there for you when you need me just as you have been there for me.

CONTENTS

ABSTRACT	ii
ACKNOWLEDGEMENTS	v
TABLE OF CONTENTS	vii
LIST OF TABLES	x
LIST OF FIGURES	xi
LIST OF APPENDICES	xiv
CHAPTER 1.0 INTRODUCTION	1
1.1 Hydrothermal Synthesis	1
1.2 Phosphate Hideout in Steam Generators	3
1.3 Standard State Properties of Aqueous Species and Solids	5
1.3.1 Solids	5
1.3.2 Aqueous Species	9
1.4 Activity Coefficients in High Temperature Water	13
1.5 The Sodium-Phosphate-Water System	15
1.6 The Sodium-Iron-Phosphate-Water System	20
1.7 NiO-Sodium Phosphate Interactions	25
1.8 Decomposition of NTA Complexes	31
1.9 All-Volatile Treatment	33
1.10 Project Objectives	36
CHAPTER 2.0 EXPERIMENTAL	38
2.1 Chemicals and Materials	38
2.2 Apparatus	39
2.2.1 Teflon-Lined Filtration Cells	39
2.2.2 Stirred Reaction Vessel	40
2.3 Analytical Methods	45
2.3.1 Powder X-Ray Diffraction	45
2.3.2 Single Crystal X-Ray Diffraction	46
2.3.3 ICP Emission Spectroscopy	46
2.3.4 Electron Microscopy	47
2.4 Synthesis and Characterization of Hideout Reaction Products	48
2.4.1 Experimental Design	48
2.4.2 Synthesis of Maricite ($\text{NaFe}^{\text{II}}\text{PO}_4$)	50

2.4.3	Syntheses of Sodium Iron Hydroxy Phosphate (“SIHP”)	51
2.4.3.1	Iron Nitriloacetate ($\text{Fe}^{\text{III}}\text{NTA}$) Experiments	51
2.4.3.2	Iron Tartrate ($\text{Fe}^{\text{III}}_2(\text{C}_4\text{H}_4\text{O}_6)_3$) Experiments	52
2.4.3.3	Iron Oxalate ($\text{Fe}^{\text{III}}_2(\text{C}_2\text{O}_4)_3 \cdot 5\text{H}_2\text{O}$) Experiments	53
2.4.4	Syntheses of Ammonium Iron(II,III) Phosphate ($(\text{NH}_4)\text{Fe}^{\text{II}}\text{Fe}^{\text{III}}(\text{PO}_4)_2$)	53
2.4.4.1	Hematite Experiments	53
2.4.4.2	Iron Tartrate Experiments	54
2.4.5	Synthesis of Ammonium Iron Phosphate Hydrate ($(\text{NH}_4)\text{Fe}^{\text{II}}(\text{PO}_4) \cdot \text{H}_2\text{O}$)	55
2.4.5.1	Iron Nitriloacetate Experiments	55
2.4.6	Syntheses of $\text{Na}_2\text{Ni}(\text{OH})\text{PO}_4$ (“SNHP”)	56
2.4.6.1	Nickel Oxide (NiO) Experiments	56
2.4.6.2	Nickel Nitriloacetate ($\text{H}^+[\text{NiNTA}^-]$) Experiments	57
2.5	Solubility Measurements on Sodium Nickel Hydroxy Phosphate in the Stirred Reaction Vessel	57
2.5.1	Kinetics	57
2.5.2	Solubility vs Temperature	59
2.5.3	Recovery of the Equilibrium Solid Reaction Product	61

CHAPTER 3.0 HYDROTHERMAL SYNTHESIS OF HIDEOUT REACTION

	PRODUCTS	63
3.1	Maricite	63
3.2	SIHP	65
3.2.1	The $\text{Fe}^{\text{III}}\text{NTA}$ Reaction	65
3.2.2	The $\text{Fe}^{\text{III}}_2(\text{C}_4\text{H}_4\text{O}_6)_3$ Reaction	69
3.2.3	The $\text{Fe}^{\text{III}}_2(\text{C}_2\text{O}_4)_3 \cdot 5\text{H}_2\text{O}$ Reaction	70
3.3	$(\text{NH}_4)\text{Fe}^{\text{II}}\text{Fe}^{\text{III}}(\text{PO}_4)_2$	72
3.4	$(\text{NH}_4)\text{Fe}^{\text{II}}(\text{PO}_4) \cdot \text{H}_2\text{O}$	77
3.5	SNHP	82
3.5.1	The NiO Reaction	82
3.5.2	The $\text{H}^+[\text{NiNTA}^-]$ Reaction	86

CHAPTER 4.0 SOLUBILITY AND REACTION KINETICS OF SODIUM NICKEL

	HYDROXY-PHOSPHATE	90
4.1	Solubility of Nickel Oxide-Sodium-Phosphate Reaction	90
4.2	Kinetics of $\text{Na}_2\text{Ni}(\text{OH})\text{PO}_4$ Equilibration.....	92
4.3	A Thermodynamic Model	96
4.3.1	Phosphate Ionization Equilibria	96
4.3.2	Equilibrium Constants and Thermodynamic Properties of SNHP	104
4.4	Comparison with Data From Other Workers	115
4.5	Future Work	119

CHAPTER 5.0 CONCLUSIONS	122
CHAPTER 6.0 BIBLIOGRAPHY	124
APPENDIX I: Powder X-ray Diffraction Results.....	132
APPENDIX II: X-ray Crystal Structure of $(\text{NH}_4)\text{Fe}^{\text{II}}(\text{PO}_4)\cdot\text{H}_2\text{O}$	162
APPENDIX III: Kinetic and Solubility Data for $\text{Na}_2\text{Ni}(\text{OH})\text{PO}_4$ Formation Equilibria with Nickel Oxide.....	172

LIST OF TABLES

Table 1.1	Corrosion rates of Inconel Alloy 600 in high temperature phosphate solutions compared with those of other alloys	35
Table 3.1	Positional parameters for $(\text{NH}_4)\text{Fe}^{\text{II}}(\text{PO}_4)\cdot\text{H}_2\text{O}$ from single crystal analysis.....	80
Table 4.1	Experimental equilibrium constants for the SNHP formation reaction	98
Table 4.2	Standard state properties of the first and second ionizations of phosphoric acid	99
Table 4.3	Standard state properties of the third ionization of phosphoric acid	100
Table 4.4	Standard state properties of the dissociation of water	102
Table 4.5	Standard state properties of aqueous species at 25 °C and 1 bar	106
Table 4.6	HKF equation of state coefficients for aqueous species	107
Table 4.7	Maier-Kelley coefficients for heat capacities of solids	108
Table 4.8	Experimental data calculations for the SNHP formation reaction	110
Table 4.9	Equilibrium constants for the isocoulombic reaction	111
Table 4.10	Standard state properties of the SNHP formation reaction	117

LIST OF FIGURES

Figure 1.1	Two-liquid phase and solution-solid boundaries for aqueous solution mixtures of sodium phosphate salts of mole ratios, Na/PO ₄ from 1.00 to 3.00 at 200-400 °C	18
Figure 1.2	Schematic representation of part of the sodium-phosphate-water isothermal phase diagram near 300 °C	19
Figure 1.3	A schematic diagram of the reaction process of Fe ^{II} Fe ^{III} ₂ O ₄ at 275 °C with varying mole ratios of aqueous Na/PO ₄ solutions	23
Figure 1.4	Approximate stability diagram for the sodium-iron-phosphate-water system, calculated with m(Na ⁺ ,aq)=0.1 mol·kg ⁻¹ , showing the hideout reaction paths during heating: (a) Na/PO ₄ = 2.0; (b) Na/PO ₄ = 2.2; and (c) Na/PO ₄ = 3.5	24
Figure 1.5	Distribution of nickel(II) ion complexes present in solution at 25 °C (298 K; top) and 287 °C (560 K; bottom) where Na/PO ₄ = 2.3	28
Figure 1.6	Possible process for dissolution of reaction product formed by NiO and aqueous sodium phosphate (Na/PO ₄ = 2.5)	30
Figure 2.1	Modified Parr 4744 reaction vessel used for hydrothermal synthesis and <i>in situ</i> filtration	41
Figure 2.2	45 mL Teflon lined cells. On the left, vessels before the reaction, and after the filtration. On the right, vessels during the reaction	42
Figure 2.3	Schematic diagram of Parr 450 mL stirred reaction vessel	44
Figure 2.4	Experimental design for zirconium stirred reaction vessel experiments: Solubility of zirconium oxide reaction products, and nickel oxide reaction products under uncontrolled redox conditions	60
Figure 3.1	Scanning electron micrographs of (a) maricite (Quinlan, 1996) and (b) a solid reaction product obtained from Fe ^{III} NTA and aqueous sodium phosphate (Na/PO ₄ = 2.15) at 200 °C for 28 days	64

Figure 3.2	Scanning electron micrographs of solid reaction products obtained from Fe ^{III} NTA and aqueous sodium phosphate (Na/PO ₄ = 4.0) at 200 °C for 5-14 days [(a) (PO ₄)=0.6 molal, (b) repeat of (a) at a higher Fe/PO ₄ mole ratio, (c) (PO ₄)=1.0 molal]66
Figure 3.3	Scanning electron micrograph of a solid reaction product obtained from iron(III) tartrate and aqueous sodium phosphate (Na/PO ₄ = 2.8) at 200 °C for 3 weeks71
Figure 3.4	Scanning electron micrograph of a solid reaction product obtained from iron(III) oxalate and aqueous sodium phosphate (Na/PO ₄ = 2.5) at 250 °C for 8 days73
Figure 3.5	Scanning electron micrograph of solid reaction products obtained from iron(III) tartrate and aqueous ammonium phosphate (NH ₄ /PO ₄ = 1.0) at 250 °C for 1 week [(b) is an enlarged view of (a)]75
Figure 3.6	Scanning electron micrograph of a solid reaction product obtained from iron(III) tartrate and aqueous ammonium phosphate (NH ₄ /PO ₄ = 1.0) at 200 °C for 1 week76
Figure 3.7	Scanning electron micrograph of a solid reaction product obtained from Fe ^{III} NTA and aqueous ammonium phosphate (NH ₄ /PO ₄ = 2.8) at 200 °C for 9 days78
Figure 3.8	Crystal Structure of (NH ₄)Fe ^{II} (PO ₄)·H ₂ O81
Figure 3.9	Scanning electron micrograph of a solid reaction product obtained from iron(III) tartrate and aqueous ammonium phosphate (NH ₄ /PO ₄ = 2.8) at 200 °C for 8 days83
Figure 3.10	Scanning electron micrograph of a solid reaction product obtained from nickel oxide and aqueous sodium phosphate (Na/PO ₄ = 2.5) at 250 °C for 1 week85
Figure 3.11	Scanning electron micrograph of a solid reaction product obtained from H ⁺ [NiNTA ⁻] and aqueous sodium phosphate (Na/PO ₄ = 2.5) at 250 °C for 4 days87
Figure 3.12	Scanning electron micrographs of solid reaction products obtained from H ⁺ [NiNTA ⁻] and aqueous sodium phosphate (Na/PO ₄ = 4.0) for 5 days at (a) 200 °C and (b) 250 °C respectively89

Figure 4.1	Scanning electron micrographs of solid reaction products obtained from nickel oxide and aqueous sodium phosphate ($\text{Na}/\text{PO}_4 = 2.5$), solubility run from (a) the basket and (b) the bottom of the vessel.....	91
Figure 4.2	Kinetics of precipitation and re-dissolution of SNHP (all runs combined)	93
Figure 4.3	Kinetics of precipitation and re-dissolution of SNHP (data obtained from the best runs)	94
Figure 4.4	Phosphate ionization equilibria calculated from SUPCRT'92 and literature data from Mesmer and Baes, 1974	101
Figure 4.5	Water ionization equilibria calculated from SUPCRT'92 and literature data from Sweeton et al., 1974	103
Figure 4.6	The relative difference between experimental values of log K (Mesmer and Baes, 1974; Sweeton et al., 1974) and those calculated from SUPCRT'92	105
Figure 4.7	Extended van't Hoff plot of the isocoulombic reaction	113
Figure 4.8	Comparison of experimental data and values calculated from SUPCRT'92 for the SNHP formation reaction	116
Figure 4.9	Comparison of experimental and equilibrium constants calculated from SUPCRT'92 model with those of Ziemniak and Opalka (1988) for the SNHP formation reaction	118
Figure 4.10	Comparison of experimental and Gibbs free energy data calculated from SUPCRT'92 model with those of Ziemniak and Opalka (1988) for the SNHP formation reaction	120

LIST OF APPENDICES

APPENDIX I	Powder X-ray Diffraction Results.....	132
APPENDIX II	X-ray Crystal Structure of $(\text{NH}_4)\text{Fe}^{\text{II}}(\text{PO}_4)_2 \cdot \text{H}_2\text{O}$	162
APPENDIX III	Kinetic and Solubility Data for $\text{Na}_2\text{Ni}(\text{OH})\text{PO}_4$ Formation Equilibria with Nickel Oxide.....	172

1.0 INTRODUCTION

1.1 Hydrothermal Synthesis

In the last thirty years, the chemistry of inorganic and organic systems under hydrothermal conditions has received increasing interest from researchers in many different fields of scientific studies. The first definition for the term “hydrothermal” was proposed by Sir Roderick Murchison (1840s) who described it as the action of water at elevated temperature and pressure in bringing about changes in the earth’s crust leading to the formation of various rocks and minerals (Byrappa and Yoshimura, 2001). Byrappa and Yoshimura (2001) proposed the basic definition that a hydrothermal reaction is “any heterogeneous chemical reaction in the presence of a solvent (whether aqueous or non-aqueous) above room temperature and at pressure greater than 1 atm in a closed system”. The first use of experimental hydrothermal techniques came from a geological point of view, to understand natural mineral formation in the presence of water under high temperatures and pressures. Researchers have now developed a wide variety of pressure vessel equipment to simulate these natural processes in the laboratory under hydrothermal conditions (Ulmer and Barnes, 1983).

The first successful commercial application of hydrothermal techniques was the use of NaOH to leach bauxite as a process for obtaining pure aluminum hydroxide which could then be converted to pure Al_2O_3 suitable for processing to metal (Goranson, 1931). Such “pressure leaching” processes were widely used today for a large variety of metals (Habasi, 1994). Hydrothermal techniques have also been used for the synthesis of large

single crystals of quartz (Nacken, 1946), zeolites (Barrer, 1948), and other minerals for use as gemstones or advanced materials. Modern methods for the hydrothermal synthesis of single crystals are summarized by Byrappa et al. (1994). In the last decade, new homogeneous precipitation methods have been developed as a means of synthesizing monodisperse crystallites by decomposing aqueous solutions of metal chelates under hydrothermal conditions (Booy and Swaddle, 1978; Bridson et al., 1998). In this project, this method was utilized to synthesize the desired sodium metal phosphate and ammonium metal phosphate reaction products that can form under boiler conditions.

All hydrothermal systems are closed. Therefore one can study the influence of temperature, pressure and composition separately which help to understand phase behaviour, and fundamental solution chemistry in many aqueous inorganic systems. Interest in this area has also led to many studies in the solubility, kinetics, and thermodynamics of crystal growth. Advances in apparatus used in this area of research have contributed to the increasing popularity of the hydrothermal technique, among physical chemists. Studies on aqueous systems at high temperature and pressure have been done using conductivity, potentiometric, spectrophotometric, solubility, PVT and calorimetric, neutron diffraction, EXAFS, and other related methods (Byrappa and Yoshimura, 2001).

In this work, we want to observe “hideout” behaviour under boiler conditions. Low concentrations of sodium phosphate are added to the boiler water of electric power stations as a means of controlling pH. Hideout is the phenomenon by which phosphate in the water is observed to be retained in the boiler during conditions of high temperature

and pressure, only to be released back into the water upon cooling. Several workers have used boiler tube simulators, flow systems, or batch systems under a range of conditions in this area of research (Straub, 1950; Pollard and Edwards, 1963; Economy et al., 1975; Balakrishnan, 1977; Wetton, 1980; Ziemniak et al., 1981; Connor and Panson, 1983; Tremaine et al., 1992, 1993, 1996, 1998). In our studies, we incorporated simple acid digestion bombs for hideout product syntheses and stirred autoclave systems for kinetic and solubility experiments.

1.2 Phosphate Hideout in Steam Generators

Before the 1970s, sodium-phosphate treatments had been successfully used for the control of pH and scale formation in steam generating stations with little understanding of how the physical chemistry of the system worked. In the early 1970s many power stations were beginning to see thinning of boiler tubes and pressure-tube denting which eventually led some power stations to replace their current sodium phosphate treatment with all-volatile treatments (AVT).

What was happening to these boiler tubes could be attributed to phosphate hideout. Studies by Panson et al. (1975), Broadbent et al. (1977), and Taylor et al. (1979) have shown that hideout can be caused by the precipitation of sodium phosphate phases under scale deposits, in crevices, and in other local hot spots. Because of the incongruent precipitation of acidic phosphate salts, the basicity of the boiler water greatly increased when hideout occurred at high sodium phosphate mole ratios ($\text{Na}/\text{PO}_4 > 3.0$), eventually leading to the boiler tube damage described above. The introduction of “congruent”

phosphate control in the 1980s was intended to keep low concentrations within an area of the sodium-phosphate-water phase diagram that would avoid pH excursions, even at temperatures greater than 300 °C (Panson et al., 1975; Aschoff et al., 1986).

In order to investigate the chemistry involved, Economy et al. (1975) and Conner and Panson (1983) studied the effects that aqueous sodium phosphate had on metal oxides at temperatures up to 315 °C. The metals involved were those typically used in the construction of boiler tubes. However, modern steam generators operate at higher temperatures and pressures than 315 °C. Tremaine et al. (1993) extended the experimental temperature range up to 360 °C for magnetite and three of the major components of sludge, Cu, NiO, and ZnO. The same results were observed in both studies, the metal oxides reacted with sodium phosphate to produce phosphate-metal corrosion products.

Two of the major corrosion products that were observed when magnetite, iron, and carbon steel were exposed to concentrated phosphate at temperatures greater than 200 °C were “maricite”, $\text{NaFe}^{\text{II}}\text{PO}_4$, and sodium iron(III) hydroxyphosphate “SIHP”, $\text{Na}_3\text{Fe}^{\text{III}}(\text{PO}_4)_2 \cdot (\text{Na}_{4/3}\text{H}_{2/3}\text{O})$. Recent work in our group (Bridson et al., 1998; Tremaine et al., 1998) resulted in the development of a chemical equilibrium model and database for predicting the precipitation of these iron compounds.

The objective of this project is to investigate phosphate hideout under conditions associated with the changeover from congruent phosphate treatment to AVT at the Point Lepreau nuclear station. Most modern nuclear stations operate at temperatures as high as 300 °C and pressures as high as 200 bars, and use volatile amines as chemical additives to

control impurities and pH in boiler water. However, recent experience has shown that severe corrosion damage can occur during changeover as the result of incongruent release of sodium-phosphate hideout reaction products, and subsequent reactions with the protective transition metal oxide layer. Therefore the purpose of this research is to identify solid reaction products that could form under typical phosphate hideout conditions with Inconel Alloy 800 in Candu boiler tubes by both powder and single crystal XRD analysis, and to determine equilibrium constants for sodium nickel hydroxyphosphate “SNHP”, $\text{Na}_2\text{Ni}(\text{OH})\text{PO}_4$, which is one of the major nickel reaction products known to form at steam generator temperatures (Ziemniak, 1988).

1.3 Standard State Properties of Aqueous Species and Solids

1.3.1 Solids

Gibbs energies of reaction for the formation and dissolution of solid reaction products, $\Delta_r G_{T,p}^\circ$, are calculated from the standard Gibbs energies of formation of the solid, aqueous, gaseous reactants and products. These are represented by the following equation (Atkins, 1993):

$$\Delta_r G_T^\circ = \sum \Delta_f G_T^\circ(\text{products}) - \sum \Delta_f G_T^\circ(\text{reactants}) \quad (1.1)$$

The enthalpies of formation can be represented by a similar equation. Using the following solubility reaction as an example:



the standard Gibbs energies and enthalpies of formation of the species $\text{A}_2\text{B(s)}$ at high temperature and pressure are calculated from the elements at the same temperature and the reference pressure, p_r (1bar):

$$\Delta_f G_{\text{A}_2\text{B},T,p}^{\circ} = G_{\text{A}_2\text{B},T,p}^{\circ} - 2G_{\text{A},T,p_r}^{\circ} - G_{\text{B},T,p_r}^{\circ} \quad (1.3)$$

$$\Delta_f H_{\text{A}_2\text{B},T,p}^{\circ} = H_{\text{A}_2\text{B},T,p}^{\circ} - 2H_{\text{A},T,p_r}^{\circ} - H_{\text{B},T,p_r}^{\circ} \quad (1.4)$$

The standard partial molar entropies, isobaric heat capacities, and volumes of minerals, gases, and aqueous species are designated by $S_{p,T}^{\circ}$, $C_{p,T}^{\circ}$, and $V_{p,T}^{\circ}$, respectively. Gibbs energy, enthalpy, and entropy are related through the following well-known equation:

$$\Delta_f G_{i,T,p}^{\circ} = \Delta_f H_{i,T,p}^{\circ} - T\Delta_f S_{i,T,p} \quad (1.5)$$

The heat capacity of formation $\Delta_f C_{p,T}^{\circ}$ and the volume of formation $\Delta_f V^{\circ}$ are used in the expressions for the high temperature thermodynamic properties in Equation (1.5). The standard Gibbs free energy at a specified temperature can be calculated from the following equation:

$$\Delta_f G_{T,p}^o = \Delta_f G_{T_r,p_r}^o - \Delta_f S_{T_r,p_r}^o (T - T_r) + \int_{T_r}^T \Delta_f C_p^o dT - T \int_{T_r}^T \frac{\Delta_f C_p^o}{T} dT + \int_{p_r}^p \Delta_f V^o dp \quad (1.6)$$

at some reference temperature and pressure. The value for the heat capacity of a solid can be represented by the Maier-Kelly equation (1932):

$$C_p^o = a + bT + cT^{-2} \quad (1.7)$$

where a, b, and c are constants. More complex equations are also used (Anderson and Crerar, 1993), for example:

$$C_p^o = a + bT + cT^{-2} + fT^2 + gT^{\frac{-1}{2}} \quad (1.8)$$

and

$$C_p^o = a + bT^{\frac{1}{2}} + cT^{-2} + dT^{-3} \quad (1.9)$$

The volume of a solid can be expressed as:

$$V_{p,T}^o = V_{p_r,T_r}^o + \sum_{i=1}^n \Delta V_i^o \quad (1.10)$$

where V^o designates the standard molal volume of the specified solid at the subscripted

pressure and temperature, and ΔV_t° represents the change in standard molal volume associated with the i th of the n solid/solid phase transitions (t) that occur along the straight-line p-T path from p_r, T_r to p, T (Johnson et al, 1992; Helgeson et al., 1978). However, there are only slight variations in volume with changes in temperature and pressure. Therefore the volume may be assumed to be constant.

The standard molal Gibbs free energies and enthalpies of minerals, gases, and aqueous species are more conveniently defined as *apparent* standard molar Gibbs free energies ($\Delta_a G_{p,T}^\circ$) and enthalpies ($\Delta_a H_{p,T}^\circ$) of formation from the elements at the reference pressure, $p_r = 1$ bar, and temperature, $T_r = 298.15$ K (Benson, 1968; Helgeson et al., 1978; 1981). Using reaction (1.2) as an example, the apparent Gibbs free energy and enthalpy of formation are defined as:

$$\begin{aligned}\Delta_a G_{A_2B,T,p}^\circ &= G_{A_2B,T,p}^\circ - 2G_{A,T_r,p_r}^\circ - G_{B,T_r,p_r}^\circ \\ &= \Delta_f G_{A_2B,T_r,p_r}^\circ + (G_{A_2B,T,p}^\circ - G_{A_2B,T_r,p_r}^\circ)\end{aligned}\quad (1.11)$$

$$\begin{aligned}\Delta_a H_{A_2B,T,p}^\circ &= H_{A_2B,T,p}^\circ - 2H_{A,T_r,p_r}^\circ - H_{B,T_r,p_r}^\circ \\ &= \Delta_f H_{A_2B,T_r,p_r}^\circ + (H_{A_2B,T,p}^\circ - H_{A_2B,T_r,p_r}^\circ)\end{aligned}\quad (1.12)$$

where $\Delta_f G^\circ$ and $\Delta_f H^\circ$ are the standard molar Gibbs free energy and enthalpy of formation of the species from the elements in their stable phase at the reference pressure ($p_r = 1$ bar) and the temperature ($T_r = 298.15$ K). The terms $G_{p,T}^\circ - G_{p_r,T_r}^\circ$ and $H_{p,T}^\circ - H_{p_r,T_r}^\circ$ refer to differences in the standard molar Gibbs free energy and enthalpy of the species from

changes in pressure ($p - p_r$) and temperature ($T - T_r$). In comparison with equation (1.6), the temperature dependence of $\Delta_a G_{T,p}^{\circ}$ is expressed by the following equation:

$$\Delta_a G_{T,p}^{\circ} = \Delta_f G_{T_r,p_r}^{\circ} - S_{T_r,p_r}^{\circ} (T - T_r) + \int_{T_r}^T C_p^{\circ} dT - T \int_{T_r}^T \frac{C_p^{\circ}}{T} dT + \int_{p_r}^p V^{\circ} dp \quad (1.13)$$

The Gibbs energies of reaction $\Delta_r G_{T,p}^{\circ}$ can be calculated from the Gibbs free energies of the elements incorporating the previous Equation (1.13) for each element by:

$$\begin{aligned} \Delta_r G_T^{\circ} &= \sum \Delta_a G_T^{\circ}(\text{products}) - \sum \Delta_a G_T^{\circ}(\text{reactants}) \\ &= \sum \Delta_f G_T^{\circ}(\text{products}) - \sum \Delta_f G_T^{\circ}(\text{reactants}) \end{aligned} \quad (1.14)$$

The equilibrium constants of a reaction are related to $\Delta_r G_{T,p}^{\circ}$, and can be calculated by the following well known equation:

$$\Delta_r G^{\circ} = -RT \ln K \quad (1.15)$$

1.3.2 Aqueous Species

Models for evaluating the heat capacity (C_p°) and standard molal volumes (V°) of aqueous species have only been developed in the last twenty years because data for C_p° and V° have only recently been determined at elevated pressure and temperature.

Because of the experimental difficulties involved in such measurements, semi-empirical equations are needed to predict the values of these thermodynamic properties at high temperatures.

The standard partial molar thermodynamic property of an aqueous species is the sum of the intrinsic properties of the ions involved and that of the electrostatic contributions from the ion-solvent interactions present (Helgeson and Kirkham, 1976; Tanger and Helgeson, 1988). The intrinsic properties are normally referred to as a “nonelectrostatic” or a “nonsolvation” contribution to the equation of state. The Born model is used to represent the electrostatic or solvation contribution. SUPCRT’92 (Johnson et al., 1992) is an interactive Fortran 77 program that contains a large thermodynamic database of many minerals, gases, and aqueous species. The revised Helgeson-Kirkham-Flowers (HKF) equation of state (Tanger and Helgeson, 1988; Shock et al., 1991) is used by SUPCRT’92 to calculate thermodynamic properties over a range of temperatures and pressures.

The revised HKF equation of state for standard molal volumes at varying temperature and pressure can be expressed as:

$$V^o = [\Delta V_n^o] + [\Delta V_s^o] \quad (1.16)$$

$$V^o = \left[a_1 + \frac{a_2}{\psi + p} + \frac{a_3}{T - \Theta} + \frac{a_4}{(\psi + p)(T - \Theta)} \right] + \left[-\omega Q + \left(\frac{1}{\epsilon} - 1 \right) \left(\frac{\partial \omega}{\partial p} \right)_T \right] \quad (1.17)$$

where n and s are the non-solvation and solvation parts of the volume equation

respectively, a_1 , a_2 , a_3 , and a_4 are species-dependent fitting parameters, ψ (2600 bars) and Θ (228 K) are solvent-dependent parameters, and Q refers to the solvent Born functions defined by the following equation (ϵ is the static dielectric constant of water):

$$Q = \epsilon^{-1} \left(\frac{\partial \ln \epsilon}{\partial p} \right)_T \quad (1.18)$$

The remaining ω term is the conventional Born coefficient defined as:

$$\omega = \frac{Z^2 \eta}{r_e} \quad (1.19)$$

where Z is the charge of the ion, $\eta = 1.6603 \cdot 10^{-5} \text{ cal} \cdot \text{m}^{-1} \cdot \text{mol}^{-1} = 6.9466 \cdot 10^{-5} \text{ J} \cdot \text{m}^{-1} \cdot \text{mol}^{-1}$, and r_e is an effective electrostatic radius of the ion. The value for r_e is different for cations and anions, defined by the expressions $r_e = r_{\text{cryst}} + 0.94Z$ and $r_e = r_{\text{cryst}}$ respectively (Shock and Helgeson, 1988).

The standard molal heat capacity at varying temperature and pressure can be obtained from:

$$C_p^o = [\Delta C_{p,n}^o] + [\Delta C_{p,s}^o] \quad (1.20)$$

$$C_p^o = \left[c_1 + \frac{c_2}{(T - \Theta)^2} - \left(\frac{2T}{(T - \Theta)^3} \right) \left[a_3(p - p_r) + a_4 \ln \left(\frac{\psi + p}{\psi + p_r} \right) \right] \right] \quad (1.21)$$

$$+ \left[\omega T X + 2TY \left(\frac{\partial \omega}{\partial T} \right)_p - T \left(\frac{1}{\epsilon} - 1 \right) \left(\frac{\partial^2 \omega}{\partial T^2} \right)_p \right]$$

where X and Y are the Born functions associated with heat capacity which are defined as:

$$X = \varepsilon^{-1} \left[\left(\frac{\partial^2 \ln \varepsilon}{\partial T^2} \right)_T - \left(\frac{\partial \ln \varepsilon}{\partial T} \right)_p^2 \right] \quad (1.22)$$

$$Y = \frac{1}{\varepsilon^2} \left(\frac{\partial \varepsilon}{\partial T} \right)_p \quad (1.23)$$

At constant pressure, the revised HKF equations (1.17) and (1.21) become:

$$V^o = a_1 + \left\{ \frac{a_3}{(T - \Theta)} \right\} - \omega Q \quad (1.24)$$

$$C_p^o = c_1 + \left\{ \frac{c_2}{(T - \Theta)^2} \right\} + \omega TX \quad (1.25)$$

Equations (1.16) to (1.25) are the theoretical basis for the thermodynamic modeling code used in SUPCRT'92. The heat capacity and volume functions for aqueous species become a little more complex as compared to solids, resulting in more complex formulas for standard partial molar thermodynamic properties of aqueous species. Shock et al. (1992) gives a summary of the references describing the derivation of these equations, and examples of the practical application of these theories and data to model equilibrium processes at high temperatures and pressures.

1.4 Activity Coefficients in High Temperature Water

In order to describe solubility equilibria at defined molalities, a model is needed to calculate the activity coefficients of the aqueous species. Using Equation (1.2) as an example, the equilibrium quotient, Q , is found in the following way:

$$Q = \frac{m(A^+, aq)^2 \cdot m(B^{2-}, aq)}{a(A_2B, s)} \quad (1.26)$$

and the equilibrium constant, K , can be written as:

$$K = \frac{m(A^+, aq)^2 \cdot \gamma(A^+, aq)^2 \cdot m(B^{2-}, aq) \cdot \gamma(B^{2-}, aq)}{a(A_2B, s)} \quad (1.27)$$

$$\log K = \log Q + \log \left[\frac{\gamma(A^+, aq) \cdot \gamma(B^{2-}, aq)}{a(A_2B, s)} \right] \quad (1.28)$$

The activity of the solid, $a(A_2B)$, is usually unity. Since the aqueous molalities are known, the only remaining variables are the activity coefficients which represent the ion-ion interactions in solution. For many high temperature systems, the semi-empirical model reported by Pitzer (1991) can be used to calculate activity coefficients. When activity coefficients are not known, Lindsay's model (Lindsay, 1989, 1990) can be used at temperatures in the range of 150-325 °C. This model relates activity coefficients at a given ionic strength to those of NaCl. The EPRI computer code MULTEQ (Lindsay,

1989; Baes and Lindsay, 1996; Alexander et al., 1989) incorporates Lindsay's model. As a result, Lindsay's model was used in this study.

Ionic strength is defined by the following equation:

$$I = \frac{1}{2} \sum_i z_i^2 m_i \quad (1.29)$$

where z_i is the ionic charge and m_i is the molality of the ionic species. Activity coefficients are calculated as follows, according to the Lindsay model (Lindsay, 1990):

$$\gamma_i = (\gamma_{NaCl})^{z_i^2} \quad (1.30)$$

where z_i is the charge of ion i . The expression for $\gamma_{(NaCl)}$ is taken from the Meisner equation (Alexander and Luu, 1989):

$$\log \gamma_{(NaCl)} = F(I) = \frac{-AI^{\frac{1}{2}} \log 10}{1 + CI^{\frac{1}{2}}} + \log [1 + B(1 + 0.1I)^q - B] \quad (1.31)$$

where

$$B = 0.75 + 0.065q \quad (1.32)$$

$$C = 1 + 0.0055q e^{-0.028I^{\frac{1}{2}}} \quad (1.33)$$

$$q = 2.95869 - 3.21502 \times 10^{-3} t_c - 1.7233 \times 10^{-5} t_c^2 \quad (1.34)$$

$$A = 0.484582 + 0.00158173t_c - 2.14065 \times 10^{-5} t_c^2 + 2.56199 \times 10^{-7} t_c^3 - 1.05332 \times 10^{-9} t_c^4 + 1.57603 \times 10^{-12} t_c^5 \quad (1.35)$$

and t_c is the Celcius temperature.

The properties of water were an important component of the MULTEQ database which was used in our study, to calculate equilibrium speciation at high temperatures. The most important properties of water are the osmotic coefficient (Φ) and the activity (a_w), of water. These two properties, which must satisfy the Gibbs-Duhem equation, are expressed as follows:

$$\Phi - 1 = \frac{1}{\sum_{sol} m_i} \sum_i \int_0^{\sum_{sol} m_i} \left(\frac{d \ln \gamma_i}{d \sum_i m_i} \right)_x d \sum_i m_i \quad (1.36)$$

$$a_w = \exp(-0.018015 \Phi \sum_{sol} m_i) \quad (1.37)$$

where $\sum_{sol} m_i$ is the total concentration of all dissolved constituents in the solution.

1.5 The Sodium-Phosphate-Water System

The complex phase behaviour of the sodium-phosphate-water system below 100 °C has been determined by Van Wazer (1958) and Wendrow and Kobe (1955). At room temperature, several hydrated phases of the Na_2HPO_4 and Na_3PO_4 salts are present

along with two complex salts, $\text{Na}_3\text{PO}_4 \cdot 12\text{H}_2\text{O} \cdot 1/4\text{NaOH}$ and $\text{Na}_2\text{HPO}_4 \cdot 2\text{NaH}_2\text{PO}_4 \cdot 2\text{H}_2\text{O}$, but these become less stable as temperature is raised, leaving less hydrated and anhydrous phases above 100 °C. The major phosphate species present in high temperature water are H_2PO_4^- , HPO_4^{2-} , and PO_4^{3-} . A complete review of the aqueous chemistry of phosphates has been reported by Tremaine et al. (1992).

At high temperatures, the solubility and phase behaviour of the monosodium phosphate system has been studied by Morey (1953) up to 600 °C, whereas that of the disodium phosphate system has been extensively studied by Ravich and Scherbakova (1955), Panson et al. (1975), Broadbent et al. (1977), and Wetton (1981) up to 350 °C.

The tri-sodium phosphate system differs from the previous two systems in that solubility decreases with increasing temperature above 120 °C. This has been observed by Schroeder et al. (1937) and references therein. It was found in the more recent studies that the stable phase, at temperatures above 200 °C and up to 350 °C, was the solid solution $\text{Na}_{2.8}(\text{H}_3\text{O})_{0.2}\text{PO}_4$ and not Na_3PO_4 as originally thought. Ravich and Scherbakova (1955) also reported that the incongruent precipitation of $\text{Na}_{2.8}(\text{H}_3\text{O})_{0.2}\text{PO}_4$ caused a dramatic increase in pH in the $\text{Na}_3\text{PO}_4\text{-H}_2\text{O}$ system at mole ratio of $\text{Na}/\text{PO}_4 \geq 2.8$. This conclusion about the tri-sodium phosphate system became an important aspect in boiler water chemistry control.

Broadbent et al. (1977) and Marshall (1982) reported that aqueous systems with sodium phosphate mole ratios between 1.0 and 2.1, showed a liquid-liquid phase separation at 275 °C. Marshall and Begun (1989) showed that these liquid phases mainly

consist of orthophosphates. The boundaries of the two phase regions are plotted as a function of temperature in Figure 1.1 along with the solubilities of di- and tri- sodium phosphate reported earlier.

Incongruent phosphate precipitation is thought to be the cause of pressure-tube damage observed in some power stations, because of the high increase in pH that resulted from the hideout process. Observing this, Marcy and Halstead (1964) first recommended the use of “congruent phosphate” control in the power industry. Congruent phosphate control maintains a position in the sodium-phosphate phase diagram at ($2.2 < \text{Na}/\text{PO}_4 < 2.8$) by employing low concentrations of sodium phosphate, which would avoid pH excursions. Further solubility studies on the sodium-phosphate system at higher temperatures and a wider range of sodium phosphate compositions were done by Panson et al. (1975), Broadbent et al. (1977), and Wetton (1981). These new measurements and those by Taylor et al. (1979), extended the phase diagram to include the equilibrium solids recovered from dry-out experiments as shown in Figure 1.2. Figure 1.2 illustrates the complex sodium phosphates and pyrophosphates that can exist under boiler conditions and the region of liquid-liquid phase separation at sodium-phosphate ratios around 2.0. All these results showed that no excursions to highly acidic or basic conditions occurred when pure sodium phosphate solutions ($2.2 < \text{Na}/\text{PO}_4 < 2.7$) are evaporated to dryness, because the solution composition is trapped between the congruent composition at 2.8 and the invariant point at 2.15. Panson et al. (1975) suggested that this feature of the phase diagram could be used as the basis for an improved treatment for

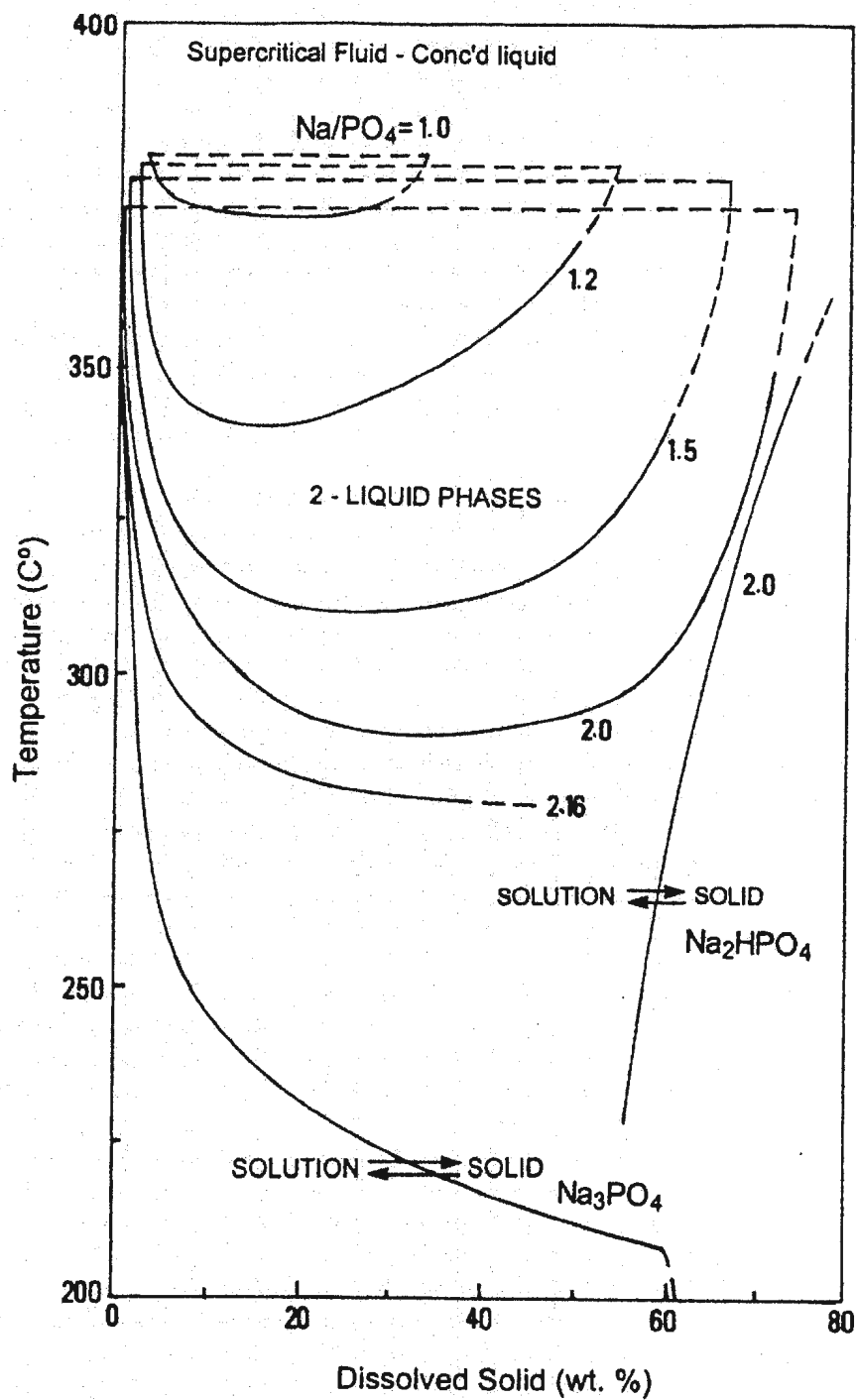


Figure 1.1: Two-liquid phase and solution-solid boundaries for aqueous solution mixtures of sodium phosphate salts of mole ratios, Na/PO₄ from 1.00 to 3.00 at 200-400 °C (Marshall, 1982)

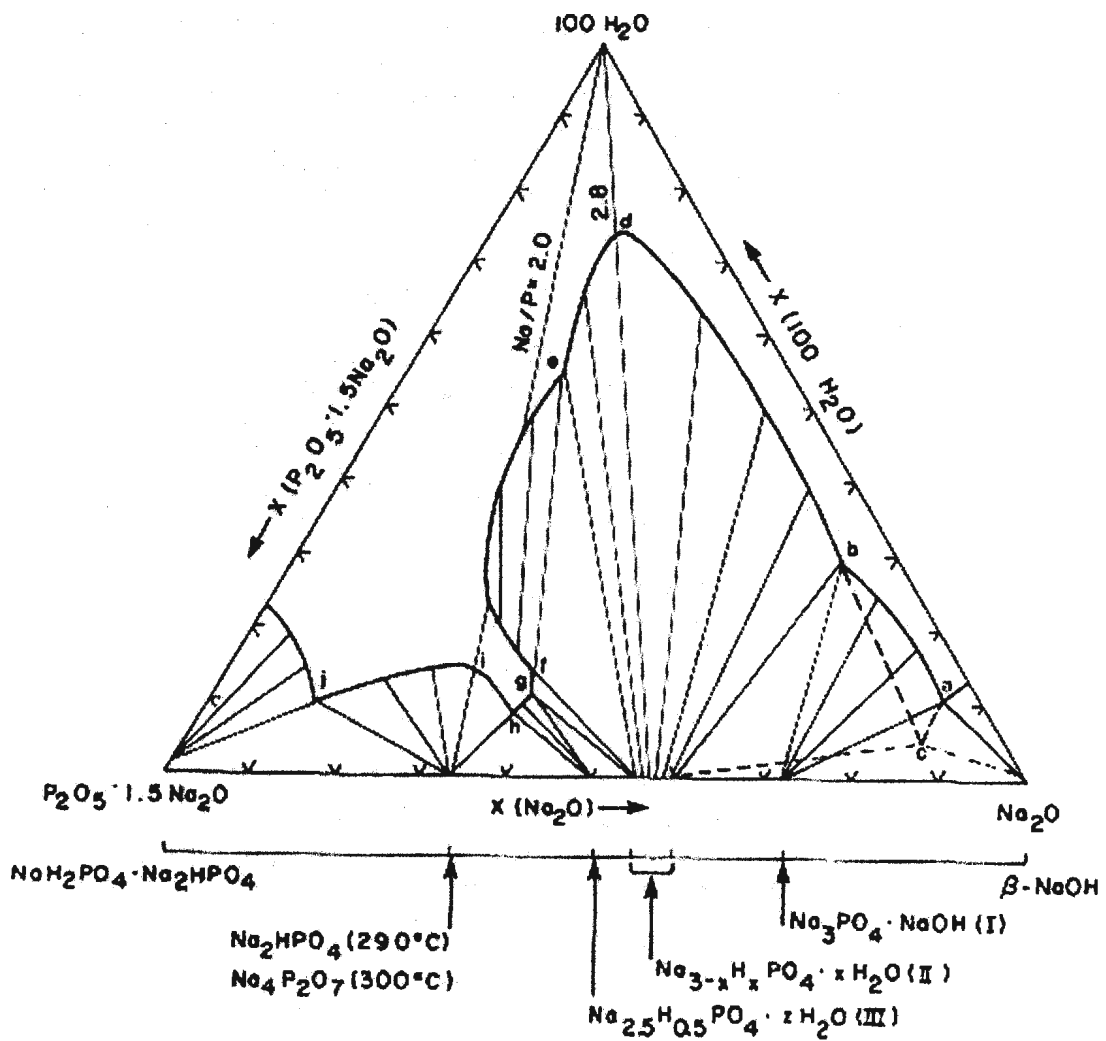


Figure 1.2: Schematic representation of part of the sodium-phosphate-water isothermal phase diagram near 300 °C (Taylor et al., 1979)

boiler water chemistry control, and coined the term “invariant point” phosphate treatment.

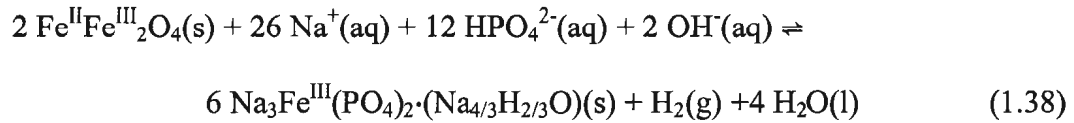
1.6 The Sodium-Iron-Phosphate-Water System

Power plant boilers would be able to operate using congruent phosphate treatment ($\text{Na}/\text{PO}_4 \leq 2.8$) without experiencing caustic conditions in their systems if hideout only involved sodium-phosphate precipitates. However phosphate has been shown to react readily with metal oxides (Economy et al., 1975; Balakrishnan, 1977; Broadbent et al., 1978; Connor and Panson, 1983) and Na/PO_4 mole ratios can rise to above 3.0. Therefore a more complex process for phosphate hideout occurs, that includes transition metal reactions.

The transition metal phosphate compound ludlamite, $\text{Fe}^{\text{II}}\text{HPO}_4$, was identified in boilers as early as 1939 by Partridge and Hall (1939). Kirsh (1964) observed such compounds as wolfite and triploideite, both with the formula $\text{Fe}^{\text{II}}_2\text{PO}_4(\text{OH})$. Around this time, researchers were observing other hideout products that contained sodium within the compound as well. The product $\text{Na}_3\text{Fe}^{\text{II}}(\text{OH})(\text{HPO}_4)_2$ was identified by Broadbent et al. (1978) whereas a related compound $\text{NaFe}^{\text{III}}_3(\text{PO}_4)_2(\text{OH})_4 \cdot 2\text{H}_2\text{O}$ was identified by Harada et al. (1978). One major sodium-iron-phosphate precipitate identified by various researchers (Pollard and Edwards, 1963; Marcy and Halstead, 1964; Broadbent et al., 1978; Jonas and Layton, 1988) was maricite, $\text{NaFe}^{\text{II}}\text{PO}_4$. This iron(II) hideout product was determined to play a major role in phosphate hideout and more recently in the corrosion behaviour observed in boiler systems (Dooley and Paterson, 1994; Dooley et

al., 1994; Dooley and McNaughton, 1996)). Another major product identified around this time was a brick-red reaction product (Broadbent et al., 1978; Ziemniak et al., 1981; Connor and Panson, 1983). This precipitate was later abbreviated as “SIHP” for sodium iron(III) hydroxy phosphate, and Ziemniak and Opalka (1993) proposed that its formula was $\text{Na}_4\text{Fe}(\text{OH})(\text{PO}_4)_2 \cdot 1/3\text{NaOH}$, however the correct formula was determined by Bridson et al. (1998), and found to be $\text{Na}_3\text{Fe}(\text{PO}_4)_2 \cdot (\text{Na}_{4/3}\text{H}_{2/3}\text{O})$ or $\text{Na}_3\text{Fe}^{\text{III}}(\text{PO}_4)_2 \cdot (\text{Na}_{2(1-x)}\text{H}_{2x}\text{O})$ where $x = 0.226$. Both formulas are similar but not identical.

Using flow experiments, Tremaine et al. (1993) determined the reaction products of magnetite, $\text{Fe}^{\text{II}}\text{Fe}^{\text{III}}_2\text{O}_4$, in equilibrium with aqueous sodium phosphate at various temperatures and Na/PO_4 mole ratios. Their results were consistent with other research at temperatures below 320 °C (Economy et al., 1975; Connor and Panson, 1983). When the solubility threshold has been reached, the magnetite reacts to form one or more reaction products. During phosphate hideout, the aqueous system becomes more basic, whereas during reverse reaction product re-dissolution, more acidic. The same observations have been seen in boilers. At 320 °C and $\text{Na}/\text{PO}_4 < 2.5$, the main hideout reaction products were maricite and SIHP. When the $\text{Na}/\text{PO}_4 > 2.5$, SIHP was observed, along with a stable solid solution of cubic $\text{Na}_{2.6}\text{Fe}_{0.2}\text{PO}_4$. Equations for each process can be found in work published by Tremaine et al. (1993). The results at 350 °C were similar to those found at 320 °C however SIHP was the major reaction product. The results at this temperature showed that iron(II) in magnetite was oxidized to iron(III) found in SIHP according to the following equation:



The schematic diagram of the phosphate hideout processes involved can be seen in Figure 1.3. Extensive damage to the magnetite film covering the boiler tube is observed at low Na/PO₄ mole ratios producing maricite and hematite, and an acidic environment. In the range 2.0 ≤ Na/PO₄ ≤ 3.0, maricite and SIHP are both produced, whereas, at Na/PO₄ > 3.0, SIHP is the only reaction product and the presence of H₂(g) produced very strong reducing conditions and a more basic environment (Tremaine et al., 1998).

Figure 1.4 is a stability diagram that represents the paths of the hideout reactions. In other words, the diagrams can be used to identify the hideout reactions that occur when magnetite is exposed to different temperatures and H₂ pressures while in equilibrium with a given sodium phosphate solution, and to understand the effects of redox conditions arising from hideout processes. Figure 1.4a shows iron(II) being removed from magnetite to form maricite, thus oxidizing magnetite to form hematite. Figure 1.4c shows the formation of SIHP and H₂. At Na/PO₄ = 2.2, a true invariant point is observed in which the four solid phases co-exist, as seen by Figure 1.4b. At this point, the redox potential is buffered at much lower reducing conditions. Tremaine et al. (1996) concluded that the redox chemistry of magnetite in boiler water during hideout is controlled by the sodium phosphate species concentrations, not those of dissolved O₂ or redox buffers which were added.

Several chemical equilibrium models have been developed to describe the

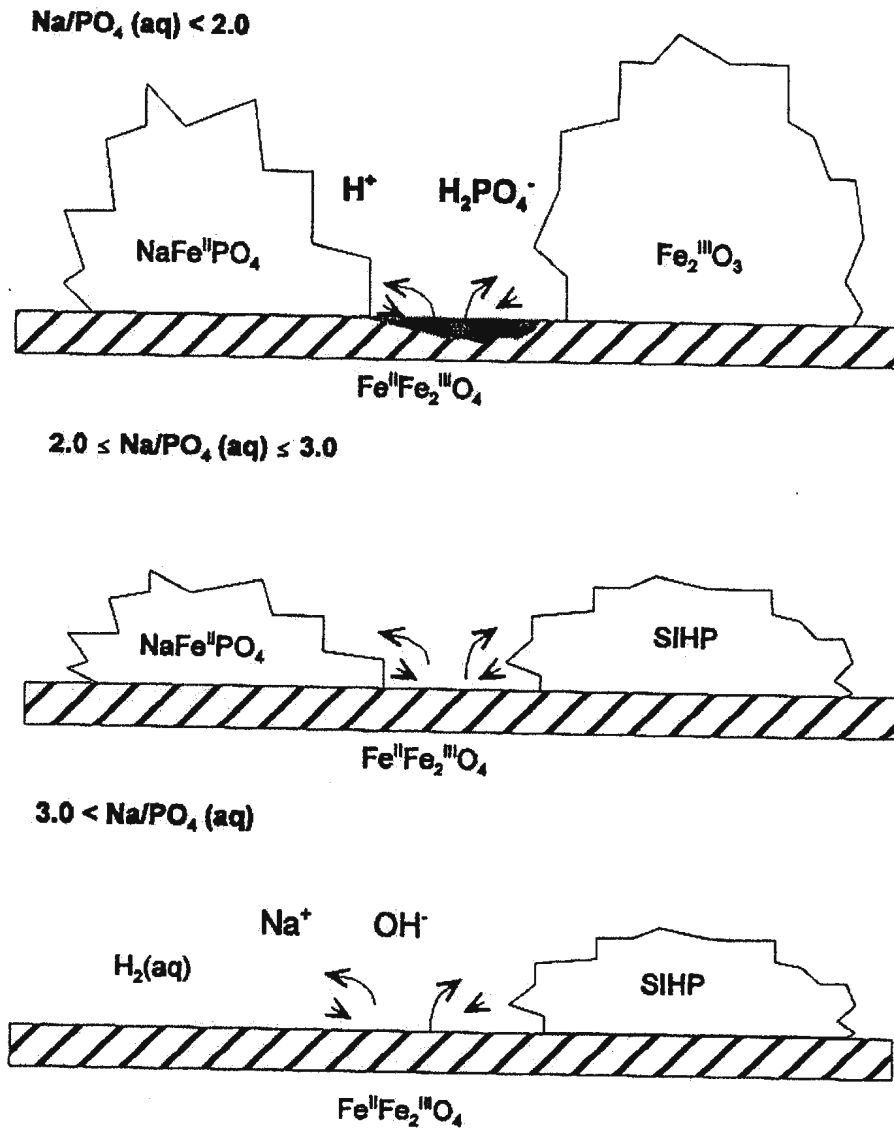


Figure 1.3: A schematic diagram of the reaction process of $\text{Fe}^{\text{II}}\text{Fe}_2^{\text{III}}\text{O}_4$ at 275 °C with varying mole ratios of aqueous Na/PO_4 solutions (Tremaine et al., 1998)

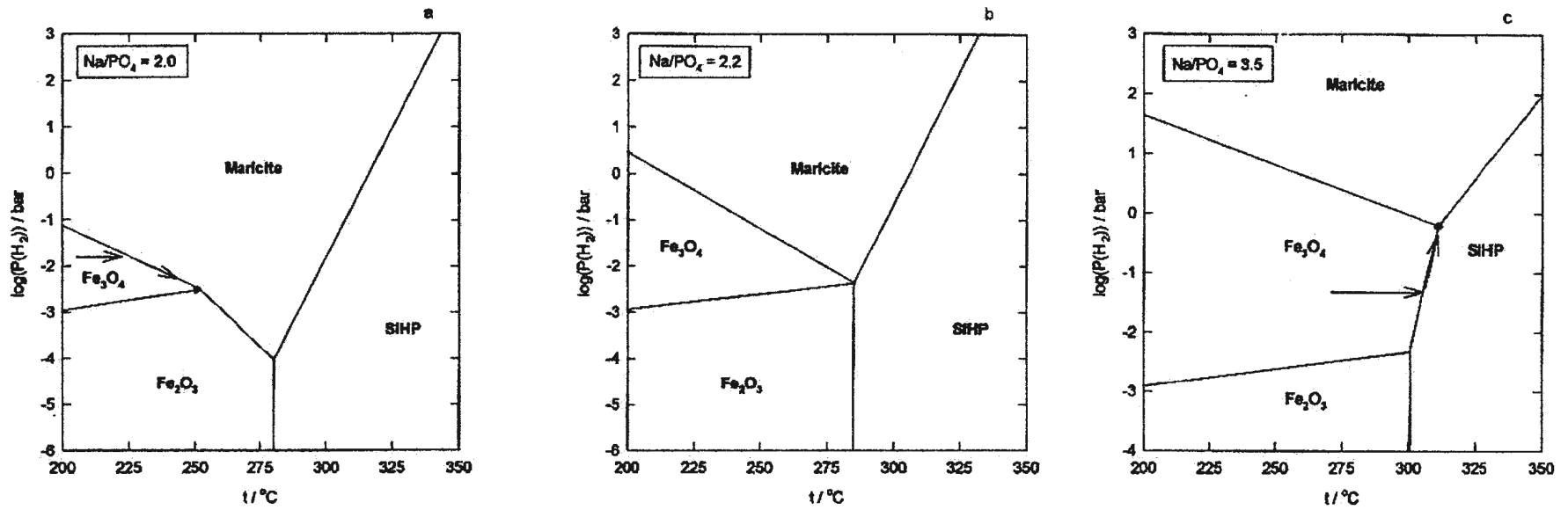
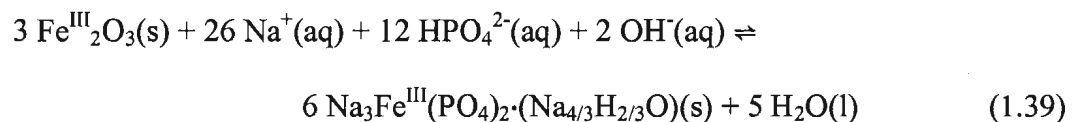


Figure 1.4: Approximate stability diagram for the sodium-iron-phosphate-water system, calculated with $m(\text{Na}^+, \text{aq}) = 0.1 \text{ mol} \cdot \text{kg}^{-1}$, showing the hideout reaction paths during heating: (a) $\text{Na}/\text{PO}_4 = 2.0$; (b) $\text{Na}/\text{PO}_4 = 2.2$ and (c) $\text{Na}/\text{PO}_4 = 3.5$ (Tremaine et al., 1998)

solubility and phase relations of precipitates in high temperature water (Alexander and Luu, 1989; Lindsay, 1989; Greenberg and Moller, 1989; Pitzer, 1986) but more information was needed before equilibrium models could be developed for this system. The main source of iron in a boiler system is magnetite, $\text{Fe}^{\text{II}}\text{Fe}^{\text{III}}_2\text{O}_4$, which acts as a protective coating on carbon steel components and also exists as loose deposits in the boiler tube. Ziemniak and Opalka (1992, 1993) reported results for the solubility of SIHP with magnetite as the iron source but did not measure the hydrogen concentrations needed for their thermodynamic calculations. Quinlan (1996) avoided this problem by using excess hematite, $\text{Fe}^{\text{III}}_2\text{O}_3$, instead of magnetite to measure the solubility of SIHP according to the reaction:

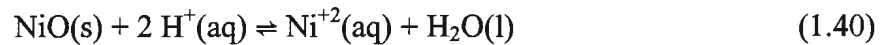


Tremaine et al. (1998) obtained solubility data for maricite in equilibrium with $\text{Fe}^{\text{II}}\text{Fe}^{\text{III}}_2\text{O}_4$ and at measured hydrogen pressures, and re-fitted the data for SIHP to derive a new equilibrium constant model based on the Helgeson-Kirkham-Flowers database and the Miessner activity coefficient model used in MULTEQ.

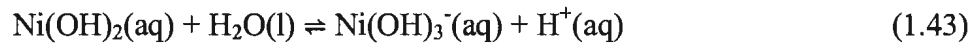
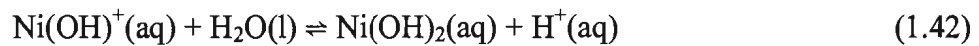
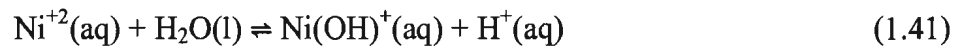
1.7 NiO-Sodium Phosphate Interactions

Nickel has been found to exist along with iron oxide solids in solid sludge deposits from steam generators (Stodola, 1986; Jonas et al., 1987). Nickel can be

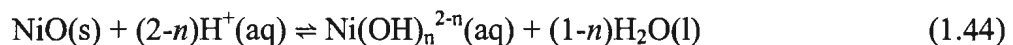
introduced from stainless steel vessels and piping, and from Inconel tubing. Ziemniak et al. (1989) investigated the solubility/phase behaviour of nickel oxide in alkaline sodium phosphate solutions at elevated temperatures. Nickel oxide becomes soluble in high temperature aqueous solutions according to the following reaction:



The dissolved nickel(II) ion becomes stabilized in aqueous solutions by the formation of hydroxo-complexes where the nickel can become surrounded by an inner hydration sphere of six water molecules. As the pH of the solution rises, dissociation occurs as follows:

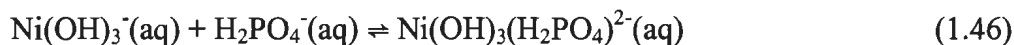
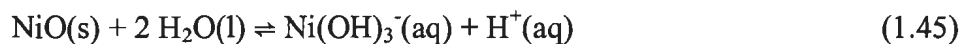


The overall nickel oxide dissolution reaction becomes the following:



where n equals the ionic state of hydrolysis and can be 0, 1, 2, 3, or 4. If phosphate is present in the aqueous solution, the nickel-phosphate complex, $\text{Ni}(\text{HPO}_4)$, and multiple, hydrolyzed forms such as $\text{Ni}(\text{OH})_n(\text{HPO}_4)_m^{(2-n-2m)+}$ ($n = 1, 2, 3; n + m \leq 6$) are possible. Figure 1.5 shows the distribution of nickel(II) ion hydrolytic and phosphate-complex species present in solution at 25 and 287 °C as a function of sodium phosphate concentration (Ziemniak et al., 1989). It can be seen that phosphate-complexes are the major nickel(II) ion species in solution at phosphate concentrations $> 5 \text{ mmol}\cdot\text{kg}^{-1}$. Ziemniak et al. (1989) also determined that $\text{Ni}(\text{II})\text{-H}_2\text{PO}_4$ complexes predominate over the $\text{Ni}(\text{II})\text{-OH}$ complexes normally present at elevated temperatures, so much so that a sodium salt of the phosphato-complex can precipitate, rather than nickel oxide.

The major reaction product of aqueous sodium phosphate with nickel under boiler conditions has been shown to be sodium nickel hydroxyphosphate, $\text{Na}_2\text{Ni}(\text{OH})\text{PO}_4$ (Ziemniak and Opalka, 1988). The hideout and release behaviour of NiO is very similar to that observed for magnetite (Tremaine et al, 1992). Ziemniak and Opalka (1988) have reported solubility data and structural data for $\text{Na}_2\text{Ni}(\text{OH})\text{PO}_4$. Ziemniak and Opalka (1988) suggest that the transformation of nickel oxide to sodium nickel hydroxy-phosphate proceeds by the following reactions:



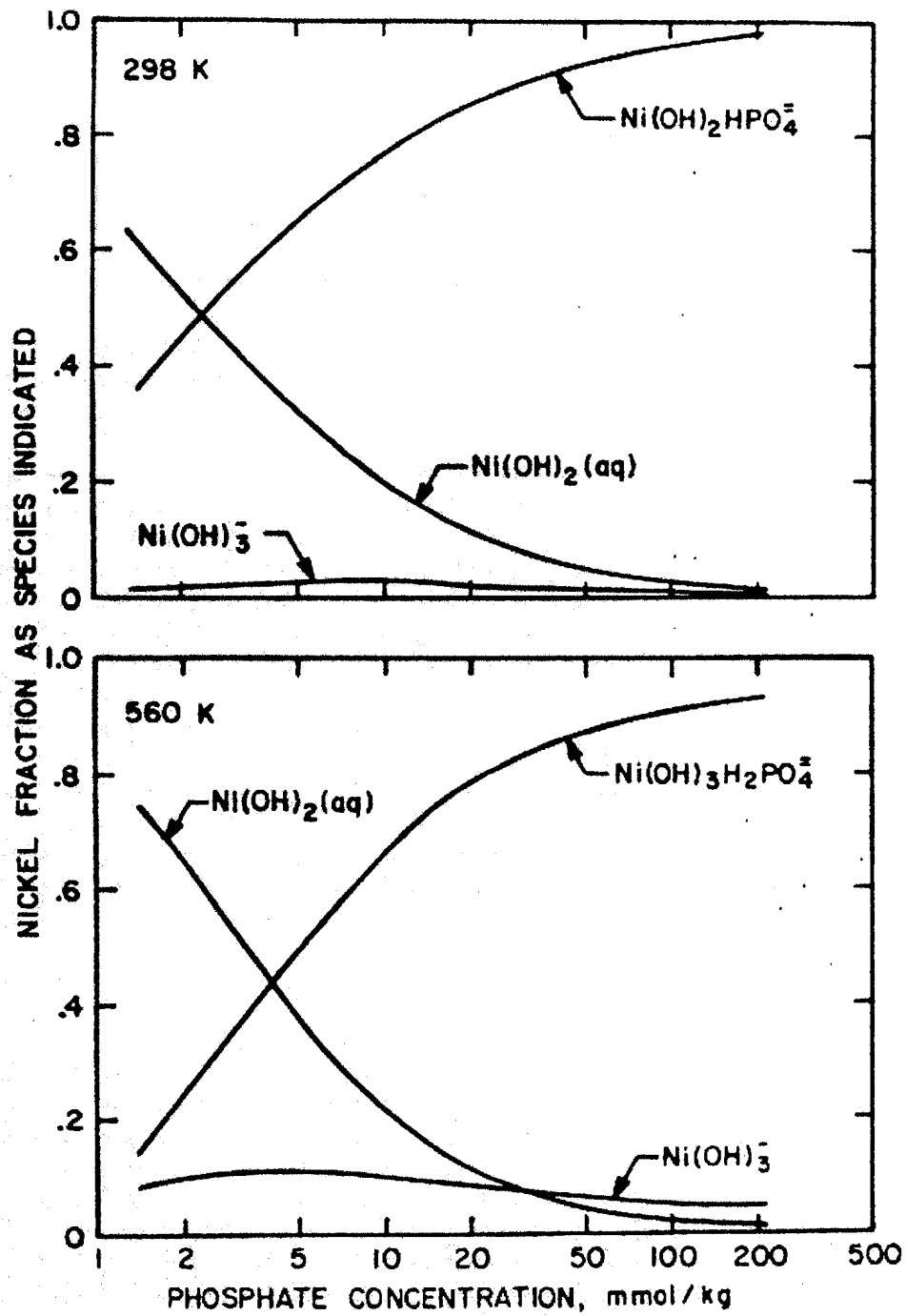
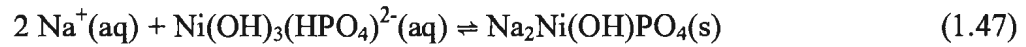
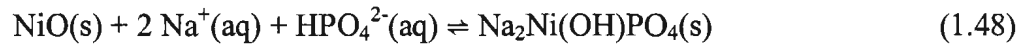


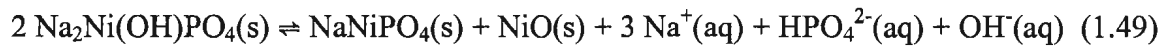
Figure 1.5: Distribution of nickel(II) ion complexes present in solution at 25 °C (298 K; top) and 287 °C (560 K; bottom) where Na/PO₄ = 2.3 (Ziemniak et al., 1989)



Combining Equations (1.45), (1.46), and (1.47) gives the solubility reaction for $\text{Na}_2\text{Ni}(\text{OH})\text{PO}_4(\text{s})$:



which is believed to be more soluble than SIHP and maricite under boiler conditions. In the flow experiments reported in the CEA Report (Tremaine et al., 1992), the dissolution process involves the formation of nickel phosphate, pyrophosphate, or possibly NaNiPO_4 (Tremaine et al. 1992) according to the following reaction:



and is schematically represented by Figure 1.6. Whether $\text{Na}_2\text{Ni}(\text{OH})\text{PO}_4(\text{s})$ can form on Inconel Alloy 800 during the chemistry excursions that occur during iron hideout reactions is unclear.

Sanz et al. (1999) have synthesized a mixed-anion phosphate, $\text{Na}_4\text{Ni}_5(\text{PO}_4)_2(\text{P}_2\text{O}_7)_2$, and reported a crystal structure for this compound along with X-ray diffraction results. Unlike the hydrothermally synthesized $\text{Na}_2\text{Ni}(\text{OH})\text{PO}_4$, this

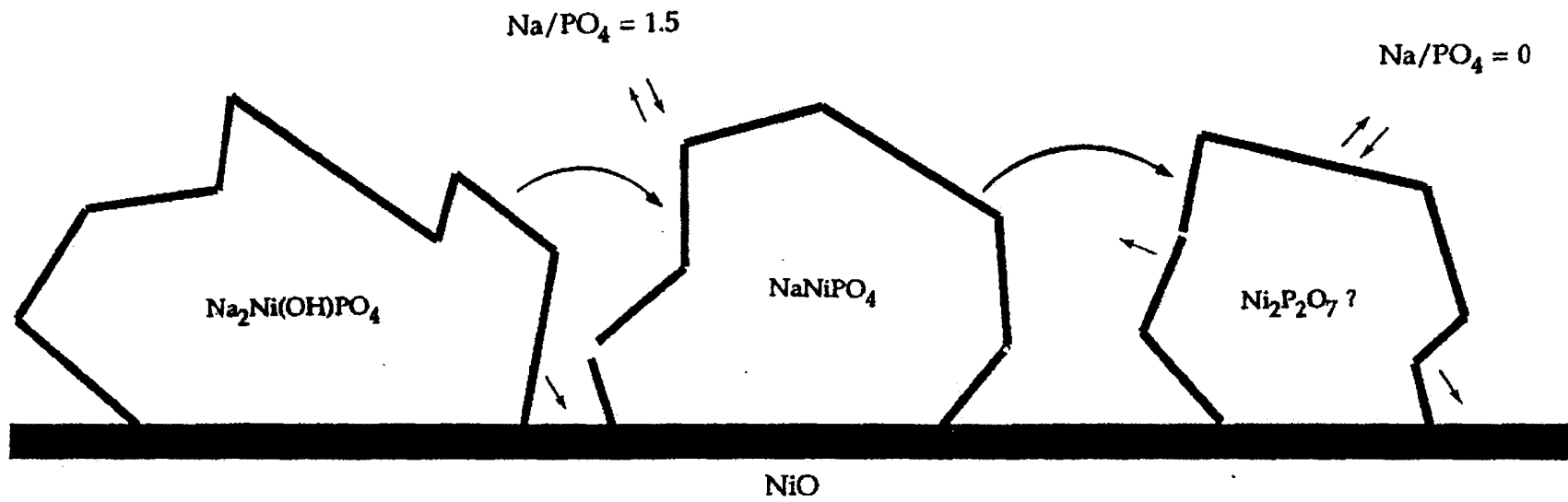


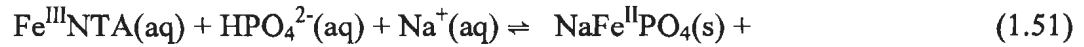
Figure 1.6: Possible process for dissolution of reaction product formed by NiO and aqueous sodium phosphate (Na/PO₄ = 2.5) (proposed by Tremaine et al. (1992))

compound was synthesized in a furnace at 900 °C. Another sodium-nickel-phosphate compound $\text{NaNi}_4(\text{PO}_4)_3$ was synthesized by Daidouh et al. (1999) using a sol-gel method in aqueous solutions at temperatures of 100-800 °C. A crystal structure and X-ray diffraction data for this compound were also reported. It remains unclear if either compound could be a possible corrosion product that forms in boilers under hydrothermal conditions.

1.8 Decomposition of NTA Complexes

The properties and applications of metal chelates have been widely studied and reported in the literature (Martell and Calvin, 1956; Bell, 1977; Chang et al., 1983, and references cited therein). Metal chelates can form in aqueous solutions by simple reactions (Bell, 1977). The most highly effective chelating ligands are ethylenediaminetetraacetic acid, EDTA, and nitrilotriacetic acid, NTA; and they form stable, water-soluble complexes with many metal ions. Chelating agents have primarily been used for the absorption or dissolution of metal oxides (Chang et al., 1983). The behavior and usefulness of metal chelate decomposition has also been studied as a means of synthesizing single crystals under hydrothermal conditions (Booy and Swaddle, 1978; Bridson et al., 1998).

Martell et al. (1975) reported that at high temperatures, NTA is not stable in aqueous solutions. NTA decomposes through a stepwise decarboxylation reaction. Equation (1.50) shows that NTA decomposes to give (a) *N*-methyliminodiacetic acid, (b) methylsarcosine and (c) trimethylamine (Martell et al., 1975):



decomposition products of $\text{HNTA}^{2-}(\text{aq})$

This method may provide a foundation for a desirable approach for the hydrothermal syntheses of other crystalline solids that have low oxidation states. This approach was also used in an attempt to synthesize SIHP, but no suitable oxidizing medium was found to produce the iron(III) complex (Bridson et al., 1998).

1.9 All-Volatile Treatment

The use of amines as additives for conditioning the secondary circuit of pressurized water reactors (PWR) is widespread. Ammonia or other amines can reduce the corrosion of materials in the steam cycle, particularly in regions subject to two-phase flow-accelerated corrosion (Bursik, 2002). In other words, amines are used in an effort to reduce corrosion product transport of iron species from tube components made of carbon steel, released due to flow-accelerated corrosion, into the steam generator. Consequences of corrosion deposits are drops in steam pressure and, in case of large deposits, a reduction in power output. Moreover, the production of corrosion products and their subsequent transport from the feedwater to the steam generator tubing has a detrimental influence on the risk of intergranular stress corrosion cracking (IGA/SCC) of Inconel Alloy 600 steam generator tubes. In addition to fouling and a decrease in thermal transfer, corrosion products may partially plug flow holes, leading to flow instability (Nordmann et al., 2001). Pessall et al. (1977) tested the corrosion resistance of Inconel

Alloy 600 and other alloys in sodium-phosphate at the Point Lepreau generating station. It was found to exhibit similar corrosion behaviour as Inconel Alloy 800 in high temperature phosphate solutions. Table 1.1 shows the results obtained by Pessall et al. (1977). It can be seen that the maximum corrosion weight loss observed in Inconel Alloy 600 in saturated phosphate solutions at $\text{Na}/\text{PO}_4 = 1.6$ was also observed in Incoloy Alloy 800, however Incoloy Alloy 800 appears less resistant than Inconel Alloy 600 in solutions with $\text{Na}/\text{PO}_4 \leq 1.6$. Observation of the areas of attack on Inconel Alloy 600 in boilers, have shown the presence of a greenish scale deposit. Pessall et al. (1977) reported that in their study, samples immersed in solutions with $\text{Na}/\text{PO}_4 \leq 1.6$, showed green scale deposits where the sample corroded. In contrast, yellow and yellow-green scale deposits were observed in $\text{Na}/\text{PO}_4 = 2$ solutions, and brown and grey-black deposits in $\text{Na}/\text{PO}_4 > 2.3$ solutions. All scale deposits consisted of Na, P, Ni, Fe, and Cr, and that the green and yellow scales contained higher concentrations of Fe and Ni. The precipitation of phosphate salts and their reaction with the metal in the boilers may account for the observed localized high corrosion rates. Despite these findings, Point Lepreau generating station has been operating with phosphate treatment for 20 years, apparently without corrosion, but it is unclear if any corrosion problems will be encountered during the changeover.

The initial group of plants that switched from phosphate to AVT had many problems. Changing to AVT introduces a whole new set of operating parameters and brings up the question as to whether or not the system should be cleaned before a changeover and, if so, how thoroughly.

Table 1.1: Corrosion rates of Inconel Alloy 600 in high temperature phosphate solutions compared with those of other Alloys (Pessall et al., 1977)

Test Environment				Corrosion Wt Loss Based on Parabolic Relationship (mg/dm ² in 1 yr)				
Na/P (r)	Concentration (Molality)	Temp. (C)	Maximum Exposure Time (Hour)	Inconel ⁽¹⁾ 600	Inconel ⁽²⁾ 690	Incoloy ⁽³⁾ 800	304 SS ⁽⁴⁾	Croloy ⁽⁵⁾
1.35	6.0	325	312	680	1600	620	2139	40000
1.6	6.0	325	480	2800	5600	6400	5989	—
2.0	5.0	325	504	510	600	600	599	—
2.2	0.18	325	504	86	43	43	257	1600
2.3	5.0	325	451	470	471	1200	11123	6800
1.6	6.0	275	1344	2400	—	—	3000	—
2.3	5.0	275	1226	86	150	260	—	—
2.3	0.4	275	1560	540	—	340	—	—
2.6	0.15	275	1176	43	1000	100	—	—

(1) Ni-15.4Cr-7.92Fe-0.22Si-0.17Mn-0.15Cu-0.06C-0.007S

(2) Ni-29.82Cr-9.38Fe-0.15Si-0.17Mn-0.03C-0.007S

(3) Fe-21.81Cr-31.55Ni-0.32Si-0.81Mn-0.37Ti-0.28Al-0.23Cu-0.03C-0.007S

(4) Fe-18.22Cr-8.93Ni-0.49Si-1.89Mn-0.19Cu-0.06C-0.005S-0.022P-0.29Mo-0.11Co

(5) Fe-2.28Cr-0.89Mo-0.25Si-0.42Mn-0.1C-0.009P

1.10 Project Objectives

The objectives of this project were two-fold; (i) syntheses of hydrothermal reaction products that can form under boiler conditions and (ii) kinetic and solubility studies on $\text{Na}_2\text{Ni}(\text{OH})\text{PO}_4$ to develop a chemical equilibrium model for the major nickel-sodium-phosphate reaction product.

The first compounds to be synthesized were from the sodium-iron-phosphate system. One objective was to prove that the maricite synthesis previously reported by Quinlan (1996) is reproducible and is a reliable hydrothermal means of synthesizing the iron(II) reaction product. Another was to develop hydrothermal synthetic methods for producing a reliable means of obtaining crystalline sodium iron(III) hydroxyphosphate, SIHP.

The second synthetic objective was to determine whether ammonium-iron-phosphate compounds could be produced under all-volatile amine treatment boiler conditions. Boudin and Lii (1998) showed that a mixed-valence iron phosphate, $(\text{NH}_4)\text{Fe}^{\text{II}}\text{Fe}^{\text{III}}(\text{PO}_4)_2$, can be synthesized by a hydrothermal method at 500 °C using a sealed gold ampoule. Our experiments were to determine whether it would form under boiler conditions, to synthesize it using a more simple method, and to identify any other ammonium-iron-phosphate compounds that can form hydrothermally.

The final system that was studied was the sodium-nickel-phosphate system. Sodium nickel hydroxy-phosphate, $\text{Na}_2\text{Ni}(\text{OH})\text{PO}_4$, (“SNHP”), is known to form under boiler conditions by the reaction of NiO with aqueous sodium phosphate; thus one objective was to synthesize a pure sample for calorimetric measurements. The initial

route that was taken to synthesize SNHP was to use the homogeneous thermal decomposition of $\text{H}^+[\text{NiNTA}^-]$ as a nickel source instead of NiO, in a process similar to that used for maricite by Quinlan (1996).

Another objective of this study was to undertake solubility measurements on $\text{Na}_2\text{Ni}(\text{OH})\text{PO}_4$, in order to develop a chemical equilibrium model for the sodium-nickel-phosphate system. Kinetic and solubility experiments were conducted at elevated temperatures using excess NiO and aqueous sodium-phosphate. Solution samples were taken from the system at each temperature increment and analyzed for total sodium and phosphorus. The results were used to derive thermodynamic data for SNHP, which was added to the database for “hideout” reactions that take place between transition metals and aqueous sodium phosphate under steam-generator conditions.

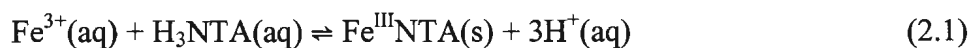
The experimental designs used throughout this project to meet the above objectives are listed in the following chapter. The remaining chapters of this thesis describe the results obtained from our studies and the conclusions that can be made from this project as a whole.

2.0 EXPERIMENTAL

2.1 Chemicals and Materials

The sodium-phosphate solutions were prepared from reagent grade Na_2HPO_4 (Aldrich, ACS Reagent Grade, 99 %), NaH_2PO_4 (Aldrich, 99 %), and NaOH (Fisher Scientific, 50 % w/w solution) with Nanopure water (resistivity > 18 $\text{M}\Omega\text{ cm}$). The ammonium-phosphate solutions were prepared from reagent grade $(\text{NH}_4)_2\text{HPO}_4$ (Aldrich, 99 %), $(\text{NH}_4)\text{H}_2\text{PO}_4$ (Aldrich, ACS Reagent Grade, 98+ %), and NaOH solution with Nanopure water. The concentrations of the sodium- and ammonium-phosphate solutions were determined by mass (i.e. $\text{mol}\cdot\text{kg}^{-1}$).

$\text{Fe}^{\text{III}}_2\text{O}_3$ (Aldrich, 99+ %), $\text{Fe}_2(\text{C}_4\text{H}_4\text{O}_6)_3$ (Sigma, 19.0-21.0 % Fe), $\text{Fe}^{\text{III}}_2(\text{C}_2\text{O}_4)_3\cdot 5\text{H}_2\text{O}$ (BDH reagent, no purity given), and $(\text{NH}_4)\text{Fe}^{\text{III}}(\text{SO}_4)_2\cdot 12\text{H}_2\text{O}$ (BDH, 99.0-102.0 %) were the iron sources used in this study. The $\text{Fe}^{\text{III}}\text{NTA}$ complex used in this study was prepared according to the following procedure reported by Booy and Swaddle (1978). Ammonium ferric sulphate (20 g), $(\text{NH}_4)\text{Fe}^{\text{III}}(\text{SO}_4)_2\cdot 12\text{H}_2\text{O}$ and nitrilotriacetic acid (8 g), H_3NTA were added to 400 mL of deionized water and brought to a boil for one hour. The following reaction occurred:



The resulting mixture was suction filtered and washed with deionized water. The yellow-

green Fe^{III}NTA complex isolated was transferred to a Petri dish and allowed to air dry overnight.

The nickel source in this study was NiO (Fisher Scientific reagent grade). Ni(OH)₂ (Aldrich, nickel content ~61 %) was also used but only as a precursor in the synthesis of another nickel starting material used in this study. H⁺[NiNTA⁻] was prepared much in the same way as Fe^{III}NTA by boiling 3-5 g of nickel hydroxide, Ni(OH)₂ with 9 g of nitrilotriacetic acid (Aldrich, 99 %), H₃NTA, in 400 mL of deionized water for one hour according to the following reaction:



The resulting purple-blue solid was suction filtered, washed with cold deionized water and dried in air overnight.

2.2 Apparatus

2.2.1 Teflon-Lined Filtration Cells

Parr 4744 general purpose bombs were used to synthesise the solids at high temperature, with the modifications to the vessels previously made by Quinlan (1996). These are 45 mL 316 stainless steel pressure vessels with Teflon liners that were widened to allow for the insertion of an inner Teflon cup with a removable cap containing a stainless steel filter; dividing the vessel into separate upper and lower compartments. The

filters, for use at high temperatures, were purchased from Small Parts Inc. in Miami Lakes Florida and were made from 316 stainless steel 325 mesh.

A schematic diagram of this vessel is shown in Figure 2.1. The design of the vessel allows *in situ* isolation of the solid reaction products from the aqueous phase by simply inverting the cell while in a high-temperature oven. When the vessel is first placed in the high temperature oven, the solid starting materials are placed in the filter separating them from the aqueous starting materials in the bottom of the Teflon liner. Once the vessel is inverted in the oven, the starting materials are allowed to mix, and after the reaction has come to completion, re-inverting the vessel permits the liquid to drain through the stainless steel filter, trapping the solid reaction products in the filter. Figure 2.2 is a diagram of this filtration step.

In addition to the filtration step, in order to avoid refluxing the filtrate and re-dissolving the reaction product, the cell was cooled to room temperature by placing it on an aluminium plate in cold flowing water so that the lower compartment of the cell was colder than the top during the cooling process.

2.2.2 Stirred Reaction Vessel

For the kinetic and solubility experiments, a 450 mL Model 4562 Parr Stirred Mini-Reactor was used. The reaction vessel used previously in our lab was made of Hastelloy C, an alloy with high nickel content. Thus it could not be used in our experiments because the solubility equilibria being studied involve nickel-containing phases. Any corrosion of the Hastelloy C vessel would give unreliable kinetic and

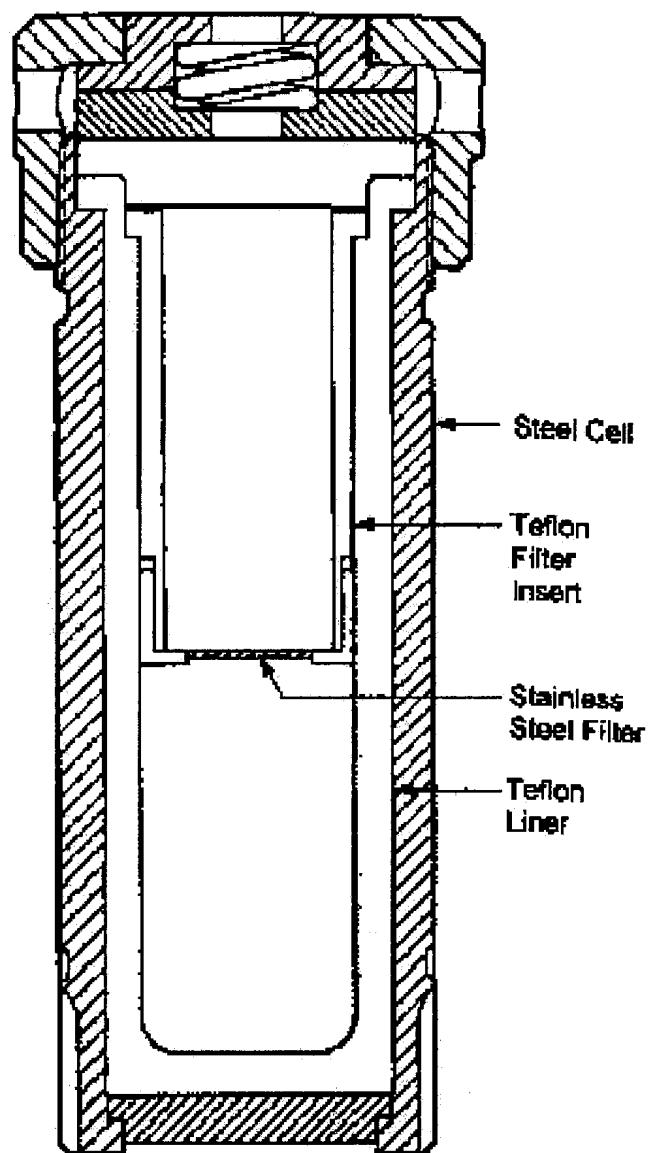


Figure 2.1 Modified Parr 4744 reaction vessel used for hydrothermal synthesis and *in situ* filtration (Bridson, 1998)

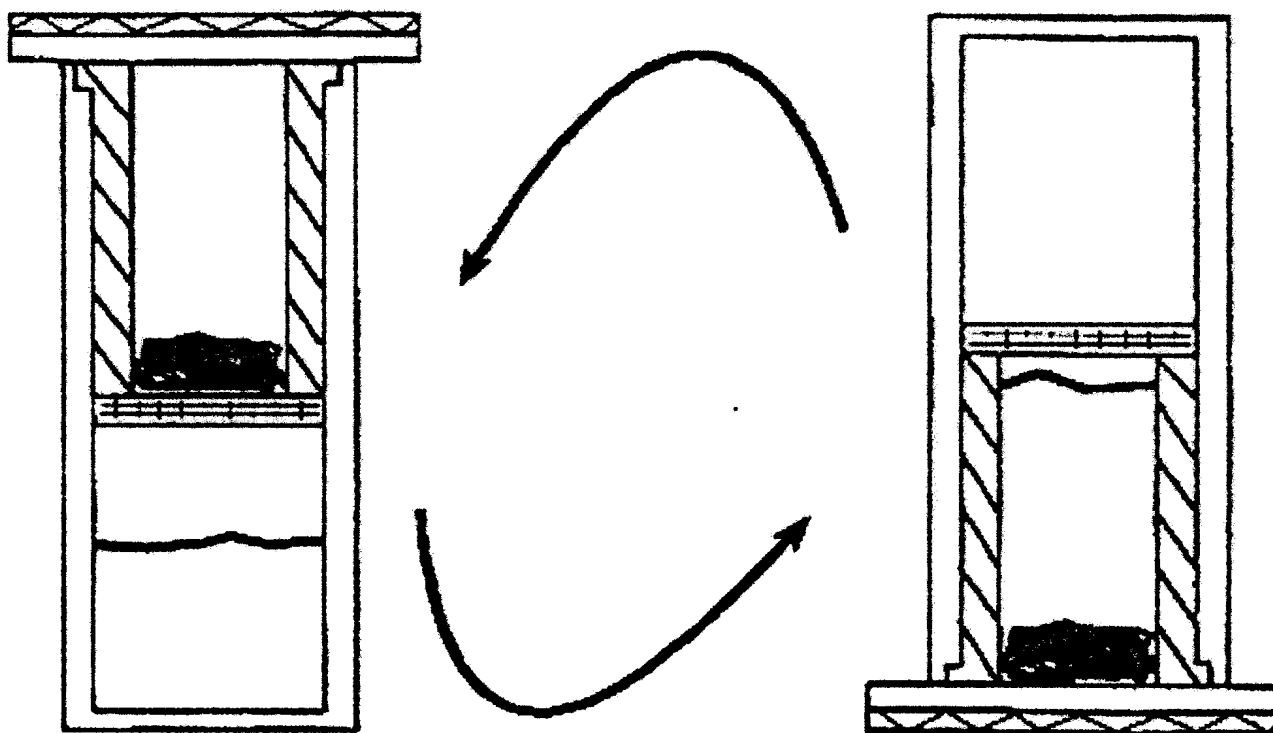


Figure 2.2: 45 mL Teflon lined cells. On the left, vessels before the reaction, and after the filtration. On the right, vessels during the reaction. (Quinlan, 1996)

solubility results. A new zirconium vessel and stirrer head was purchased for this study.

A schematic diagram of the reactor system is presented in Figure 2.3. The Parr 4562 Mini-Reactor is rated for a maximum pressure of 1600 psi at 300 °C. The Parr 4843 temperature controller has a microprocessor-based control module, which provided full PID control with adjustable tuning parameters, with an operating range of 0 to 750 °C. The system is accurate to ± 2 °C and is equipped with two high temperature cut-offs. If the temperature exceeds the set limit, an alarm light will appear, the lockout relay will be tripped, and power to the heater around the vessel will be shut off.

Previously, Quinlan (1996) had made modifications to the Hastelloy C vessel which increased its suitability for his project. Several of the same modifications were made to the new zirconium reactor. A wider and lower impeller was added to provide increased agitation, which was intended to reduce deposition of solids. The reactor head was equipped with a gold lined rupture disk, which is less vulnerable to corrosion and thus reduces the chance of premature rupture. Before kinetic and solubility experiments, the zirconium vessel was treated with dilute NaOH to form a protective oxide layer on the inside of the cylinder and the stirrer head. A condenser was attached to the autoclave head just before the liquid sampling valve to allow sampling at high temperature. It consisted of a valve attached to a length of 0.125 inch stainless steel tube inside a 0.25 inch copper tube, and was cooled by cold flowing water. A filter was connected to the end of the liquid sampling tube inside the vessel which consisted of several layers of 325 mesh 316 stainless steel filters inside a modified 0.25 inch Swagelok union. Quinlan (1996) showed that this modification should prevent any solid from clogging up the

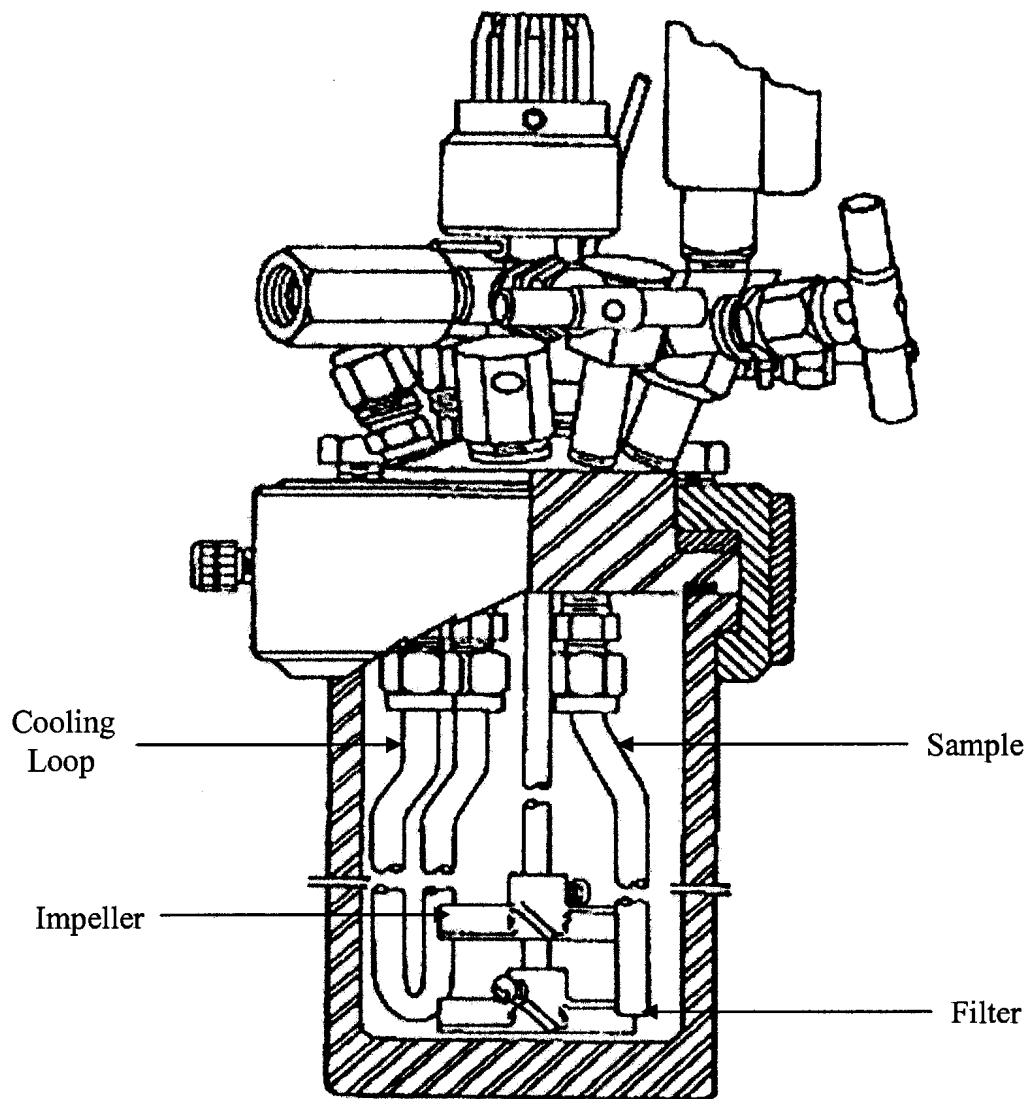


Figure 2.3: Schematic diagram of Parr 450 mL stirred reaction vessel. (Quinlan, 1996)

liquid sampling tube and the condenser. However, some carry-over of solid material was frequently encountered.

Another addition to the system was a stainless steel mesh basket. It was connected between the two ends of the cooling loop and its purpose was to isolate any reaction product during the kinetic and solubility experiments for analysis.

2.3 Analytical Methods

2.3.1 Powder X-Ray Diffraction

X-Ray diffraction studies of solid reaction products were performed using a Rigaku RU-200 X-ray diffractometer (XRD) which was operated at 40 kV and 180 mA. It contained a 12 kW rotating anode Cu K α X-ray source, that scanned the sample at 10° (2 θ) per minute, and a diffracted beam monochromator. Samples for analysis were prepared by grinding them to a fine powder (<10 μ m) with a mortar and pestle, to which methanol was added, and the resulting mixture was transferred to a slide via a disposable pipette and allowed to air dry for 15 minutes. A current software version of the JCPDS database (i.e. ICDD; International Center for Diffraction Database), equipped with the MDI Jade+ search-match algorithm, was used to identify the XRD powder patterns from the samples. X-Ray diffraction results of synthesized reaction products are listed in Appendix I.

2.3.2 Single Crystal X-Ray Diffraction

Dr. John Bridson and Mr. David Miller at the Department of Chemistry/MUN analyzed the structure of the single crystal isolated in this study with a Rigaku AFC6S diffractometer and a VAX3100 workstation and the teXsan crystallographic software package (Molecular Structure Corporation Inc.). A more detailed report of the analysis can be found in Appendix II.

2.3.3 ICP Emission Spectroscopy

During the kinetic and solubility experiments, liquid samples were taken from the autoclave at regular intervals and diluted by mass in order to obtain sodium and phosphorus concentrations between 50-200 ppm. The diluted samples were analyzed using a TJA Iris HR ICP-OE spectrometer with a TJA 300 sample changer, at the Department of Mines and Energy by Mr. Chris Finch. The spectrometer was controlled by ThermoSpec software.

To calibrate the instrument a blank solution was run that contained 0 ppm sodium and phosphorus followed by a standard solution of 250 ppm sodium and phosphorus. Two samples of deionized water were then run for baseline measurement, then another 125 ppm standard solution. Each sample was flushed through the sample line for a minute to remove any possible contaminants before the concentrations of the sample was measured, and the 125 ppm standard was re-run after every ten samples to ensure the instrument was giving accurate readings. Included in each batch of unknown samples were four known standard solutions which provided a second check for instrument

accuracy. The results showed that the ICP ES measurements were within 2.4 % of the expected phosphorus concentrations, and 7 % of the expected sodium concentrations. Each original sample was diluted to give two aliquots within the range 50-200 ppm in Na and P, and agreement was within ± 3 %.

The results that were received from ICP-ES analysis were the elemental concentrations (ppm) of the diluted samples. Using a Microsoft Excel spreadsheet and the mass dilution factors of each diluted sample, the sodium and phosphorus molality concentrations of each original sample taken from the stirred reactor were calculated.

2.3.4 Electron Microscopy

From the synthesis experiments, the solid reaction products of specific interest to this study were analyzed by scanning electron microscopy (SEM) at an accelerating voltage of 20 kV in a Hitachi S570 SEM equipped with a Tracor Northern 5500 energy-dispersive X-ray analyzer and a Microtrace Model 70152 silicon X-ray spectrometer, located in the Department of Biology/MUN. Detector/sample positioning gave an effective takeoff angle of 30° and SEM images were recorded on Polaroid Type 655 Positive/Negative film. Samples were placed on double sided sticky tabs on aluminium stubs and carbon coated in a Denton 502A High Vacuum Evaporator before SEM analysis.

2.4 Synthesis and Characterization of Hideout Reaction Products

2.4.1 Experimental Design

In the sodium-iron-phosphate study conducted previously in our laboratory (Quinlan, 1996; Bridson et al., 1998), the Parr 4744 reaction vessel was modified in order to isolate SIHP from the reaction mixture because other workers have reported (Taylor et al., 1979; Broadbent et al., 1978; Tremaine et al., 1993) that it is unstable at temperatures lower than 180 °C in the presence of water. The experimental design of the reaction vessel thus prevented the reaction product from coming in contact with liquid water during the isolation step and also prevented dehydration of the equilibrium phase. The same experimental design was applied to all the experiments conducted throughout this study.

The experimental procedure is as follows. The sodium-phosphate or ammonium-phosphate solution was initially placed in the Teflon liner. Because of the thermal expansion effect, the vessels were not overloaded with solution in order to prevent a pressure build up. The solid starting materials were added once the Teflon filter cup was positioned above the level of the solution and a Teflon lid was put into place. The Teflon assembly was then placed inside the stainless steel pressure vessel to which a corrosion disc and a rupture disc were added, followed by a stainless steel pressure vessel lid. The lid was hand tightened and tightened a further 1/8 revolution by a specially designed pressure vessel wrench. The vessel was then placed in a high temperature oven at either 200 °C or 250 °C and inverted. As seen in Figure 2.2, the solution passes through the filter and is allowed to react with the solid starting materials once inverted. The vessels

remained in the oven for 5 days - 4 weeks, and were shaken periodically. Before being removed from the oven, the vessels were set upright to filter any reaction product from solution. This step was done in the oven to prevent hydration of solid reaction products during cooling.

After filtering for a day, the vessels were carefully removed from the oven. They were placed on aluminium plates being cooled by cold running water in a sink. This prevented the solution in the lower part of the Teflon vessel from refluxing and in turn preventing any solid reaction product in the filter from coming in contact with condensation and possibly re-dissolve. Solid reaction products were also prevented from dehydration due to the presence of unsaturated moisture above the filter. After cooling to room temperature (approx. 2 hrs), the pressure vessels were opened and the resulting solids and solutions were collected. The solids recovered from the filter were analyzed by X-ray diffraction, and samples of further interest were analyzed by SEM.

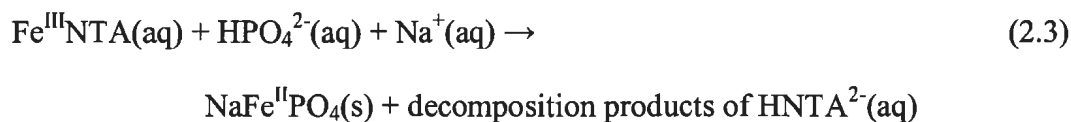
When the solid and aqueous starting materials were originally placed in the reaction vessel at room temperature, they were separated thus preventing any reaction at non-boiler conditions. The solid metal-NTA complexes and other starting reactants were placed on the screen above the solutions, and only when the vessel had reached the desired boiler temperature, was the vessel inverted, allowing the contents to mix. Any reaction product eventually isolated would have formed at the boiler water temperature and not at room temperature. This gives us a more accurate account of what corrosion products can form at the higher temperatures at which power stations operate.

Several solid starting materials were used as a source of iron, including hematite, ferric tartrate, ferric oxalate, and iron nitriloacetate ($\text{Fe}^{\text{III}}\text{NTA}$). Nickel oxide and nickel nitriloacetate ($\text{H}^+[\text{NiNTA}^-]$) were the two different solid starting materials used as a source of nickel. The following sections summarize the synthetic experiments carried out with the above mentioned solids.

2.4.2 Synthesis of Maricite ($\text{NaFe}^{\text{II}}\text{PO}_4$)

Quinlan (1996) synthesized single crystals of maricite using an adaptation of the procedure reported by Booy and Swaddle (1978) for synthesizing magnetite crystals. The reducing conditions created by the thermal decomposition of aqueous $\text{Fe}^{\text{III}}\text{NTA}$ in the presence of sodium phosphate solution provided the right conditions for homogeneous nucleation of maricite. The purpose of synthesizing maricite in this study was to determine whether Quinlan's synthesis is reproducible.

Maricite was synthesized by the same recipe used by Quinlan (1996), in that 0.6 g of $\text{Fe}^{\text{III}}\text{NTA}$ was reacted with 10 mL of $0.6 \text{ mol}\cdot\text{kg}^{-1}$ sodium phosphate solution with a Na/PO_4 mole ratio of 2.15 at 200°C , according to the following reaction:



Two additional experiments were attempted with $\text{Fe}^{\text{III}}\text{NTA}$ in order to observe if it is possible to synthesis maricite from an initial sodium phosphate solution with an

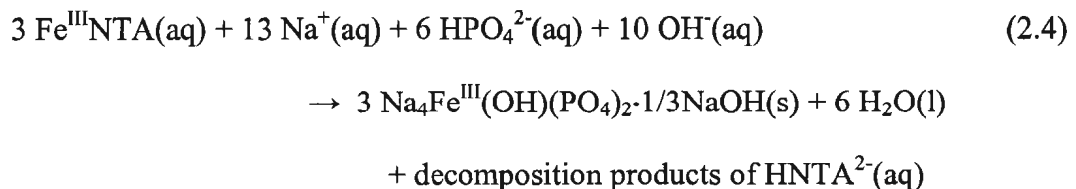
identical Na/PO₄ mole ratio as that of the solid maricite (i.e. 1:1) at 200 °C. These runs were unsuccessful in producing maricite, the reaction vessel contained unreacted starting materials.

2.4.3 Syntheses of Sodium Iron Hydroxy Phosphate (“SIHP”)

2.4.3.1 Iron Nitriloacetate (Fe^{III}NTA) Experiments

Quinlan (1996) obtained SIHP by three different synthetic routes. Samples of SIHP were produced by reacting (i) iron phosphate and aqueous sodium phosphate (Na/PO₄ = 2.15), (ii) magnetite and aqueous sodium phosphate (Na/PO₄ = 2.15), and (iii) hematite and aqueous sodium phosphate (Na/PO₄ = 2.5), all at 250 °C for three weeks. Quinlan also attempted to synthesis SIHP by thermally decomposing the Fe^{III}NTA complex in the presence of an oxidizing agent, to create a more suitable environment for synthesizing the iron(III) reaction product. Both CuO and NaNO₃ were used as possible oxidizing agents for the reaction but the experiments were unsuccessful in producing SIHP.

In principle, SIHP could be synthesised according to the following reaction with Fe^{III}NTA as the iron source:

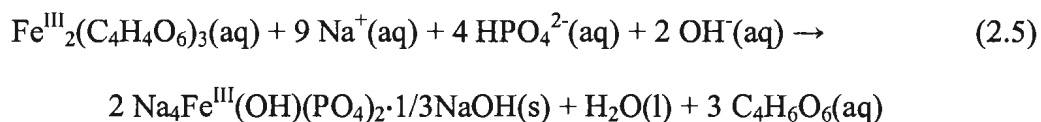


In our Fe^{III}NTA experiments, instead of using oxidizing agents, the sodium-phosphate mole ratio was increased from 2.15 to 4.0 in order to push the reaction stoichiometry towards producing the high sodium-phosphate mole ratio observed in SIHP.

Fe^{III}NTA was used as a starting material in 11 runs with sodium-phosphate mole ratios of 4.0-8.0, and introduced as a solid. The initial masses of Fe^{III}NTA were from 0.16-0.85 g, and the initial concentrations of phosphate were 0.6-1.5 mol·kg⁻¹. Runs with Fe^{III}NTA were maintained at 200 or 250 °C for 5-14 days with periodic shaking.

2.4.3.2 Iron Tartrate (Fe^{III}₂(C₄H₄O₆)₃) Experiments

It was mentioned in Section 2.4.3.1, that reactions involving the hydrothermal decomposition of Fe^{III}NTA in the presence of oxidizing agents have been attempted, with no success in synthesizing SIHP. The next step in our study was to use an iron chelate source that yielded more oxidizing conditions on decomposition. It was thought that iron tartrate, Fe^{III}₂(C₄H₄O₆)₃, might be a suitably oxidizing chelate, according to the following reaction:

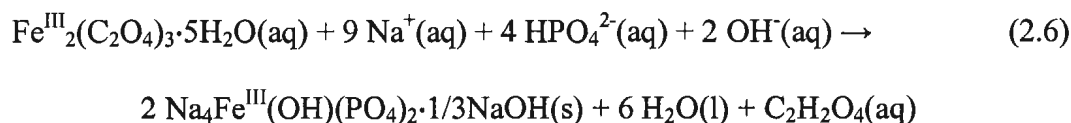


Fe^{III}₂(C₄H₄O₆)₃ was used as a starting material in 8 runs with sodium-phosphate mole ratios of 2.15-2.8, and introduced as a solid. The initial masses of iron tartrate were from 0.39-0.50 g, and the initial concentrations of phosphate were

0.6-1.5 mol·kg⁻¹. Runs with Fe^{III}₂(C₄H₄O₆)₃ were maintained at 200 or 250 °C for 4-22 days with periodic shaking.

2.4.3.3 Iron Oxalate (Fe^{III}₂(C₂O₄)₃·5H₂O) Experiments

Iron oxalate was also used as a starting material in order to create a more oxidizing environment for the synthesis of SIHP according to the following reaction:



Fe^{III}₂(C₂O₄)₃·5H₂O was used as a solid starting material in 4 runs with sodium-phosphate mole ratios of 2.15-2.8. The initial masses of iron oxalate were from 0.37-0.41 g, and the initial concentrations of phosphate were 0.6-1.0 mol·kg⁻¹. Runs with Fe^{III}₂(C₂O₄)₃·5H₂O were maintained at 250 °C, for 8 days with periodic shaking.

2.4.4 Synthesis of Ammonium Iron(II,III) Phosphate ((NH₄)Fe^{II}Fe^{III}(PO₄)₂)

2.4.4.1 Hematite Experiments

The first example of a mixed-valence ammonium iron phosphate was synthesised by Boudin and Lii (1998), and was obtained at very high temperature and high pressure. This phosphate, (NH₄)Fe^{II}Fe^{III}(PO₄)₂, was initially synthesized by heating a mixture of (NH₄)H₂PO₄ (0.132 g), (NH₄)₂HPO₄ (0.152 g), Fe^{III}₂O₃ (0.032 g), and water (0.3 mL) in a sealed gold ampule at 500 °C and an estimated pressure of 32000 psi for 24 hours, which

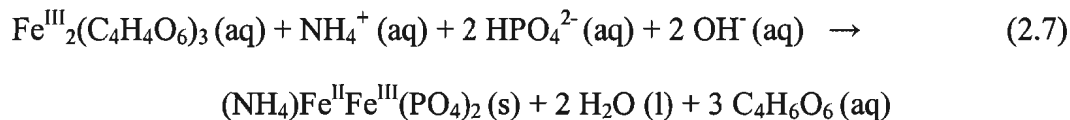
was then cooled at 3 °C/h to 250 °C and quenched to room temperature by removing the autoclave from the furnace. This gave a mixture of black crystals of $(\text{NH}_4)\text{Fe}^{\text{II}}\text{Fe}^{\text{III}}(\text{PO}_4)_2$ and colorless thin plates. However, hydrothermal treatment of $(\text{NH}_4)\text{H}_2\text{PO}_4$ (0.460 g), $\text{Fe}^{\text{III}}_2\text{O}_3$ (0.032 g), $\text{Fe}^{\text{II}}\text{O}$ (0.0288 g), and water (0.65 mL) in a gold ampule under the same reactions conditions gave a pure product of $(\text{NH}_4)\text{Fe}^{\text{II}}\text{Fe}^{\text{III}}(\text{PO}_4)_2$. Boudin and Lii (1998) obtained a single crystal XRD structure, however they did not report any powder XRD data for $(\text{NH}_4)\text{Fe}^{\text{II}}\text{Fe}^{\text{III}}(\text{PO}_4)_2$. Though, through email contact with Dr. Lii, the complete single crystal XRD data set was provided which was used to generate a powder XRD spectrum using the SHELXTL software program. No solubility data or thermodynamic constants were reported however. In this study, attempts to reproduce ammonium iron phosphate from the hydrothermal methods used in the lab, using roughly the same starting materials as that of Boudin and Lii's paper. The purpose was to see if the mixed valence compound would form under boiler conditions and whether the synthesis could be done using a more simple method.

$(\text{NH}_4)\text{H}_2\text{PO}_4$ (0.27-0.32 g), $(\text{NH}_4)\text{HPO}_4$ (0.30-0.33 g), and $\text{Fe}^{\text{III}}_2\text{O}_3$ (0.06-0.08 g) were used as starting materials in 6 runs with varying amounts of deionized water from 2-10 mL. Syntheses were carried out at 200 °C or 250 °C for 5-7 days with periodic shaking.

2.4.4.2 Iron Tartrate Experiments

For the same reasons as in the SIHP experiments, similar syntheses to Boudin and Lii (1998) were conducted with an alternate iron source, iron tartrate.

Syntheses were attempted using ammonium phosphate solutions and iron tartrate, according to the following reaction:



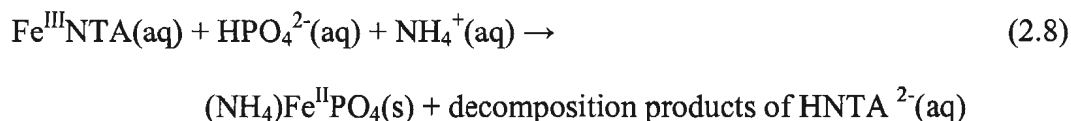
$(\text{NH}_4)\text{H}_2\text{PO}_4$ (0.29-0.47 g), $(\text{NH}_4)_2\text{HPO}_4$ (0.29-0.31 g), and $\text{Fe}^{\text{III}}_2(\text{C}_4\text{H}_4\text{O}_6)_3$ (0.07-0.08 g) were used as starting materials in 4 runs with varying amounts of deionized water from 2-10 mL. Runs were maintained at 200 °C for 7 days with periodic shaking.

$\text{Fe}^{\text{III}}_2(\text{C}_4\text{H}_4\text{O}_6)_3$ was used as a starting material in 7 runs with ammonium phosphate mole ratios of 1.00-2.8. The initial masses of iron tartrate were from 0.39-0.41 g and the initial concentrations of phosphate were 0.6-0.7 mol·kg⁻¹. Runs with $\text{Fe}^{\text{III}}_2(\text{C}_4\text{H}_4\text{O}_6)_3$ were maintained at 200 or 250 °C for 4-8 days with periodic shaking.

2.4.5 Synthesis of Ammonium Iron Phosphate Hydrate $((\text{NH}_4)\text{Fe}^{\text{II}}(\text{PO}_4)\cdot\text{H}_2\text{O})$

2.4.5.1 Iron Nitriloacetate Experiments

Quinlan (1996) synthesized maricite, $\text{NaFe}^{\text{II}}\text{PO}_4$, by thermally decomposing $\text{Fe}^{\text{III}}\text{NTA}$ in the presence of sodium phosphate solution. Experiments were conducted by the same method using ammonium phosphate solution instead; in order to explore the possibility of synthesizing an ammonium analogue of maricite under boiler conditions, and obtain a pure compound for calorimetry. The reaction was thought to proceed as follows:



$\text{Fe}^{\text{III}}\text{NTA}$ was used as a starting material in 13 runs with ammonium-phosphate mole ratios of 1.0-2.8. The initial masses of iron nitriloacetate were from 0.59-0.75 g, and the initial concentrations of phosphate were 0.6-0.9 mol·kg⁻¹. Runs with $\text{Fe}^{\text{III}}\text{NTA}$ were maintained at 200 or 250 °C, for 6-9 days with periodic shaking.

2.4.6 Syntheses of $\text{Na}_2\text{Ni}(\text{OH})\text{PO}_4$ (“SNHP”)

2.4.6.1 Nickel Oxide (NiO) Experiments

Ziemniak and Opalka (1988) have shown that NiO transforms to a sodium nickel hydroxy phosphate compound in concentrated sodium phosphate solutions at elevated temperatures. The following reaction was used for the synthesis of SNHP from nickel oxide using our experimental design:

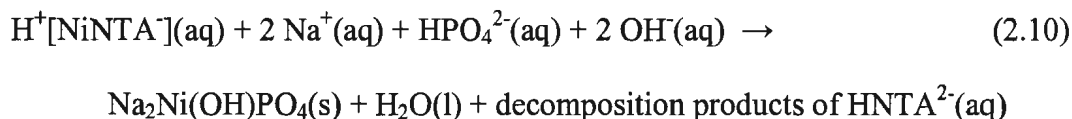


Nickel oxide was used as a starting material in 2 runs, with a sodium-phosphate mole ratios of 2.5. The initial masses of nickel oxide were 0.56 and 0.69 g and the concentration of the phosphate solution were 1.5 mol·kg⁻¹. Both runs were maintained at 250 °C for 1 week with periodic shaking.

2.4.6.2 Nickel Nitriloacetate ($\text{H}^+[\text{NiNTA}^-]$) Experiments

An alternate nickel source used in this study was nickel nitriloacetate. The rationale for using $\text{H}^+[\text{NiNTA}^-]$ in our experiments was to have a route where Ni(II) was slowly released into the system and possibly form single SNHP crystals, much like the studies with $\text{Fe}^{\text{III}}\text{NTA}$.

Twenty-eight experiments were done with $\text{H}^+[\text{NiNTA}^-]$ as a starting material according to the following reaction:



The sodium-phosphate mole ratios ranged from 2.0-4.0. The initial masses of nickel nitriloacetate were from 0.50-1.07 g, and the initial concentrations of phosphate were 0.6-1.5 $\text{mol}\cdot\text{kg}^{-1}$. Runs with $\text{H}^+[\text{NiNTA}^-]$ were maintained at 200 or 250 °C for 4-14 days with periodic shaking.

2.5 Solubility Measurements on Sodium Nickel Hydroxy Phosphate in the Stirred Reaction Vessel

2.5.1 Kinetics

Eight kinetic experiments were attempted in order to determine the time required for mixtures of SNHP and NiO to reach equilibrium with aqueous sodium phosphate. Four of these were stopped due to leaks or clogging of the filter below the sample line.

All runs lasted up to 10 days at a time. In two separate runs, the autoclave temperature was raised to 250 °C, and the kinetics was determined approaching equilibrium from supersaturated conditions by initiating the precipitation reaction. In the other two runs, the autoclave temperature was brought up to 275 °C, allowed to reach equilibrium for 4 days and then quickly lowered to 250 °C, in order to determine the kinetics approaching equilibrium from unsaturated conditions by initiating the re-dissolution reaction. The purpose behind the two different sets of runs was to establish that the reaction was reversible.

The experiments to determine the kinetics of SNHP formation and re-dissolution at 250 °C respectively proceeded as follows. An excess of 25 g of nickel oxide was placed in the zirconium cylinder with 240-250 mL of 1.5 mol·kg⁻¹ phosphate solution with a sodium-phosphate mole ratio of 2.5. To ensure that all aqueous nickel species are in equilibrium with the nickel(II) oxide, an excess of nickel oxide was used in each experiment. The steam tables of Haar et al. (1984) were used to calculate the volume of the solution after thermal expansion, which prevented over-filling of the vessel, and subsequent pressure release, by the rupture disk. The vessel was then properly assembled, without over-filling, brought up to the desired temperature, and allowed to proceed to equilibrium under isothermal conditions. Three samples of 3-4 mL were withdrawn at regular time intervals, the first of which were discarded to ensure the sample line was adequately flushed of any previous solution. The remaining samples were analyzed by ICP ES to determine the molality of aqueous sodium and total phosphate. In determining the kinetics of SNHP formation at 250 °C, samples were taken

regularly over a period of up to 250 hours. For the re-dissolution reaction, the pressure vessel was allowed to remain at 275 °C for 4 days and then the temperature was lowered to 250 °C, and samples were withdrawn for an additional 240 hours until equilibrium was reached. The experiments were stopped when sample flow became erratic; indicating the level of the solution had dropped below the sample tube, or when approximately 140 mL of solution were calculated to remain in the vessel.

2.5.2 Solubility vs Temperature

Only two temperature-dependant solubility runs were performed. The temperature was raised in small increments, so that the solutions were supersaturated with respect to the nickel-phosphate reaction product, but unsaturated with respect to the zirconium-phosphate reaction product. A schematic plot of equilibrium phosphate concentration versus temperature for the zirconium oxide-aqueous phosphate and nickel oxide-aqueous reactions from this study can be seen in Figure 2.4. As shown in the schematic, large temperature increments could cause the solution to become supersaturated with respect to the zirconium-phosphate reaction product, and lead to possible corrosion of the zirconium vessel.

The temperature-dependant solubility experiments were performed in the following way. As in the kinetic runs, an excess of 25 g of nickel oxide was added to the zirconium vessel with approximately 250 mL of 1.5 mol·kg⁻¹ sodium phosphate solution with a sodium- phosphate mole ratio of 2.5. In the first solubility run, the vessel was raised from room temperature to 235 °C whereas; in the second solubility run the first

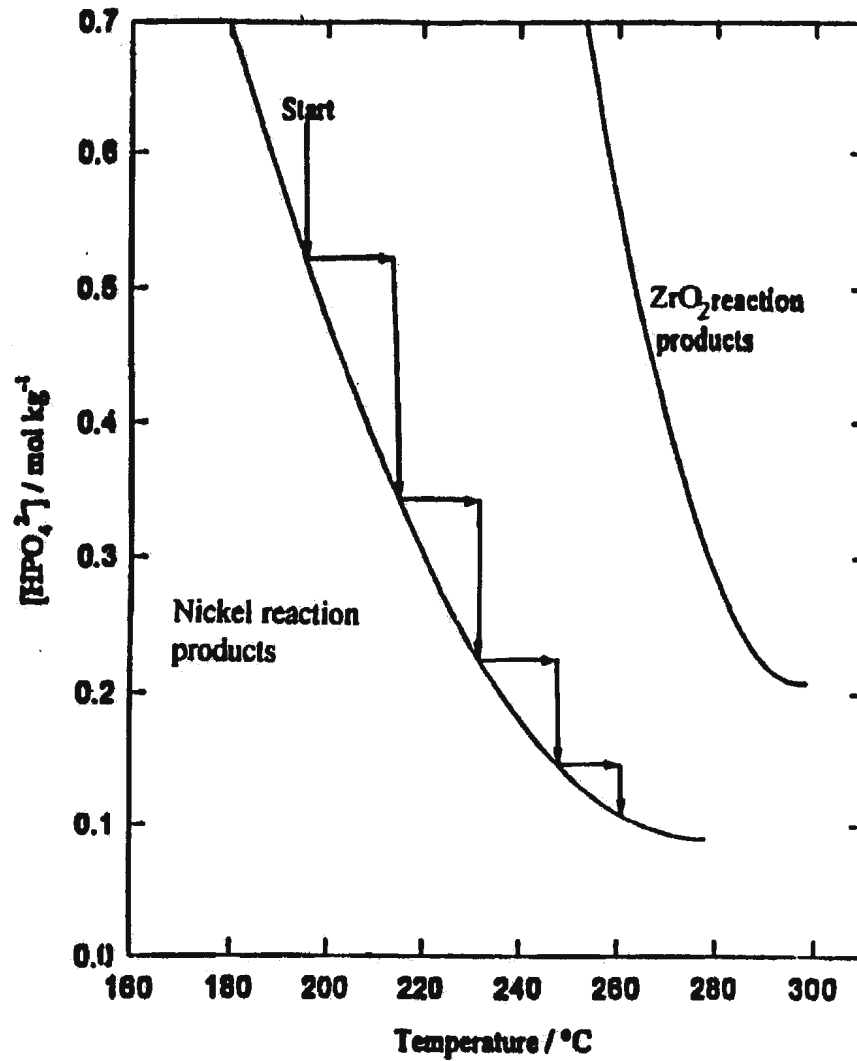


Figure 2.4: Experimental design for zirconium stirred reaction vessel experiments: Solubility of zirconium oxide reaction products, and nickel oxide reaction products under uncontrolled redox conditions. (taken from Quinlan (1996); modified to fit our reaction conditions)

temperature approached was 240 °C. The initial analysis of the kinetic data suggested that 2-2.5 days was sufficient for equilibrium to be achieved. The reaction was allowed to react for that time with constant stirring at each temperature. Approximately 3-4 mL of solution was collected to flush the sample line before two 3 mL samples were withdrawn, and the temperature was raised by 8-10 °C. Again the reaction was allowed to proceed for 2-2.5 days before the procedure was repeated. As the temperature was raised, the precipitation of SNHP removed sodium and phosphate from the solution incongruently, causing the Na/PO₄ mole ratio to rise. The highest temperature measured was 280 °C. Higher temperatures were thought to possibly cause corrosion of the autoclave vessel. Only 5-7 measurements were taken per solubility run because of time constraints. These temperature-dependant solubility runs typically required two weeks to complete.

2.5.3 Recovery of the Equilibrium Solid Reaction Product

In each of the four kinetic runs and two solubility runs, it was necessary to recover some of the solid reaction product for powder XRD analysis in order to confirm that the correct nickel-sodium-phosphate phase was synthesized and consequently being measured. A small stainless steel filter basket was placed in between the cooling tubes, located in the autoclave head. The basket contained NiO which reacted with aqueous phosphate to form the reaction product. The reaction product was then removed from contact with the liquid at high temperatures as the removal of samples lowered the level of the aqueous phase in the vessel below that of the basket. This procedure prevented re-

dissolution of SNHP and allowed the equilibrium reaction product to be recovered. Powder XRD determined the solid was a mixture of SNHP and nickel oxide. Powder patterns of the solids recovered from the impeller and the bottom of the vessel also showed SNHP present in high quantities. This confirmed that the correct phase was produced in all of the kinetic and solubility studies.

3.0 HYDROTHERMAL SYNTHESIS OF HIDEOUT REACTION PRODUCTS

3.1 Maricite

The purpose of this set of experiments was to prove that the maricite synthesis previously done by Quinlan (1996) using the hydrothermal decomposition of aqueous $\text{Fe}^{\text{III}}\text{NTA}$, was reproducible.

Product RGH05: The off-white product obtained in this study was analyzed by powder XRD and identified as maricite. The powder XRD results can be found in Table A.I.1 in Appendix I. The results were compared with powder XRD results for maricite from Quinlan (1996) and those obtained from the JCPDS database. They were an excellent match. None of the expected impurities (i.e. Na_2HPO_4 , Na_3PO_4 , $\text{Fe}^{\text{III}}_2\text{O}_3$, $\text{Fe}^{\text{II}}\text{Fe}^{\text{III}}_2\text{O}_4$) were observed (detection limit < 2 %). Figures 3.1a and b show secondary electron images of Quinlan's maricite product synthesized at 250 °C and the maricite product obtained in this study at 200 °C, respectively. An identical blossom-like growth is observed in both figures, indicating the crystals grew out of solution by rapid homogeneous nucleation. The maricite sample in Figure 3.1a was synthesized at 250 °C, but Quinlan (1996) reported that, single crystals of maricite could be isolated when the reaction was repeated at a lower temperature. In the upper right corner of the SEM image in Figure 3.1b, a single crystal is observed. It was concluded that single crystals of maricite can be synthesized at 200 °C.

(a)



(b)



Figure 3.1a and b:

Scanning electron micrographs of (a) maricite (Quinlan, 1996) and (b) a solid reaction product obtained from $\text{Fe}^{\text{III}}\text{NTA}$ and aqueous sodium phosphate ($\text{Na}/\text{PO}_4 = 2.15$) at $200\text{ }^\circ\text{C}$ for 28 days.

No single crystal XRD was performed on the maricite product since the structure is known (LePage and Donnay, 1977; Bridson et al., 1998), but the powder XRD analysis proves that the maricite hydrothermal synthesis is reproducible and that it is a reliable means of synthesizing maricite.

3.2 SIHP

3.2.1 The Fe^{III}NTA Reaction

An objective of this study was to develop hydrothermal synthetic methods for producing a reliable means of synthesizing crystalline sodium iron hydroxy phosphate (SIHP) by decomposing an aqueous complex. Fe^{III}NTA is known to produce single crystals of the iron(II) product maricite at 200 °C (Section 3.1). Our first attempt to synthesize SIHP involved decomposing Fe^{III}NTA(aq) in solutions with a higher sodium-phosphate mole ratio, in order to drive the reaction toward the iron(III) hydroxide product. The benefit of using Fe^{III}NTA is that iron is slowly released into the system over time, thus providing a better chance of growing single crystals of SIHP large enough for XRD analysis and to avoid unreacted iron oxide starting materials.

Figures 3.2a, b, and c are SEM images of a few of the products obtained from the attempted syntheses listed in Section 2.4.3. All three experiments produced solids that were mostly or all red-orange in color, and all were conducted at 200 °C.

Product RGH32B: Figure 3.2a is a SEM image of a sample of SIHP obtained from reacting Fe^{III}NTA with aqueous sodium-phosphate (Na/PO₄ = 4.0, [PO₄] = 0.6 molal) for 2 weeks. The sample was mostly red-orange solid with traces of black solid

(a)



(b)



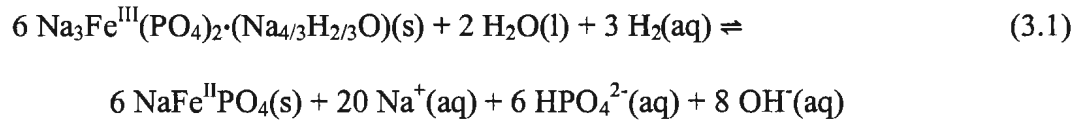
(c)



Figure 3.2a, b, and c: Scanning electron micrographs of solid reaction products obtained from $\text{Fe}^{\text{III}}\text{NTA}$ and aqueous sodium phosphate ($\text{Na}/\text{PO}_4 = 4.0$) at 200°C for 5-14 days. [(a) $(\text{PO}_4) = 0.6$ molal, (b) repeat of (a) at a higher Fe/PO_4 mole ratio, (c) $(\text{PO}_4) = 1.0$ molal]

throughout the whole sample. No yellow-green starting material could be found visually or by powder XRD analysis. Table A.I.2 in Appendix I summarizes the powder XRD results. The powder XRD patterns confirmed that SIHP was the main component, but showed that magnetite was also present in the sample, which would account for the traces of black solid observed. The JCPDS database search also identified a few peaks that matched those found in maricite and Na_3PO_4 . But these few matching peaks can also be found in powder XRD results for SIHP or magnetite. The SEM image showed that the sample contained thin, needle-like crystals, identified as SIHP. On average the crystals were 2 μm thick and 25 μm long. The SEM elemental analysis confirmed the presence of iron, sodium, and phosphorus.

The equilibrium reaction between maricite and SIHP that governs which hideout reaction product will form is as follows:



The equilibrium constant of SIHP reduction to maricite according to the above reaction is:

$$K_{\text{SIHP} \rightarrow \text{maricite}} = \frac{m(\text{Na}^+)^{20} m(\text{HPO}_4^{2-})^6 m(\text{OH}^-)^8}{m(\text{H}_2)^3} \quad (3.2)$$

and the equilibrium constant for maricite oxidation to SIHP is given by

$$K_{maricite \rightarrow SIHP} = \frac{m(H_2)^{\frac{1}{2}}}{m(Na^+)^{\frac{10}{3}} m(HPO_4^{2-}) m(OH^-)^{\frac{4}{3}}} \quad (3.3)$$

It was concluded that raising the Na^+ concentration was successful in causing SIHP to precipitate instead of maricite, but it apparently was so high that Na_3PO_4 also precipitated.

$$K_{Na_3PO_4} = \frac{1}{m(Na^+)^3 m(HPO_4^{2-})} \quad (3.4)$$

Product RGH59B: In the next set of experiments, the iron to phosphate mole ratio was increased to $Fe/PO_4 = 4.0$ in an attempt to avoid precipitation of Na_3PO_4 by reacting more of the phosphate. The reaction conditions listed in the previous paragraph were kept the same except the reaction time was reduced to 5 days. The recovered product was a mixture of red-orange, white, and black solids. The powder XRD results can be found in Table A.I.3 in Appendix I. The powder XRD analysis confirmed that SIHP was the main component of the sample but maricite and magnetite were also present, accounting for the white and black solids, respectively. The analysis also showed that hematite and Na_3PO_4 were again present as minor impurities. Figure 3.2b shows the SEM image, and the elemental analysis confirmed the presence of iron,

sodium, and phosphorus in the reaction product. The SIHP crystals were similar to those obtained in the previous run, but appear to be about half the size.

Product RGH60A: Another set of experiments was attempted under the same conditions as the previous synthesis at Na/PO₄ = 4.0 (Product RGH59B), but this time with a greater phosphate concentration ([PO₄] = 1.0 molal). The sample obtained was red-orange solid with no visible traces of white or black solid and all powder XRD results are in Table A.I.4 in Appendix I. The powder XRD analysis did not identify maricite, magnetite, or hematite in the sample, but traces of Na₃PO₄ and Fe₂PO₅ were identified from the JCPDS search and match software. The analysis did confirm that SIHP gave an excellent match. The SEM image (Figure 3.2c), reveals the thin, needle-like SIHP crystals observed in the other products are not present. However, in the upper right hand corner of the image, round clumps are found with crystals growing from them in a radial pattern suggesting that the crystals grew from a fast homogeneous reaction.

Even though the crystals obtained were not large enough to do a single crystal XRD, it can be concluded from the SEM images and powder XRD analysis, that SIHP can be synthesized from the thermal decomposition of Fe^{III}NTA at a much higher sodium phosphate mole ratio than in the studies done by Quinlan (1996), but the synthesis yields a product with a small amount of Na₃PO₄ precipitate still present as an impurity.

3.2.2 The Fe^{III}₂(C₄H₄O₆)₃ Reaction

The second approach used in synthesizing SIHP was an attempt to prevent the reduction of Fe³⁺ during decomposition by using a chelate that does not contain amine

groups. Oxidizing agents were previously used with various iron starting materials and aqueous sodium phosphate solutions to try and synthesize SIHP (Quinlan 1996), but these were unsuccessful.

Product RGH29A: In this study, iron(III) tartrate was used as the iron chelate reagent. Aqueous $\text{Fe}^{\text{III}}_2(\text{C}_4\text{H}_4\text{O}_6)_3$ was reacted with aqueous sodium phosphate ($\text{Na}/\text{PO}_4 = 2.8$, $[\text{PO}_4] = 0.6$ molal) for 3 weeks. The sample obtained from the experiment at $200\text{ }^\circ\text{C}$ was an orange-red powder with small amounts of white solid throughout. The powder XRD results are in Table A.I.5 in Appendix I. The powder XRD analysis confirmed that SIHP was the main component in the sample, but maricite and Na_3PO_4 are also present in small amounts, accounting for the white solid observed. Some of the peaks in the XRD pattern that do not match SIHP, maricite, or Na_3PO_4 are due to the presence of sodium tartrate hydrate and sodium hydrogen phosphate hydrate in the sample. Figure 3.3 is the SEM image. The SEM EDX elemental analysis confirmed the presence of iron, sodium, and phosphorus. The sample contains crystals of various types and sizes and scattered, thin needle-like SIHP crystals can be seen throughout. However no one crystal was large enough for single crystal XRD analysis. These sets of experiments gave better crystals than in the first approach described in Section 3.2.1, but the samples still contained impurities.

3.2.3 The $\text{Fe}^{\text{III}}_2(\text{C}_2\text{O}_4)_3 \cdot 5\text{H}_2\text{O}$ Reaction

Product RGH78A: Another iron chelating agent used to try to obtain SIHP in this study was iron(III) oxalate. Aqueous $\text{Fe}^{\text{III}}_2(\text{C}_2\text{O}_4)_3 \cdot 5\text{H}_2\text{O}$ was used as a starting material



Figure 3.3: Scanning electron micrograph of a solid reaction product obtained from iron(III) tartrate and aqueous sodium phosphate ($\text{Na}/\text{PO}_4 = 2.8$) at 200 °C for 3 weeks.

and reacted with aqueous sodium phosphate ($\text{Na}/\text{PO}_4 = 2.5$, $[\text{PO}_4] = 1.0$ molal) at $250\text{ }^\circ\text{C}$ for a period of 8 days to produce a red-orange, crystalline solid. The powder XRD results are listed in Table A.I.6 in Appendix I. No evidence for unreacted starting material could be found visually or in the powder XRD spectrum. This synthesis seemed to produce a solid product with little or no impurities however some extra peaks were observed that are not present in the SIHP XRD powder pattern from Quinlan (1996). The presence of Na_3PO_4 and Fe_3PO_5 in the sample accounts for some of the peaks, however the peaks observed at d-spacings of 7.9707 \AA and 7.8460 \AA could not be accounted for. Figure 3.4 is the SEM image of the product. The SEM elemental analysis confirmed the presence of iron, sodium, and phosphorus. Distinct thin, needle-like crystals can be seen, much like the SIHP products obtained from the $\text{Fe}^{\text{III}}\text{NTA}$ reactions. While the crystals were bigger than in previous SIHP syntheses, they were still too small to perform single crystal XRD. The crystals were not uniform and there appear to be many crystal fragments scattered throughout the sample. However various areas of the SEM image show that the crystals grew in layers of smaller parallel crystals.

Again this method gave better crystals than in the first approach, described in Section 3.2.1 but a few impurities were observed. Future work on this reaction could include trying the synthesis at a higher Na/PO_4 mole ratio.

3.3 $(\text{NH}_4)\text{Fe}^{\text{II}}\text{Fe}^{\text{III}}(\text{PO}_4)_2$

The mixed valence compound $(\text{NH}_4)\text{Fe}^{\text{II}}\text{Fe}^{\text{III}}(\text{PO}_4)_2$ was synthesized by Boudin and Lii (1998) at $500\text{ }^\circ\text{C}$ as a black crystalline product. The objective was to see if the mixed



Figure 3.4: Scanning electron micrograph of a solid reaction product obtained from iron(III) oxalate and aqueous sodium phosphate ($\text{Na}/\text{PO}_4 = 2.5$) at $250\text{ }^\circ\text{C}$ for 8 days.

valence compound would form under boiler conditions and to synthesize it using a more simple method. The first batch of experiments was done at 250 °C using the starting materials reported in the paper by Boudin and Lii (1998). The XRD diffraction spectra showed evidence that unreacted hematite, $(\text{NH}_4)\text{H}_2\text{PO}_4$, and $(\text{NH}_4)_2\text{HPO}_4$ were still present in the recovered product. There was no success in obtaining $(\text{NH}_4)\text{Fe}^{\text{II}}\text{Fe}^{\text{III}}(\text{PO}_4)_2$ from this method.

Product RGH51A: Another set of experiments was run, where iron tartrate was used as the iron source with varying mole ratios of aqueous ammonium phosphate (NH_4/PO_4). One such run at 250 °C for a week ($\text{NH}_4/\text{PO}_4 = 1.0$, $[\text{PO}_4] = 0.6$ molal) produced a small amount of small black crystals. The powder XRD results are listed in Table A.I.7 in Appendix I. The powder XRD performed on the synthesized product from this study matched extremely well with that generated from the supplied by Boudin and Lii (1998) suggesting that $(\text{NH}_4)\text{Fe}^{\text{II}}\text{Fe}^{\text{III}}(\text{PO}_4)_2$ was synthesized. However, hematite was found to be a major impurity, and there were also traces of $\text{Fe}^{\text{III}}(\text{PO}_4)_2 \cdot 2\text{H}_2\text{O}$ and ammonium hydrogen phosphate hydrate. The peak at a d-spacing of 3.5033 Å was due to the presence of $\text{Fe}^{\text{II}}_3(\text{PO}_4)_2$. Figures 3.5a and b are SEM images of the crystals obtained. Figure 3.5b is an enlargement of Figure 3.5a showing that the sample is a mixture of crystal clusters. Unfortunately, the crystals were not large enough to perform a single crystal XRD analysis.

Product RGH62A: In an effort to make crystals of $(\text{NH}_4)\text{Fe}^{\text{II}}\text{Fe}^{\text{III}}(\text{PO}_4)_2$ large enough to perform a single crystal XRD, the same reaction was repeated at a lower temperature (i.e. 200 °C). Figure 3.6 is the secondary electron microscopy image of this

(a)



(b)



Figure 3.5a and b:

Scanning electron micrographs of solid reaction products obtained from iron(III) tartrate and aqueous ammonium phosphate ($\text{NH}_4/\text{PO}_4 = 1.0$) at 250°C for 1 week. [(b) is an enlarged view of (a)]



Figure 3.6: Scanning electron micrograph of a solid reaction product obtained from iron(III) tartrate and aqueous ammonium phosphate ($\text{NH}_4/\text{PO}_4 = 1.0$) at 200 °C for 1 week.

sample. Table A.I.8 in Appendix I summarizes the powder XRD results. Unfortunately, the black crystals synthesized were still not large enough to perform the analysis but the powder XRD spectrum pattern confirmed that they gave a good match for $(\text{NH}_4)\text{Fe}^{\text{II}}\text{Fe}^{\text{III}}(\text{PO}_4)_2$. Again, hematite was an impurity along with $(\text{NH}_4)\text{H}_2\text{PO}_4$. The peaks at 3.1237 Å and 2.1166 Å d-spacings are due to $\text{Fe}^{\text{III}}(\text{PO}_4)\cdot 2\text{H}_2\text{O}$ present in the sample, while $\text{Fe}^{\text{III}}\text{O}(\text{OH})$ accounts for the peaks at 6.2460 Å and 1.7400 Å d-spacings.

In conclusion, crystals of $(\text{NH}_4)\text{Fe}^{\text{II}}\text{Fe}^{\text{III}}(\text{PO}_4)_2$ were synthesized however they were too small for single crystal XRD. The method run at 200 °C gave the “best” sample for calorimetry however hematite and $(\text{NH}_4)\text{H}_2(\text{PO}_4)$ were still present as impurities. This is a new, simpler synthesis for $(\text{NH}_4)\text{Fe}^{\text{II}}\text{Fe}^{\text{III}}(\text{PO}_4)_2$, and its success demonstrate that the precipitation of $(\text{NH}_4)\text{Fe}^{\text{II}}\text{Fe}^{\text{III}}(\text{PO}_4)_2$ can occur under boiler water conditions.

3.4 $(\text{NH}_4)\text{Fe}^{\text{II}}(\text{PO}_4)\cdot\text{H}_2\text{O}$

Product RGH18B: Attempts to synthesize ammonium iron phosphate hideout products at 200 °C yielded another product, ammonium iron(II) phosphate monohydrate, $(\text{NH}_4)\text{Fe}^{\text{II}}(\text{PO}_4)\cdot\text{H}_2\text{O}$. The sample of $(\text{NH}_4)\text{Fe}^{\text{II}}(\text{PO}_4)\cdot\text{H}_2\text{O}$ obtained in this study was synthesized by reacting $\text{Fe}^{\text{III}}\text{NTA}$ with aqueous ammonium phosphate ($\text{NH}_4/\text{PO}_4 = 2.8$, $[\text{PO}_4] = 0.7$ molal) for 9 days at 200 °C. The resulting crystals were clear and colorless. Figure 3.7 is the secondary electron microscope image and the elemental analysis confirmed that iron and phosphorus were present in nearly equal amounts. The SEM image shows that the crystals were stacked in an organized layered fashion. Each layer



Figure 3.7: Scanning electron micrograph of a solid reaction product obtained from $\text{Fe}^{\text{III}}\text{NTA}$ and aqueous ammonium phosphate ($\text{NH}_4/\text{PO}_4 = 2.8$) at $200\text{ }^\circ\text{C}$ for 9 days.

had crystals lying parallel to the crystals in the layer above and below. It appeared that the crystals had grown on a surface that subsequently dissolved. The coordinates of the atoms for the crystal $(\text{NH}_4)\text{Fe}^{\text{II}}(\text{PO}_4)\cdot\text{H}_2\text{O}$ obtained from single crystal analysis are given in Table 3.1 and the structure is shown in Figure 3.8. The details of the analysis are in Appendix II. From the single crystal XRD data for $(\text{NH}_4)\text{Fe}^{\text{II}}(\text{PO}_4)\cdot\text{H}_2\text{O}$, a powder pattern was generated using the SHELXTL program and the results are in Table A.I.9 in Appendix I.

The divalent metal ammonium monophosphate monohydrate, $(\text{NH}_4)\text{Fe}^{\text{II}}(\text{PO}_4)\cdot\text{H}_2\text{O}$, can exist in two polymorphs and have been synthesized by Greeden et al. (1988) and Ivanov et al. (1974, 1976). From these papers, the structure of each compound indicates a layered arrangement of MO_6 octahedra separated by ammonium ions, where the oxygen atoms forming the octahedra about the metal atoms are from the phosphate groups and the water of hydration. Polymorph A has octahedra in adjacent layers with identical orientation whereas polymorph B has layers with inverted orientation. The space groups for A and B are $\text{Pmn}2_1$ and Pnma , respectively, and the unit cell orientations are such that $a_A \approx 2(b_B)$, $b_A \approx a_B$, and $c_A \approx c_B$. Greeden et al. (1988) synthesized only polymorph A and found the unit cell dimensions to be $a = 5.684(1)$, $b = 8.803(1)$, and $c = 4.818(5)\text{\AA}$. Using these numbers, polymorph B would have calculated unit cell dimensions of $a = 17.606(2)$, $b = 5.684(1)$, and $c = 4.818(5)\text{\AA}$. The synthesized crystal structure in this study was found to have a Pnma space group and $a = 17.597$, $b = 5.667$, and $c = 4.833\text{\AA}$ unit cell dimensions. Thus, it can be concluded that polymorph B was synthesized in this study.

Table 3.1: Positional parameters for $(\text{NH}_4)\text{Fe}^{\text{II}}(\text{PO}_4)\cdot\text{H}_2\text{O}$ from single crystal analysis

atom	x	y	z
Fe(1)	0.23902(2)	0.2500	0.6192(1)
P(2)	0.15198(5)	-0.2500	0.6851(2)
O(1)	0.1439(1)	0.2500	0.3133(5)
O(3)	0.1651(1)	-0.2500	0.3714(5)
O(4)	0.19024(9)	-0.0356(3)	0.8242(3)
O(5)	0.0664(1)	-0.2500	0.7445(5)
N(1)	0.139(2)	0.2500	0.7593(7)
H(1)	-0.0157	0.2500	0.9346
H(2)	-0.0153	0.2500	0.5622
H(3)	0.0432	0.1109	0.7685
H(4)	0.1151	0.3868	0.3684
H(5)	0.1493	0.2500	0.1199

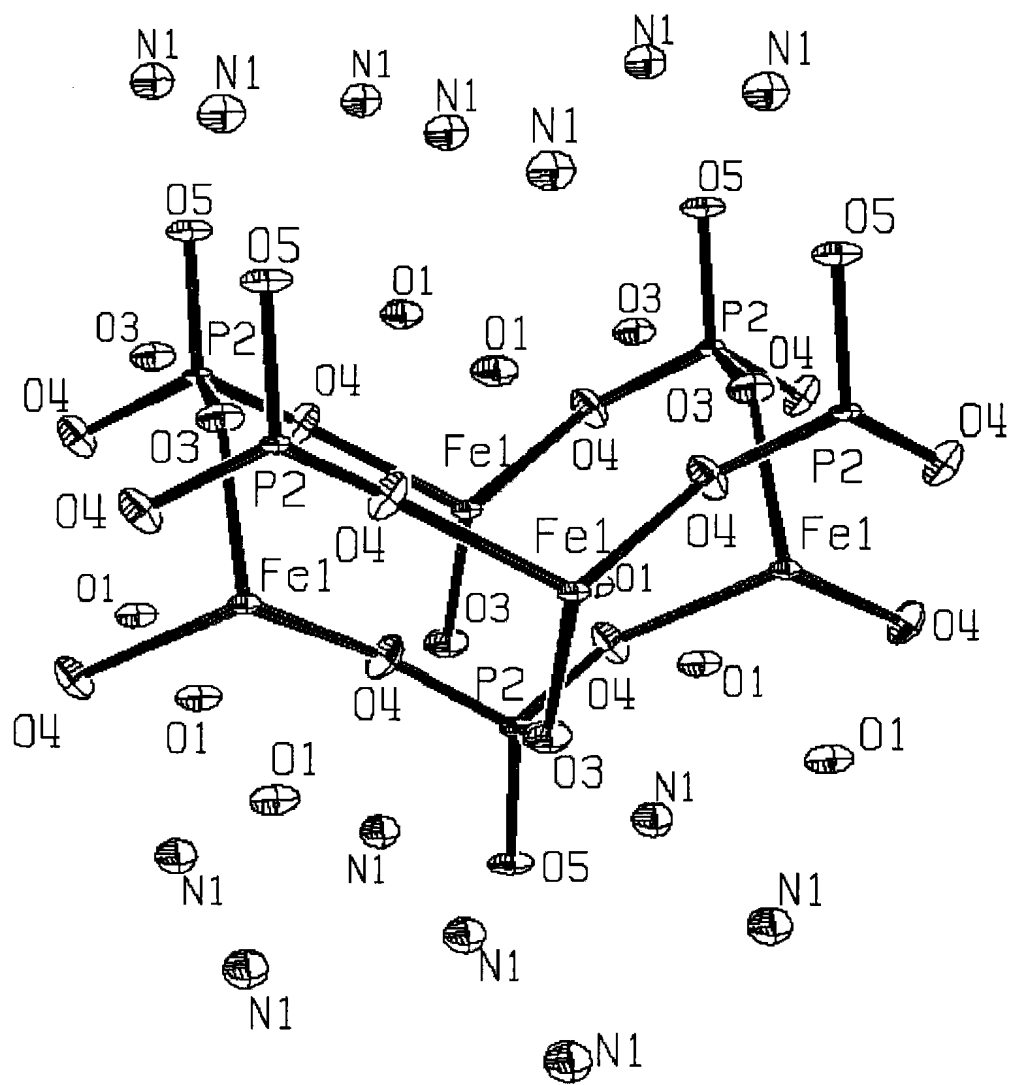


Figure 3.8: Crystal Structure of $(\text{NH}_4)\text{Fe}^{\text{II}}(\text{PO}_4)\cdot\text{H}_2\text{O}$

In a set of experiments that were an attempt to synthesize $(\text{NH}_4)\text{Fe}^{\text{II}}\text{Fe}^{\text{III}}(\text{PO}_4)_2$ (iron tartrate; $\text{NH}_4/\text{PO}_4 = 2.8$, $[\text{PO}_4] = 0.7$ molal; at $200\text{ }^\circ\text{C}$ for 8 days), a greenish grey solid was obtained. Table A.I.9 in Appendix I is a summary of the powder XRD results. While the results do not match the powder XRD pattern for $(\text{NH}_4)\text{Fe}^{\text{II}}\text{Fe}^{\text{III}}(\text{PO}_4)_2$, they do yield a good match for the calculated pattern of $(\text{NH}_4)\text{Fe}^{\text{II}}(\text{PO}_4)\cdot\text{H}_2\text{O}$. Hematite was also present in the sample. There were five peaks in the spectrum that could not be assigned. While the experiment did not yield $(\text{NH}_4)\text{Fe}^{\text{II}}\text{Fe}^{\text{III}}(\text{PO}_4)_2$, it did show that $(\text{NH}_4)\text{Fe}^{\text{II}}(\text{PO}_4)\cdot\text{H}_2\text{O}$ can be synthesized via a different route. The SEM image is shown in Figure 3.9, and the elemental analysis showed that iron and phosphorus were present in nearly equal amounts. The crystals were not large enough to perform a single crystal XRD analysis.

In conclusion, this is a new single crystal synthesis for $(\text{NH}_4)\text{Fe}^{\text{II}}(\text{PO}_4)\cdot\text{H}_2\text{O}$, and the results show that it can form in low-temperature boiler water.

3.5 SNHP

3.5.1 The NiO Reaction

Ziemniak and Opalka (1988) have shown that one reaction product of aqueous sodium phosphate with nickel under boiler conditions is sodium nickel hydroxyphosphate (SNHP), $\text{Na}_2\text{Ni}(\text{OH})\text{PO}_4$. Attempts were made to prepare pure samples of SNHP but only a few of these syntheses produced SNHP.

Product RGH92A: Utilizing the experimental methods developed in our laboratory, SNHP was synthesized by reacting NiO with aqueous sodium phosphate



Figure 3.9: Scanning electron micrograph of a solid reaction product obtained from iron(III) tartrate and aqueous ammonium phosphate ($\text{NH}_4/\text{PO}_4 = 2.8$) at 200 °C for 8 days.

($\text{Na}/\text{PO}_4 = 2.5$, $[\text{PO}_4] = 1.5$ molal) at $250\text{ }^\circ\text{C}$ for one week. The powder XRD results of the resulting green solid are listed in Table A.I.10 in Appendix I. The powder XRD analysis showed that the main component of the sample was SNHP, based on the powder XRD pattern in the paper by Ziemniak and Opalka (1988), but that unreacted NiO remained. Other impurities identified in the powder XRD pattern were Na_3PO_4 and possibly, another sodium-nickel-phosphate, $\text{Na}_4\text{Ni}(\text{PO}_4)_2$. However, the peaks in the sample XRD pattern that match $\text{Na}_4\text{Ni}(\text{PO}_4)_2$ were also present in the powder XRD pattern for $\text{Na}_2\text{Ni}(\text{OH})\text{PO}_4$. Two of the low intensity peaks could not be accounted for. In Section 1.7, it was noted that two additional anhydrous sodium-nickel-phosphate are known to exist, $\text{Na}_4\text{Ni}_5(\text{PO}_4)_2(\text{P}_2\text{O}_7)_2$ and $\text{NaNi}_4(\text{PO}_4)_3$ (Sanz et al., 1999; Daidouh et al., 1999), but they were not identified in the powder XRD results. It can be concluded that $\text{Na}_2\text{Ni}(\text{OH})\text{PO}_4$ was the major product, because the powder XRD pattern contained a greater percentage of matching peaks to that of the sample than the other compounds present.

The SEM image of this product is shown in Figure 3.10. Ziemniak and Opalka (1988) obtained an image that revealed the crystals have a lath-like shape and the laths are bundled together in most cases. Figure 3.10 shows many bundles of small (25 by 25 μm) crystals that are bundled together. The elemental analysis confirmed the presence of sodium, nickel, and phosphorus.

Other syntheses were attempted to produce a pure sample of SNHP, but there was always a NiO impurity and time constraints prevented further reactions from being run.



Figure 3.10: Scanning electron micrograph of a solid reaction product obtained from nickel oxide and aqueous sodium phosphate ($\text{Na}/\text{PO}_4 = 2.5$) at 250 °C for 1 week.

3.5.2 The $\text{H}^+[\text{NiNTA}^-]$ Reaction

Product RGH89A: In one set of experiments, $\text{H}^+[\text{NiNTA}^-]$ was reacted with aqueous sodium phosphate ($\text{Na}/\text{PO}_4 = 2.5$, $[\text{PO}_4] = 1.5$ molal) at $250\text{ }^\circ\text{C}$ for 4 days. The SEM image is given in Figure 3.11 and the EDX elemental analysis confirmed the presence of sodium, nickel, and phosphorus in the reaction product. The powder XRD results for the green crystalline solid are listed in Table A.I.11 in Appendix I. The powder XRD pattern suggests that the sample was a mixture of SNHP, $\text{H}^+[\text{NiNTA}^-]$ and sodium hydrogen phosphate. $\text{Na}_4\text{Ni}_5(\text{PO}_4)_2(\text{P}_2\text{O}_7)_2$ and $\text{NaNi}_4(\text{PO}_4)_3$ were not identified from the XRD results. Again the JCPDS database identified $\text{Na}_4\text{Ni}(\text{PO}_4)_2$ but the same matching peaks are also seen in SNHP. There were also peaks that could not be accounted for. Thus there are also other impurities present in the sample that are not listed in the powder XRD results.

Products RGH66A and RGH73A: In order to try to remove the impurities from the product, an excess of NaOH was employed to neutralize the H^+ in $\text{H}^+[\text{NiNTA}^-]$. A new batch of experiments was performed where less $\text{H}^+[\text{NiNTA}^-]$ was reacted with a solution of a higher sodium to phosphate mole ratio (but lower phosphate concentration; $\text{Na}/\text{PO}_4 = 4.0$, $[\text{PO}_4] = 1.0$ molal). The temperature was also lowered to $200\text{ }^\circ\text{C}$. A pale green powder solid was synthesized whose XRD pattern is presented in Table A.I.12. The powder XRD suggests that, even though the majority of the sample was SNHP, $\text{Ni}(\text{OH})_2$ was also present. $\text{Na}_4\text{Ni}(\text{PO}_4)_2$ showed up on the JCPDS database, but the same peaks are seen in SNHP. When the same run was performed at a higher temperature (i.e. $250\text{ }^\circ\text{C}$), the impurity $\text{Ni}(\text{OH})_2$ was not present in the solid reaction product. The XRD

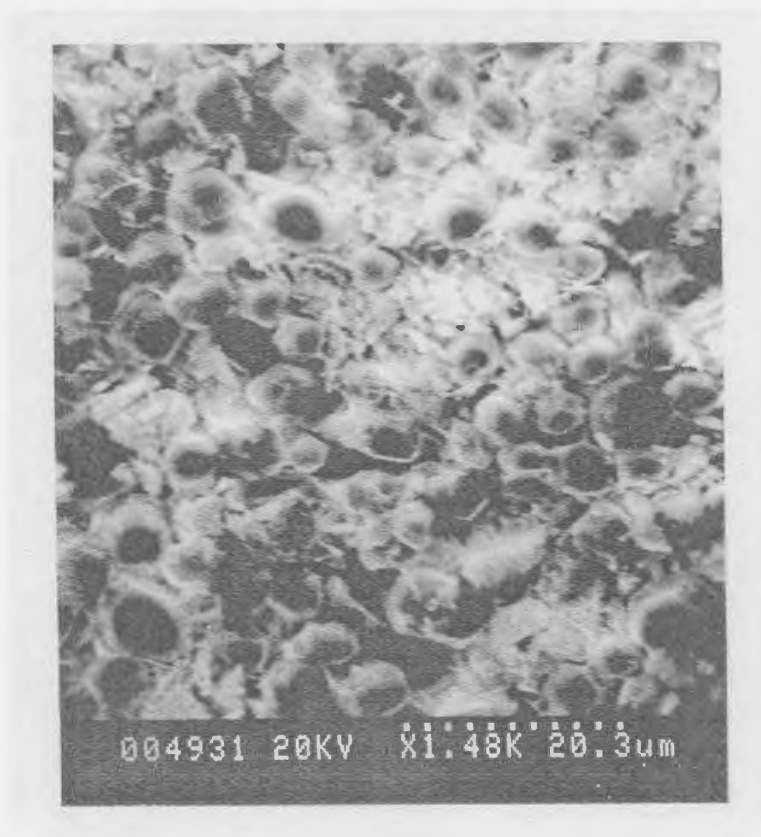
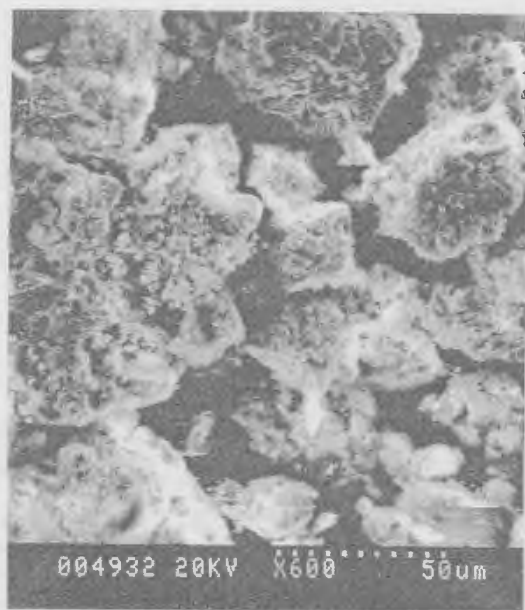


Figure 3.11: Scanning electron micrograph of a solid reaction product obtained from $\text{H}^+[\text{NiNTA}^-]$ and aqueous sodium phosphate ($\text{Na}/\text{PO}_4 = 2.5$) at 250°C for 4 days.

pattern is listed in Table A.I.13. Even though SNHP was still present in the sample, the JCPDS database identified different impurities than those in the product from the lower temperature run. Sodium phosphate and sodium phosphate hydrates accounted for most of the impurities present in the sample, but there were still peaks that could not be assigned. The SEM images of both runs are given in Figures 3.12a and b, respectively. From SEM, it can be seen the crystals are large enough to perform single crystal XRD analysis if they can be separated from the impurities. Again, as was the case with the NiO reactions, the crystals were bundled together. The well-defined crystals are smaller (5-15 μm) in size, too small for single crystal XRD. The elemental analysis confirmed the presence of sodium, nickel, and phosphorus in the reaction product.

In conclusion, using $\text{H}^+[\text{NiNTA}^-]$ as a nickel source did not give a pure sample of SNHP or large enough crystals to do a single crystal XRD analysis, as originally hoped. Time constraints prevented further investigation into this area. However, a new synthesis for SNHP has been developed. The use of NaNiNTA as a starting material could be another possible route to synthesizing SNHP for any future work in this area.

(a)



(b)



Figure 3.12a and b: Scanning electron micrographs of solid reaction products obtained from $H^+[NiNTA^-]$ and aqueous sodium phosphate ($Na/PO_4 = 4.0$) for 5 days at (a) 200 °C and (b) 250 °C respectively.

4.0 SOLUBILITY AND REACTION KINETICS OF SODIUM NICKEL HYDROXY-PHOSPHATE

4.1 Solubility of the Nickel Oxide-Sodium-Phosphate Reaction

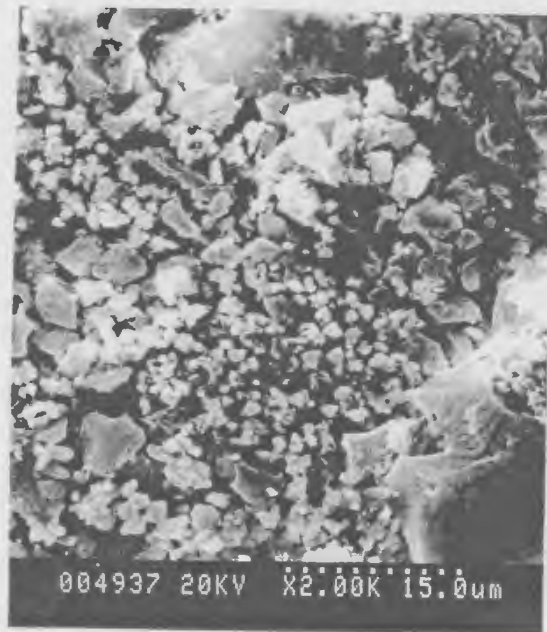
Nickel oxide undergoes reversible reactions with aqueous sodium phosphate solutions at elevated temperatures and pressures to form sodium nickel hydroxy phosphate, SNHP, according to the reaction (Ziemniak and Opalka, 1988):



In our solubility runs, samples were taken from different parts of the reaction vessel to confirm that the reaction product that had formed was indeed SNHP. Firstly, powder XRD analysis confirmed that both NiO and SNHP were present in the reaction matrix, and secondly, SEM elemental analysis showed that sodium, nickel, and phosphorus were indeed present in the crystals of reaction product. Figures 4.1a and b show the SEM images of a solid sample taken from the basket and the bottom of the vessel, respectively. Again, as previously observed, bundles or clumps of crystalline solid can be observed in both images indicating that SNHP is indeed present.

A complete description of the procedures used to determine temperature-dependant solubilities can be found in Section 2.5.2. Two separate runs were performed to determine the solubility of SNHP. The sodium-phosphate solution mole ratio was 2.5

(a)



(b)

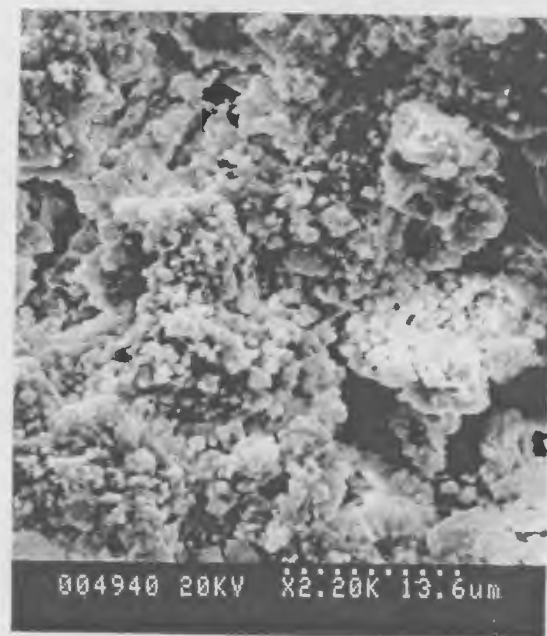


Figure 4.1a and b: Scanning electron micrographs of solid reaction products obtained from nickel oxide and aqueous sodium phosphate ($\text{Na}/\text{PO}_4 = 2.5$), solubility run from (a) the basket and (b) the bottom of the vessel.

with a phosphate concentration of $1.5 \text{ mol}\cdot\text{kg}^{-1}$. The temperature range measured was between 235-280 °C. The equilibration time used for each step was the same as that developed by Quinlan (1996) for SIHP, about 48 hours. Table A.III.3 in Appendix III contains the experimental data for the two solubility runs. The sodium and phosphate concentrations were measured by ICP-ES in ppm's but all the listed concentrations are expressed as molalities.

4.2 Kinetics of $\text{Na}_2\text{Ni}(\text{OH})\text{PO}_4$ Equilibration

The objective of the kinetic runs was to determine the time required for Equation (4.1) to reach equilibrium, and to obtain a definitive solubility of SNHP at 250 °C. Careful studies were performed from conditions of under and over saturation. The rate of SNHP precipitation was determined by raising the temperature of a vessel containing NiO and aqueous sodium phosphate ($\text{Na}/\text{PO}_4 = 2.5$) up to 250 °C. To determine the rate of SNHP re-dissolution, the system was equilibrated at 275 °C to form the reaction product, and then the temperature was lowered to 250 °C to re-dissolve it. A complete report of the experimental methods is found in Section 2.5.1. The results of two precipitation runs and two re-dissolution runs are plotted in Figure 4.2. However due to clogs in the filter, the first precipitation and the second re-dissolution attempts yielded erratic results and were discarded, leaving one good run of each. These are shown in Figure 4.3.

A simple rate equation commonly used in mineral dissolution studies (Stumm and Morgan, 1970; Blesa et al., 1994) can be used to describe the kinetic data:

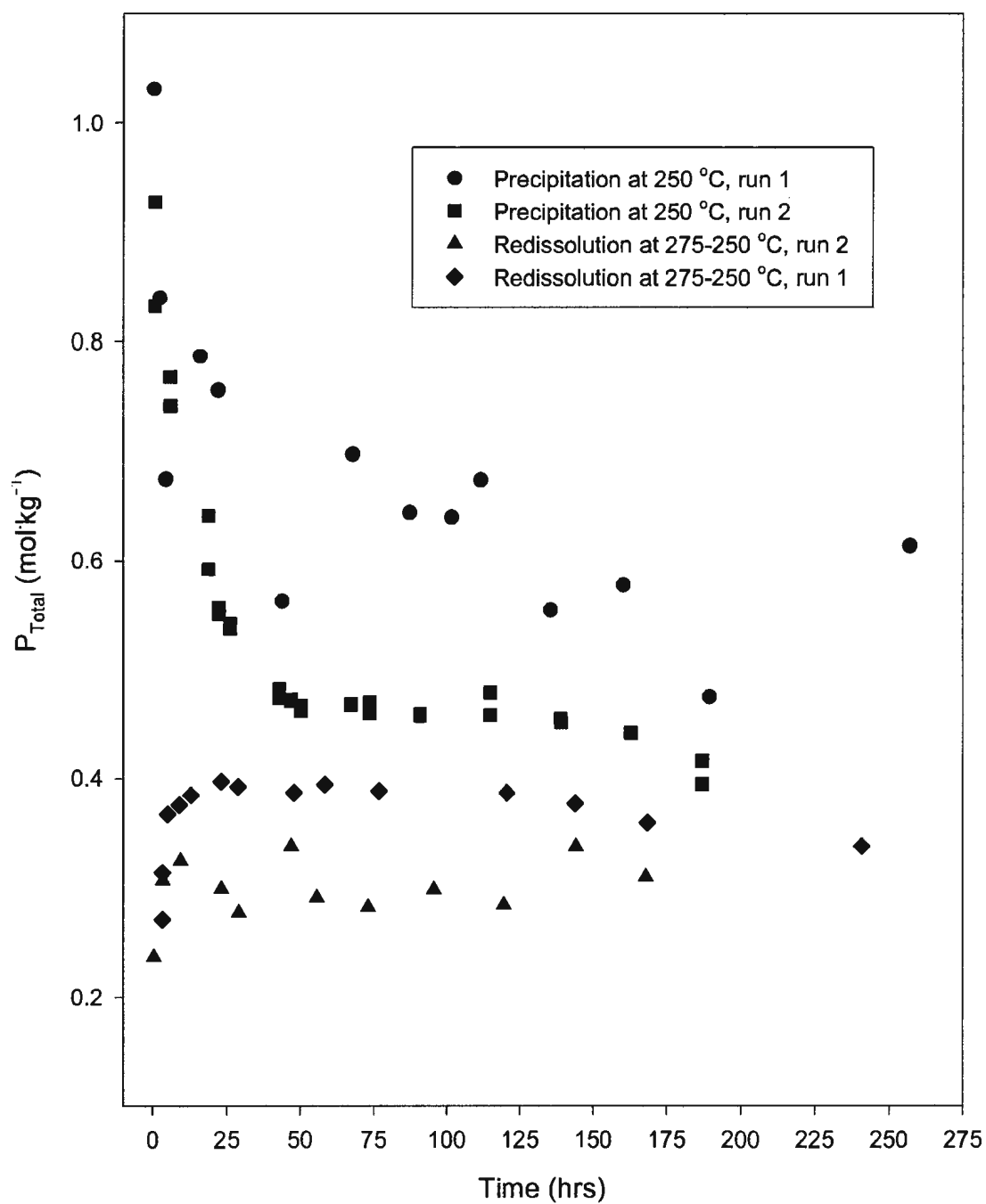


Figure 4.2: Kinetics of precipitation and re-dissolution of SNHP (all runs combined)

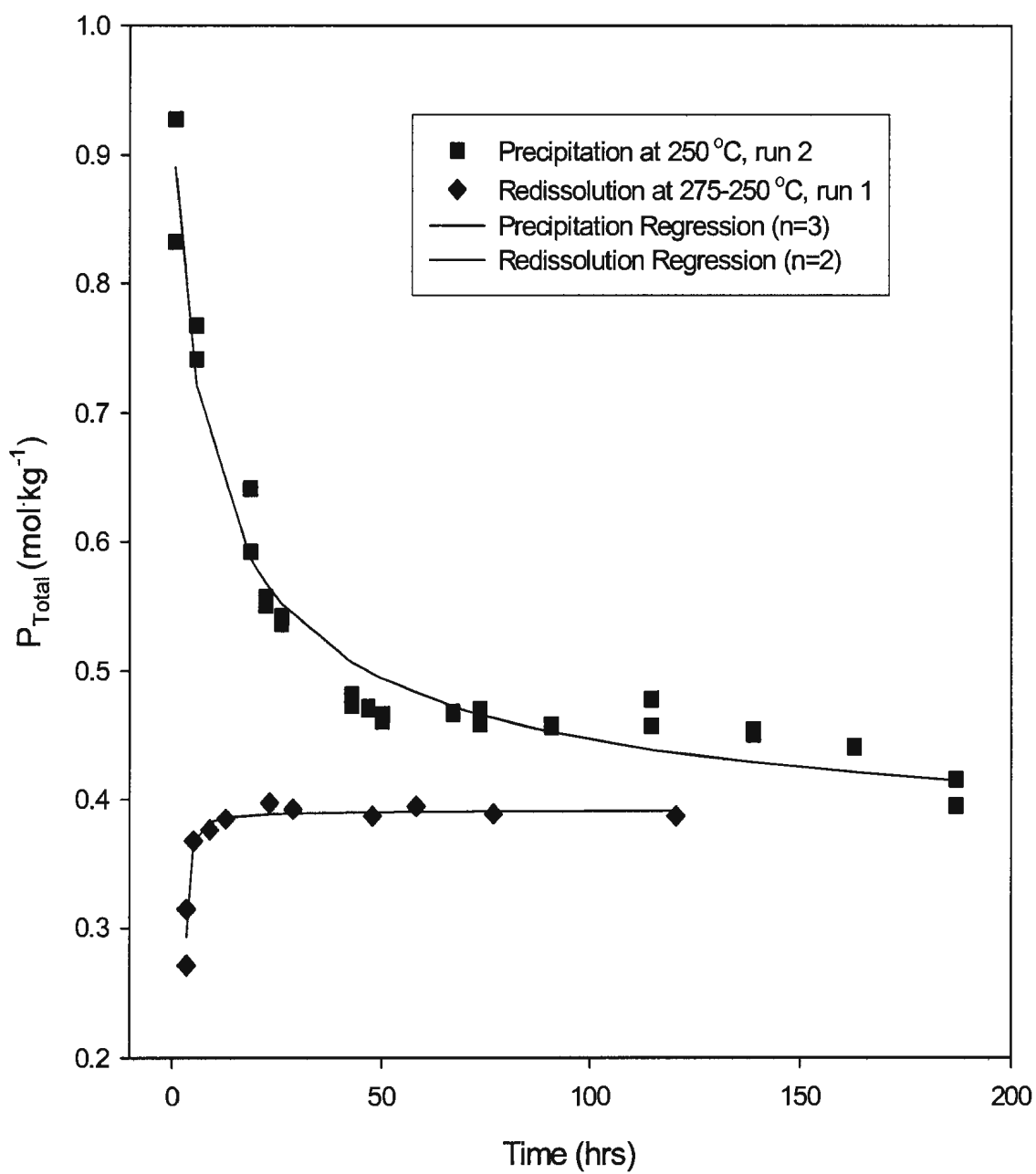


Figure 4.3: Kinetics of precipitation and re-dissolution of SNHP (data obtained from the best runs)

$$\frac{dm(\text{PO}_4, t)}{dt} = ka[m(\text{PO}_4, \text{sat}) - m(\text{PO}_4, t)]^n \quad (4.2)$$

Integration of Equation (4.2) gives the following expression

$$m(\text{PO}_4, t) = m(\text{PO}_4, \text{sat}) + [(n-1)kat + \{m(\text{PO}_4, t=0) - m(\text{PO}_4, \text{sat})\}^{(1-n)}]^{1/(1-n)} \quad (4.3)$$

The total phosphate concentration at time t is represented by $m(\text{PO}_4, t)$ whereas $m(\text{PO}_4, \text{sat})$ is the total phosphate concentration at equilibrium ($t = \infty$). In fitting Equation (4.3) to the data, the value of n was set at an arbitrary number whereas the value of the oxide surface area, a , was estimated to be equal to 1. Equation (4.3) was fitted to the kinetic data in Figure 4.3 with $n = 3$ for precipitation and $n = 2$ for re-dissolution, and the results are represented by solid curves in Figure 4.3. The rate constant for the precipitation reaction at 250 °C was $k = 0.32 \text{ mol}^{-1} \cdot \text{kg} \cdot \text{hr}^{-1} \cdot \text{m}^{-2}$ whereas $k = -16.9 \text{ mol}^{-2} \cdot \text{kg}^2 \cdot \text{hr}^{-1} \cdot \text{m}^{-2}$ was obtained for the re-dissolution reaction. The limiting values for the total solution concentrations at equilibrium ($t \rightarrow \infty$) for the precipitation reaction were $m(\text{Na}^+) = 1.3849 \text{ mol} \cdot \text{kg}^{-1}$ and $m(\text{PO}_4)_{\text{Total}} = 0.4546 \text{ mol} \cdot \text{kg}^{-1}$. The corresponding values were $m(\text{Na}^+) = 1.1901 \text{ mol} \cdot \text{kg}^{-1}$ and $m(\text{PO}_4)_{\text{Total}} = 0.3892 \text{ mol} \cdot \text{kg}^{-1}$ for the re-dissolution reaction. The averages of the two runs were taken as the “best” value at 250 °C in the thermodynamic modeling ($m(\text{Na}^+) = 1.2875 \pm 0.010 \text{ mol} \cdot \text{kg}^{-1}$, $m(\text{PO}_4)_{\text{Total}} = 0.4219 \pm 0.033 \text{ mol} \cdot \text{kg}^{-1}$).

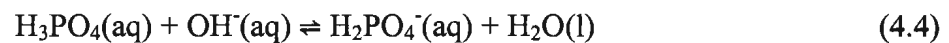
From Figure 4.3, it is shown that a time of 75 hours is needed for the precipitation reaction to equilibrate from over saturation at 250 °C. Therefore, the data used to

develop the thermodynamic model for this system were the equilibrium value at 250 °C, noted above, and values from Table A.III.3 for temperatures above 250 °C.

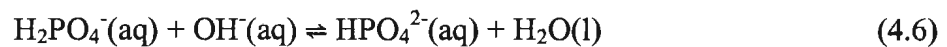
4.3 A Thermodynamic Model

4.3.1 Phosphate Ionization Equilibria

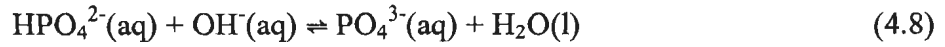
The major phosphate species in high-temperature water are the anions of orthophosphoric acid (Tremaine et al., 1992). These include dihydrogen phosphate, $H_2PO_4^-$; hydrogen phosphate, HPO_4^{2-} ; and phosphate, PO_4^{3-} . These species form according to the equilibria listed below. Because we are dealing with alkaline boiler water conditions, these are written as reactions with hydroxide, followed by their corresponding equilibrium constants:



$$K_1 = \frac{m(H_2PO_4^-)}{m(H_3PO_4)m(OH^-)} \quad (4.5)$$



$$K_2 = \frac{m(HPO_4^{2-})}{m(H_2PO_4^-)m(OH^-)} \quad (4.7)$$



$$K_3 = \frac{m(\text{PO}_4^{3-})}{m(\text{HPO}_4^{2-})m(\text{OH}^-)} \quad (4.9)$$

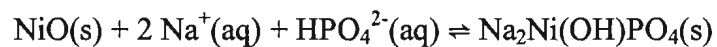


SUPCRT'92 is a software package that utilizes the HKF model presented in Section 1.3. It calculates the standard partial molal thermodynamic properties of minerals, gases and aqueous species at elevated temperatures and pressures. In this study, the same data as those used by the EPRI report and Quinlan (1996), were used for consistency between results. The program was used to calculate the thermodynamic properties for Equation (4.4), (4.6), and (4.8) from 25-300 °C, and the values are listed in Table 4.1, 4.2, and 4.3, respectively.

Figure 4.4 is a plot of log K versus temperature for the three phosphoric acid ionization reactions compared with literature data from Mesmer and Baes (1974). The agreement between the calculated data and literature data is excellent for K_1 and K_2 , but no comparison is possible in this study for K_3 because it is an extrapolation of low temperature data (Shock and Helgeson, 1988).

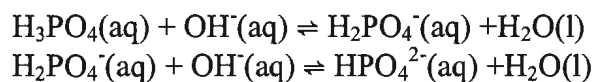
Thermodynamic properties for the dissociation of H_2O were also calculated from SUPCRT'92 and the data are listed in Table 4.4. Figure 4.5 is a plot of log K versus temperature for the calculated data compared with the literature data reported by Sweeton

Table 4.1 Experimental equilibrium constants for the SNHP formation reaction



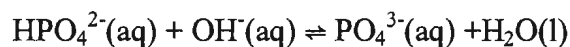
t °C	Average log Q	Average log K	Average K
243	-0.2571	2.5773	$3.779 \cdot 10^2$
245	-0.6839	2.2548	$1.798 \cdot 10^2$
250	0.4031	3.0841	$1.214 \cdot 10^3$
252	0.3619	2.6607	$4.578 \cdot 10^2$
255	-0.0124	2.9658	$9.242 \cdot 10^2$
257	0.1356	3.1103	$1.291 \cdot 10^3$
260	0.1436	3.1637	$1.457 \cdot 10^3$
265	0.5598	3.4764	$2.995 \cdot 10^3$
268	0.9847	3.7902	$6.169 \cdot 10^3$
272	0.9448	3.7904	$6.172 \cdot 10^3$
280	1.2172	4.0475	$1.116 \cdot 10^4$

Table 4.2 Standard state properties of the first and second ionizations of phosphoric acid



t °C	p bars	$d_{\text{H}_2\text{O}}$ $\text{g}\cdot\text{cm}^{-3}$	log K	$\Delta_r G^\circ$ $\text{cal}\cdot\text{mol}^{-1}$	$\Delta_r H^\circ$ $\text{cal}\cdot\text{mol}^{-1}$	$\Delta_r S^\circ$ $\text{cal}\cdot\text{mol}^{-1}\cdot\text{K}^{-1}$	$\Delta_r V^\circ$ $\text{cm}^3\cdot\text{mol}^{-1}$	$\Delta_r C_p^\circ$ $\text{cal}\cdot\text{mol}^{-1}\cdot\text{K}^{-1}$
1 st ionization								
25.00	1.000	0.997	11.825	-16133	-15240	2.9	5.5	20.2
50.00	1.000	0.988	10.972	-16224	-14789	4.3	4.0	16.5
75.00	1.000	0.975	10.261	-16347	-14395	5.5	3.3	15.2
100.00	1.013	0.958	9.662	-16498	-14019	6.5	3.2	14.9
125.00	2.320	0.939	9.152	-16673	-13645	7.5	3.3	15.1
150.00	4.757	0.917	8.714	-16873	-13265	8.4	3.8	15.3
175.00	8.918	0.892	8.336	-17094	-12882	9.3	4.5	15.3
200.00	15.536	0.865	8.008	-17337	-12499	10.1	5.3	15.5
225.00	25.479	0.834	7.721	-17599	-12108	10.9	6.2	15.9
250.00	39.736	0.799	7.469	-17880	-11726	11.7	7.2	14.2
275.00	59.431	0.759	7.247	-18176	-11484	12.1	7.5	1.6
300.00	85.838	0.712	7.043	-18471	-11870	11.5	2.6	-52.6
2 nd ionization								
25.00	1.000	0.997	6.790	-9263	-12335	-10.3	-3.7	-0.5
50.00	1.000	0.988	6.089	-9004	-12349	-10.4	-5.7	-0.7
75.00	1.000	0.975	5.489	-8744	-12372	-10.4	-6.8	-1.2
100.00	1.013	0.958	4.967	-8482	-12408	-10.5	-7.5	-1.8
125.00	2.320	0.939	4.510	-8217	-12461	-10.7	-8.1	-2.5
150.00	4.757	0.917	4.105	-7948	-12534	-10.9	-8.6	-3.3
175.00	8.918	0.892	3.743	-7675	-12627	-11.1	-9.1	-4.2
200.00	15.536	0.865	3.417	-7397	-12747	-11.3	-9.6	-5.6
225.00	25.479	0.834	3.120	-7112	-12915	-11.7	-10.4	-8.2
250.00	39.736	0.799	2.849	-6819	-13154	-12.1	-11.6	-11.5
275.00	59.431	0.759	2.597	-6515	-13456	-12.7	-13.5	-13.0
300.00	85.838	0.712	2.365	-6201	-13695	-13.1	-15.1	-3.9

Table 4.3 Standard state properties of the third ionization of phosphoric acid



t °C	p bars	d _{H2O} g·cm ⁻³	log K ₃	Δ _r G ⁰ cal·mol ⁻¹	Δ _r H ⁰ cal·mol ⁻¹	Δ _r S ⁰ cal·mol ⁻¹ ·K ⁻¹	Δ _r V ⁰ cm ³ ·mol ⁻¹	Δ _r C _p ⁰ cal·mol ⁻¹ ·K ⁻¹
25.00	1.000	0.997	1.673	-2283	-9825	-25.7	-13.9	-5.8
50.00	1.000	0.988	1.105	-1634	-9959	-26.2	-16.2	-5.2
75.00	1.000	0.975	0.612	-975	1009	-26.6	-17.7	-5.6
100.00	1.013	0.958	0.179	-306	-1024	-27.0	-18.7	-6.5
125.00	2.320	0.939	-0.205	374	-1042	-27.4	-19.7	-7.8
150.00	4.757	0.917	-0.550	1065	-1063	-28.0	-20.6	-9.1
175.00	8.918	0.892	-0.862	1768	-10875	-28.5	-21.6	-10.1
200.00	15.536	0.865	-1.148	2485	-11146	-29.1	-22.7	-11.9
225.00	25.479	0.834	-1.410	3214	-11479	-29.8	-24.1	-15.1
250.00	39.736	0.799	-1.654	3959	-11887	-30.5	-26.0	-17.4
275.00	59.431	0.759	-1.881	4719	-12247	-31.2	-27.9	-8.3
300.00	85.838	0.712	-2.089	5480	-12002	-30.7	-25.1	48.4

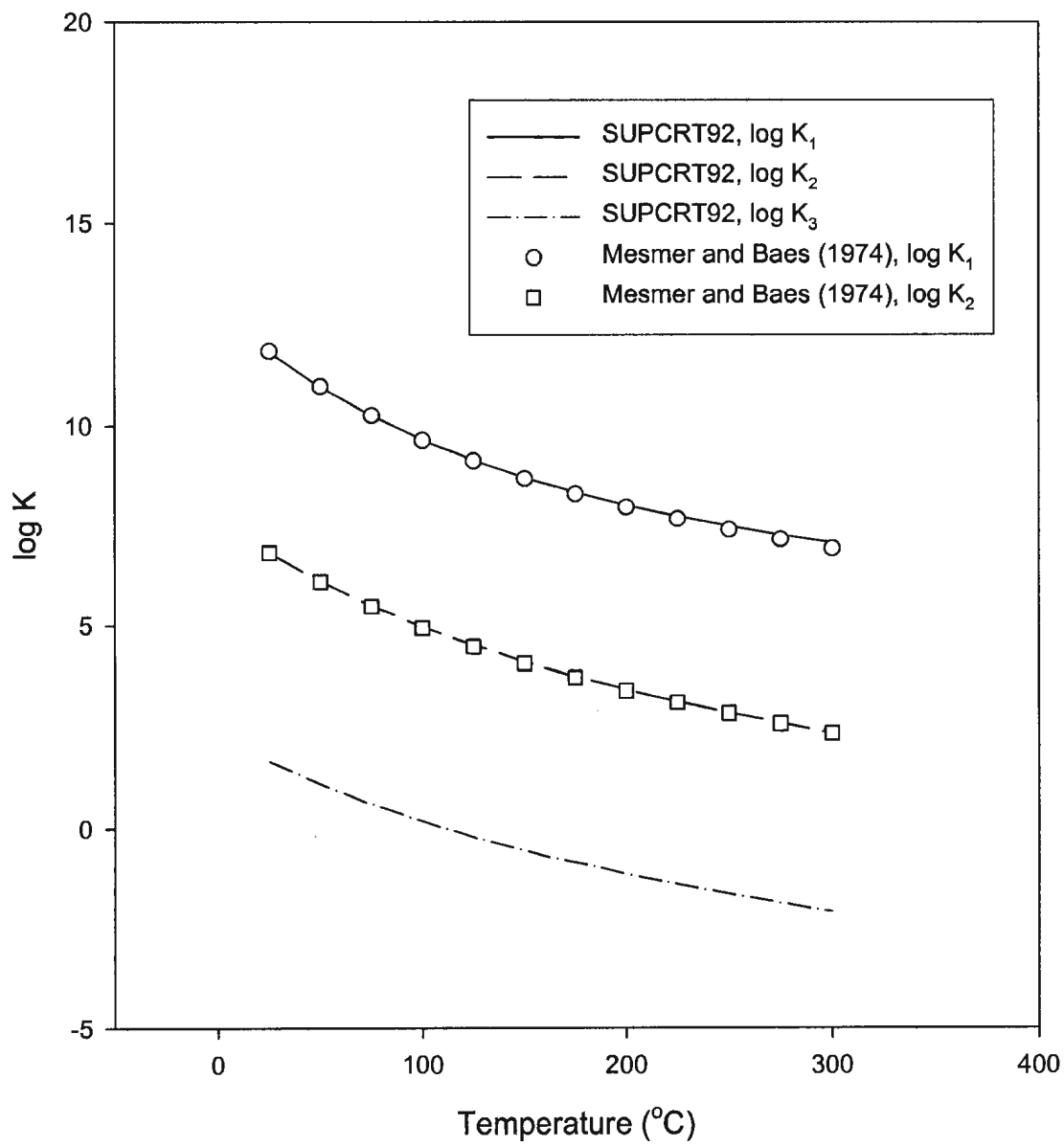
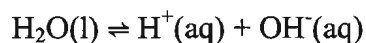


Figure 4.4: Phosphate ionization equilibria calculated from SUPCRT'92 and literature data from Mesmer and Baes, 1974.

Table 4.4 Standard state properties of the dissociation of water



t °C	p bars	$d_{\text{H}_2\text{O}}$ $\text{g}\cdot\text{cm}^{-3}$	$\log K_w$	$\Delta_r G^\circ$ $\text{cal}\cdot\text{mol}^{-1}$	$\Delta_r H^\circ$ $\text{cal}\cdot\text{mol}^{-1}$	$\Delta_r S^\circ$ $\text{cal}\cdot\text{mol}^{-1}\cdot\text{K}^{-1}$	$\Delta_r V^\circ$ $\text{cm}^3\cdot\text{mol}^{-1}$	$\Delta_r C_p^\circ$ $\text{cal}\cdot\text{mol}^{-1}\cdot\text{K}^{-1}$
25.00	1.000	0.997	-27.990	38185	26680	-38.5	-45.6	-101.2
50.00	1.000	0.988	-26.541	39245	24391	-45.9	-44.5	-85.4
75.00	1.000	0.975	-25.406	40472	22305	-52.1	-45.6	-82.9
100.00	1.013	0.958	-24.510	41849	20196	-58.0	-48.4	-86.7
125.00	2.320	0.939	-23.806	43370	17933	-63.9	-52.9	-95.1
150.00	4.757	0.917	-23.262	45039	15409	-70.0	-59.6	-107.8
175.00	8.918	0.892	-22.854	46864	12520	-76.6	-69.1	-125.4
200.00	15.536	0.865	-22.567	48858	9081	-84.0	-82.5	-154.6
225.00	25.479	0.834	-22.394	51045	4719	-93.0	-102.4	-204.6
250.00	39.736	0.799	-22.335	53465	-1149	-104.4	-134.1	-287.0
275.00	59.431	0.759	-22.398	56179	-9368	-119.6	-186.9	-422.7
300.00	85.838	0.712	-22.600	59271	-21427	-140.8	-278.5	-680.6

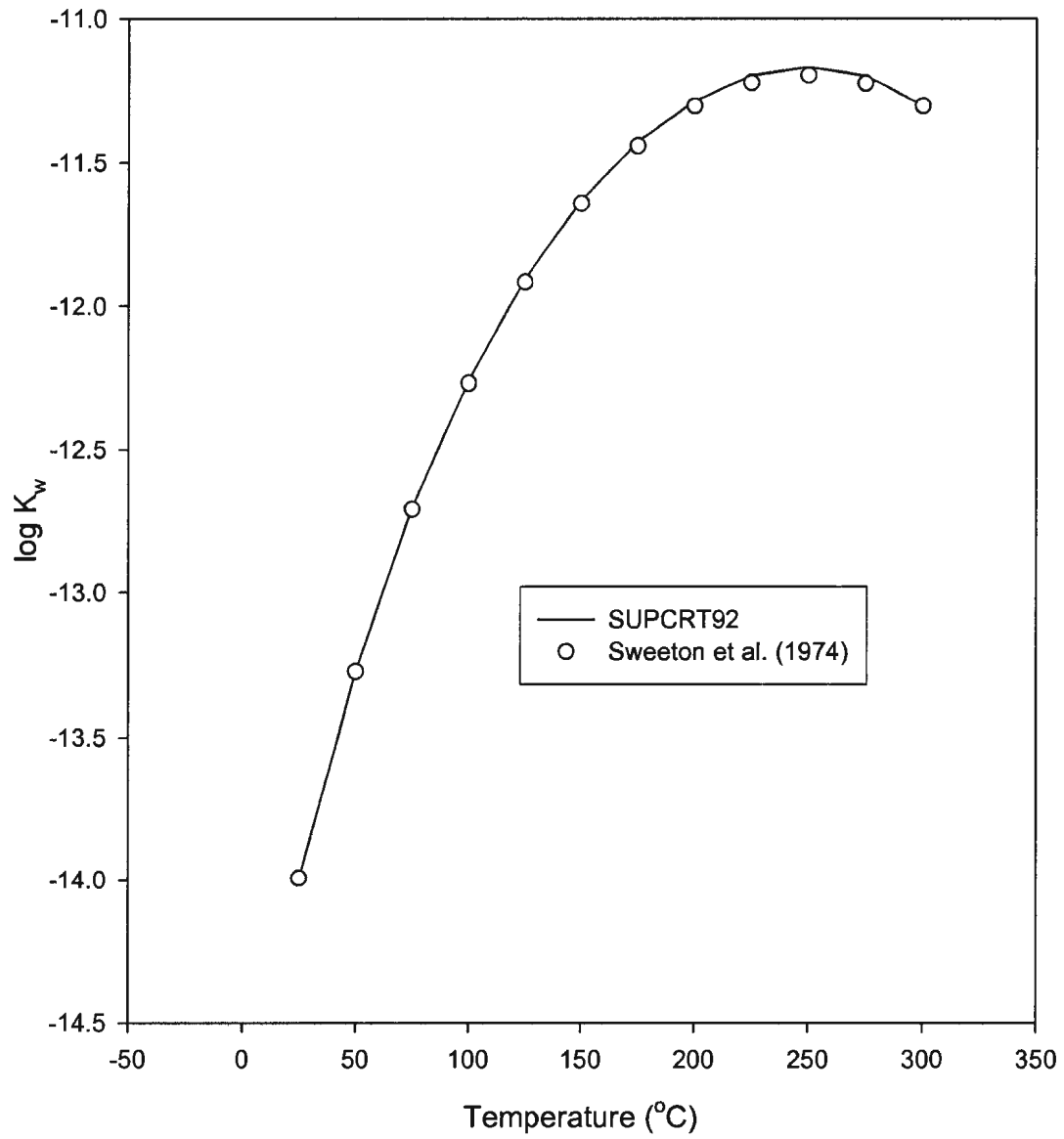


Figure 4.5: Water ionization equilibria calculated from SUPCRT'92 and literature data from Sweeton et al., 1974.

et al. (1974) and the agreement is again excellent. A difference plot of the agreement between calculated and literature data is shown in Figure 4.6. The relative difference plot shows that the highest percent difference is only ~2.1 %.

Data from SUPCRT'92 for other species used in our study are tabulated in Tables 4.5, 4.6, and 4.7. The standard state properties are listed in Table 4.5. Table 4.6 lists the HKF equation of state coefficients for these species and Table 4.7 contains the Maier-Kelley coefficients for nickel oxide and SNHP.

4.3.2 Equilibrium Constants and Thermodynamic Properties of SNHP

Once the equilibrium concentrations of total sodium and total phosphorus from solubility and kinetic measurements were converted to units of molality, MULTEQ was used to calculate the composition concentrations of relevant species at each temperature studied. The activity coefficient model described in Section 1.4, that incorporates the Meissner equation used in MULTEQ, was used to calculate the equilibrium constants for Equation (4.1) according to the following equation:

$$\ln K_{eq} = \ln Q + \ln \left(\frac{1}{(\gamma_{Na^+})^2 (\gamma_{HPO_4^{2-}})} \right) \quad (4.11)$$

$$\text{where } Q = \frac{1}{m(Na^+)^2 m(HPO_4^{2-})}$$

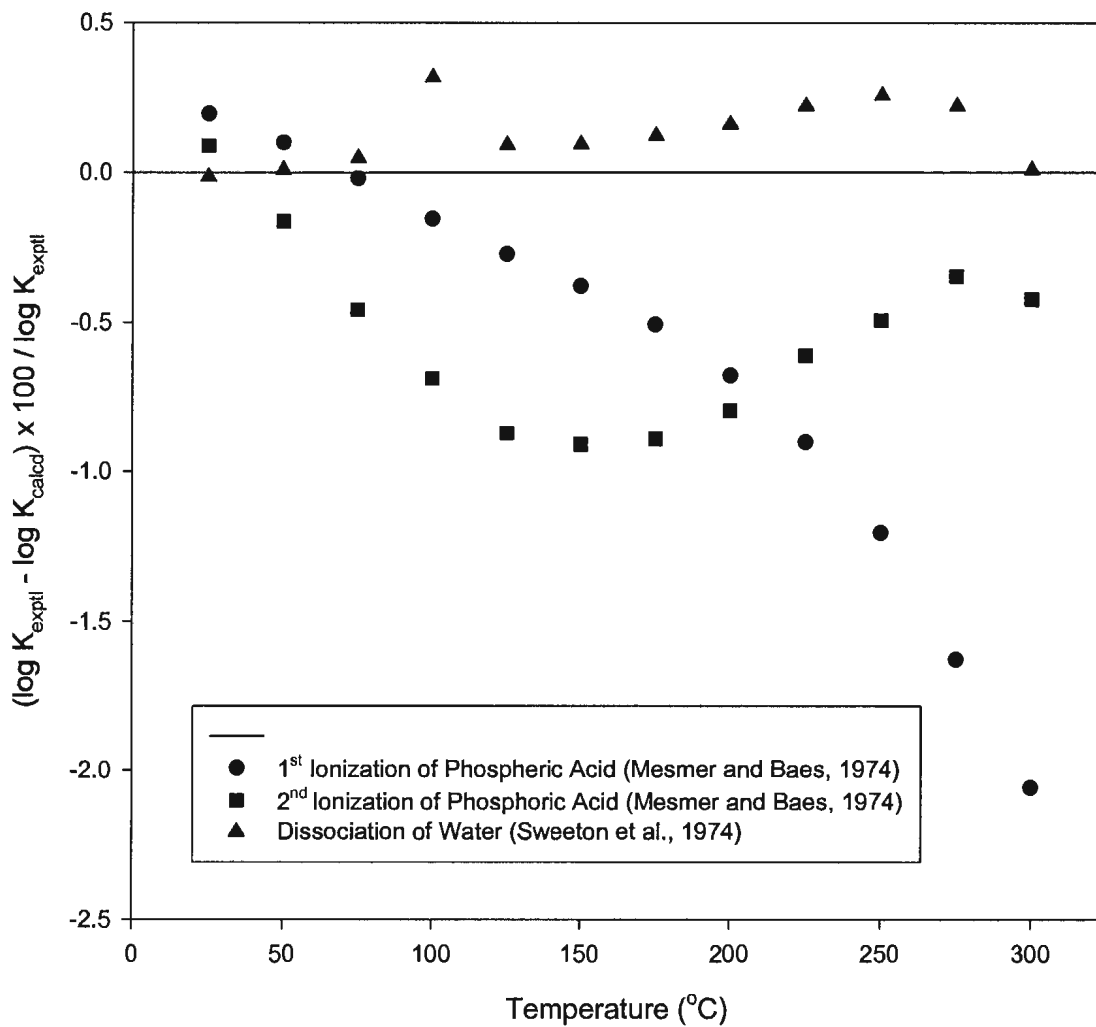


Figure 4.6: The relative difference between experimental values of log K (Mesmer and Baes, 1973; Sweeton et al., 1973) and those calculated from SUPCRT'92

Table 4.5 Standard state properties of aqueous species at 25 °C and 1 bar

	$\Delta_r G^\circ$ cal·mol ⁻¹	$\Delta_r H^\circ$ cal·mol ⁻¹	S° cal·mol ⁻¹ ·K ⁻¹	V° cm ³ ·mol ⁻¹	C_p° cal·mol ⁻¹ ·K ⁻¹
H ₃ PO ₄ (aq)	-273100	-307920	38.000	48.2	23.6
H ₂ PO ₄ ⁻ (aq)	-270140	-309820	21.600	30.9	-6.9
HPO ₄ ²⁻ (aq)	-260310	-308815	-8.000	4.4	-58.0
PO ₄ ³⁻ (aq)	-243500	-305300	-53.000	-32.3	-114.3
Na ⁺ (aq)	-62591	-57433	13.960	-1.2	9.1
H ⁺ (aq)	0	0	0	0	0
OH ⁻ (aq)	-37595	-54977	-2.560	-4.7	-32.6
H ₂ O (l)	-56688	-68317	16.712	18.1	18.0
NiO (s)	-50573	-57300	9.080	10.970	10.6
SNHP(s)	431661	468325	56.778	-	48.766

Table 4.6 HKF equation of state coefficients for aqueous species^a

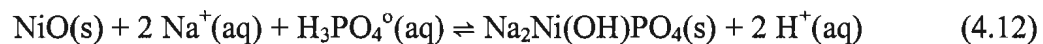
	$a_1 \times 10^1$	$a_2 \times 10^{-2}$	a_3	$a_4 \times 10^{-4}$	c_1	$c_2 \times 10^{-4}$	$\omega \times 10^{-5}$
H ₃ PO ₄ (aq)	8.2727	12.4182	0.8691	-3.2924	17.9708	1.7727	-0.2200
H ₂ PO ₄ ⁻ (aq)	6.4875	8.0594	2.5823	-3.1122	14.0435	-4.4605	1.3003
HPO ₄ ²⁻ (aq)	3.6315	1.0857	5.3233	-2.8239	2.7357	-14.9103	3.3363
PO ₄ ³⁻ (aq)	-0.5259	-9.0654	9.3131	-2.4042	-9.4750	-26.4397	5.6114
Na ⁺ (aq)	1.8390	-2.285	3.2560	-2.7260	18.1800	2.9810	0.3306
H ⁺ (aq)	0	0	0	0	0	0	0
OH ⁻ (aq)	1.2527	0.0738	1.8423	-2.7821	4.1500	-10.3460	1.7246

^a Units: a_1 , cal·mol⁻¹·bar⁻¹; a_2 , cal·mol⁻¹; a_3 , cal·K·mol⁻¹·bar⁻¹; a_4 , cal·K·mol⁻¹; c_1 , cal·mol⁻¹·K⁻¹; c_2 , cal·K·mol⁻¹; ω , cal·mol⁻¹.

Table 4.7 Maier-Kelley coefficients for heat capacities of solids

	a cal·mol ⁻¹ ·K ⁻¹	b x 10 ³ cal·mol ⁻¹ ·K ⁻²	c x 10 ⁻⁵ cal·mol ⁻¹ ·K ⁻¹	Temperature of transition (° K)
NiO (s)	-4.99	37.58	3.89	-
Bunsenite (s)	-4.99	37.58	3.89	525
	13.88	0.0	0.0	565
	11.18	2.02	0.0	-
SNHP (s)	48.766	0.0	0.0	-

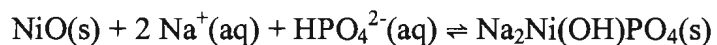
Equilibrium constants are listed in Table 4.8. Equation (4.1) is not an isocoulombic reaction, meaning that $\Delta_r C_p^\circ$ is not independent of temperature. Because the temperature-dependence of C_p° for aqueous ions is highly asymmetric, the data are very difficult to fit. Thus an isocoulombic reaction equation is desirable so that, even though $\Delta_r C_p^\circ$ is not equal to zero, it is approximately independent of temperature (Mesmer et al., 1988). This can be accomplished by adding the first and second ionizations of phosphoric acid, Equations (4.4) and (4.6) respectively, and two equivalents of the water dissociation reaction in Equation (4.10), to the experimental Equation (4.1) results calculated in this study. This results in new equilibrium constants for the following isocoulombic reaction:



The equilibrium constants for Equation (4.12) are listed in Table 4.9.

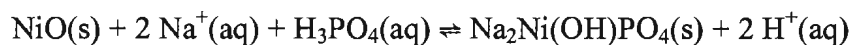
SNHP was not synthesized as a pure solid in this study; therefore no calorimetric measurements could be performed in order to obtain an experimental heat capacity of SNHP. Thus we used another method to find $C_p^\circ(\text{SNHP})$ in order to calculate a value for the heat capacity of the reaction. The value for the heat capacity of SNHP was calculated using a method by Qui and White (2001), called the “constituent additivity” model. In this method, the heat capacities of inorganic salts are calculated from additivity of the experimental heat capacities of the appropriate proportions of their

Table 4.8 Experimental data calculations for the SNHP formation reaction



t °C	ln Q	I mol·kg ⁻¹	$\gamma_{\pm}(\text{Na}^+)$	$\gamma_{\pm}(\text{HPO}_4^{2-})$	ln K
235	-2.5841	3.7398	0.3521	0.01537	3.6788
240	-1.8436	2.9115	0.3360	0.01275	4.6995
243	-0.5919	1.9406	0.3370	0.01289	5.9345
245	-1.5748	2.7250	0.3238	0.01099	5.1918
250	0.9265	1.1247	0.3499	0.01500	7.2276
252	-0.8334	2.0967	0.3135	0.00966	6.1264
255	-0.0286	1.5913	0.3189	0.01034	6.8289
257	0.3123	1.4587	0.3192	0.01039	7.1632
260	0.3307	1.4305	0.3138	0.00970	7.2840
265	1.2889	1.0090	0.3265	0.01136	8.0048
268	2.2674	0.7802	0.3407	0.01348	8.7273
272	2.1755	0.7518	0.3355	0.01267	8.7277
280	2.8026	0.6085	0.3375	0.01298	9.3196

Table 4.9 Equilibrium constants for the isocoulombic reaction



t °C	1 st ionization log K ₁	2 nd ionization log K ₂	Water Dissociation log K _w	Iso- coulombic log K	Iso- coulombic K
235	7.6170	3.0090	-11.1780	-10.1336	7.352·10 ⁻¹¹
240	7.5660	2.9550	-11.1720	-9.7830	1.648·10 ⁻¹⁰
243	7.5370	2.9220	-11.1700	-9.3029	4.979·10 ⁻¹⁰
245	7.5170	2.9010	-11.1690	-9.6644	2.166·10 ⁻¹⁰
250	7.4690	2.8490	-11.1670	-8.8778	1.325·10 ⁻⁰⁹
252	7.4510	2.8280	-11.1680	-9.3963	4.015·10 ⁻¹⁰
255	7.4230	2.7970	-11.1690	-9.1523	7.042·10 ⁻¹⁰
257	7.4040	2.7760	-11.1700	-9.0480	8.954·10 ⁻¹⁰
260	7.3770	2.7460	-11.1720	-9.0587	8.736·10 ⁻¹⁰
265	7.3330	2.6960	-11.1790	-8.8530	1.403·10 ⁻⁰⁹
268	7.3070	2.6660	-11.1840	-8.6054	2.481·10 ⁻⁰⁹
272	7.2720	2.6270	-11.1920	-8.6951	2.018·10 ⁻⁰⁹
280	7.2050	2.5490	-11.2140	-8.6253	2.370·10 ⁻⁰⁹

simple “constituent” compounds. For SNHP, the calculation is represented by the following equations:

$$C_p^\circ = \sum nC_p^\circ(\text{oxides}) \quad (4.13)$$

$$C_p^\circ = (1)C_p^\circ(\text{Na}_2\text{O}) + (0.25)C_p^\circ(\text{P}_4\text{O}_{10}) + (1)C_p^\circ(\text{NiO}) + (0.5)C_p^\circ(\text{H}_2\text{O}) \quad (4.14)$$

It was found that this model gives reasonably accurate heat capacity at or above about 150 K, provided that the coordination within the constituent solids is similar to the complex solids and there are no solid-solid phase transitions. The heat capacity value calculated for SNHP using this method is $C_p^\circ = 48.766 \text{ cal}\cdot\text{K}^{-1}\cdot\text{mol}^{-1}$.

Once the equilibrium constants for the isocoulombic reaction were calculated, the following equation was fitted to the data:

$$\ln K_{T_2} = \ln K_{T_1} - \frac{\Delta_r H^\circ}{R} \left(\frac{1}{T_2} - \frac{1}{T_1} \right) + \frac{\Delta_r C_p^\circ}{R} \left[\ln \left(\frac{T_2}{T_1} \right) + \frac{T_1}{T_2} - 1 \right] \quad (4.15a)$$

Here, $\ln K_{T_1}$ and $\Delta_r H_{T_1}^\circ$ were used as fitting parameters whereas $\Delta_r C_p^\circ$ was fixed at the room temperature value of $\Delta_r C_p^\circ = -0.134 \text{ cal}\cdot\text{mol}^{-1}\cdot\text{K}^{-1}$ (from Table 4.5). The extended van't Hoff plot is shown in Figure 4.7. The activity coefficient model works best at 250 °C, giving us a more accurate value for the equilibrium constant (Tremaine et al, 2002), thus the reference temperature was set at that temperature ($T_1 = 523.15 \text{ K}$). In our

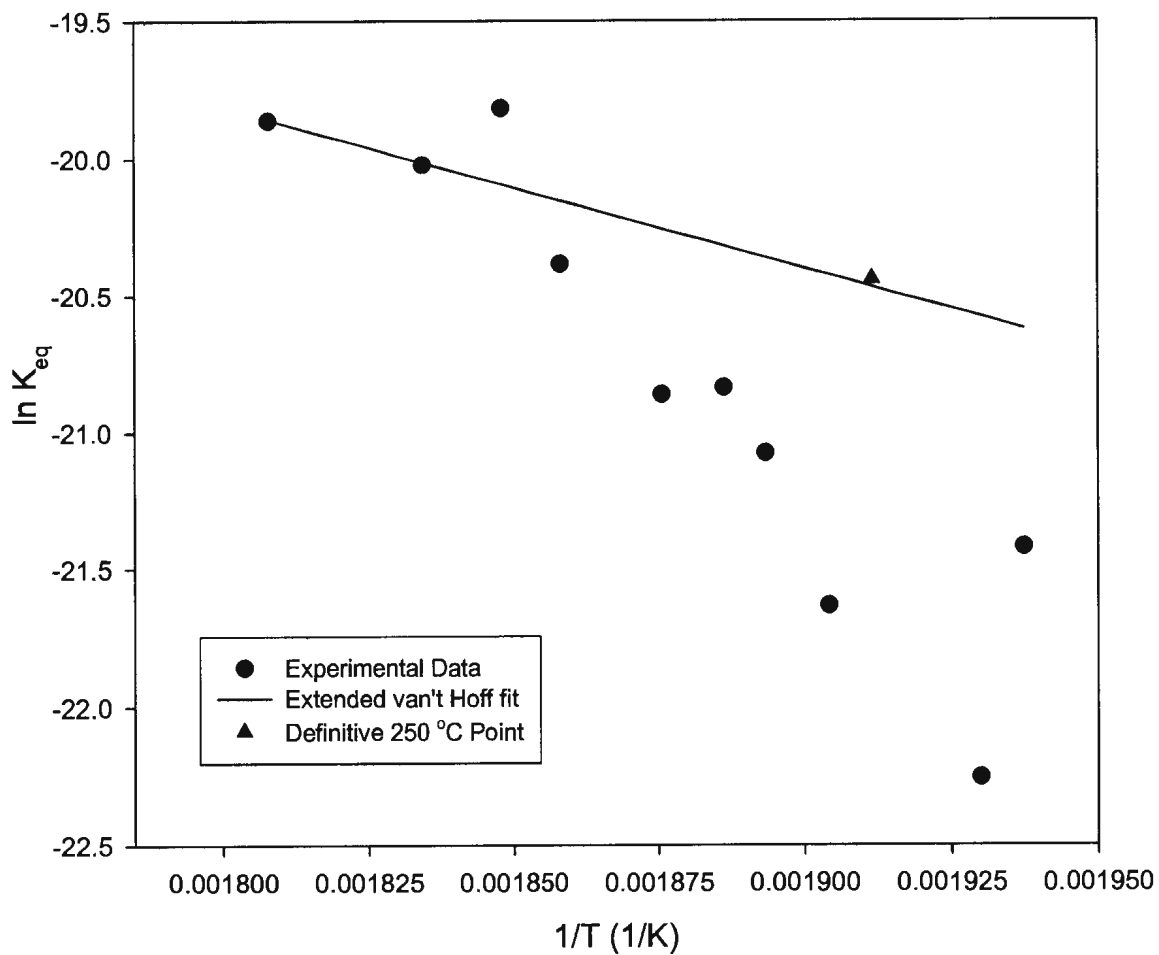
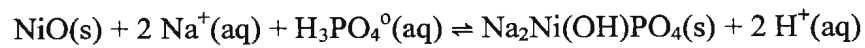


Figure 4.7: Extended van't Hoff plot of the isocoulombic reaction



solubility runs, we used the same equilibration time, 48 hrs, as that used by Quinlan (1996) for SIHP but, from our kinetic studies, it was determined that 75 hours was needed for the reaction to equilibrate at 250 °C. Therefore the best definitive solubility point was obtained from the careful kinetic experiments at 250 °C, in which equilibrium was approached from conditions of super-saturation and under-saturation. Thus the curve fit was forced to go through this data point. Furthermore, the data points at 235 and 240 °C were deleted from the curve fitting because the activity coefficients have larger errors associated with them and the reaction may not have been at equilibrium. From the plot in Figure 4.7, it can be seen that the fit also gave good agreement at the higher temperatures (t = 252 °C – 280 °C).

Equation (4.15a) with the fitted and fixed parameters included takes the form:

$$\ln K_{T_2} = -20.4691 - \frac{11730.4845}{R} \left(\frac{1}{T_2} - \frac{1}{523.15} \right) + \frac{-0.134}{R} \left[\ln \left(\frac{T_2}{523.15} \right) + \frac{523.15}{T_2} - 1 \right] \quad (4.15b)$$

From these data-fitting results, the values $\ln K = -20.4691$ and $\Delta_r H^\circ = 11730.5 \text{ cal}\cdot\text{mol}^{-1}$ at 250 °C were obtained. The value of $\ln K = -29.0191$ at 25 °C was found by extrapolation. Since $\Delta_r C_p^\circ$ was assumed independent of temperature, the value of $\Delta_r H^\circ = 11760.6 \text{ cal}\cdot\text{mol}^{-1}$ at 25 °C could be calculated from the equation:

$$\Delta_r H_{T_2}^\circ = \Delta_r H_{T_1}^\circ - (\Delta_r C_p^\circ)(T_1 - T_2) \quad (4.16)$$

where $T_1 = 523.15$ K and $T_2 = 298.15$ K. The remaining thermodynamic properties of SNHP were calculated using well known thermodynamic equations found in Section 1.3.1.

Once the standard state properties of SNHP were calculated, they were entered into the SUPCRT'92 database and the thermodynamic program was used to calculate the equilibrium constants and Gibb's free energies of the reaction in Equation (4.1). Figure 4.8 shows a comparison of the experimental and calculated results for this study. Table 4.10 contains the calculated results for SNHP formation from SUPCRT'92.

4.4 Comparison With Data From Other Workers

Ziemniak and Opalka (1988) reported solubility data for SNHP at two separate Na/PO₄ mole ratios, 2.2 and 2.5, over temperatures within the range of 256-296 °C. Unlike the present study, the reaction was only allowed to equilibrate for 4 to 16 hours at each measurement temperature before a sample was taken. From our kinetic studies, it was determined that this is not enough time for the reaction to reach completion. Also, calculations were performed using differing methods. Ziemniak and Opalka (1988) calculated equilibrium constants using the extended Debye-Huckel equation. In comparing the Ziemniak and Opalka (1998) data with those obtained in this study, the reported raw data had to be re-calculated using the same activity coefficient model used in this work. Figure 4.9 shows a comparison of the experimental and calculated

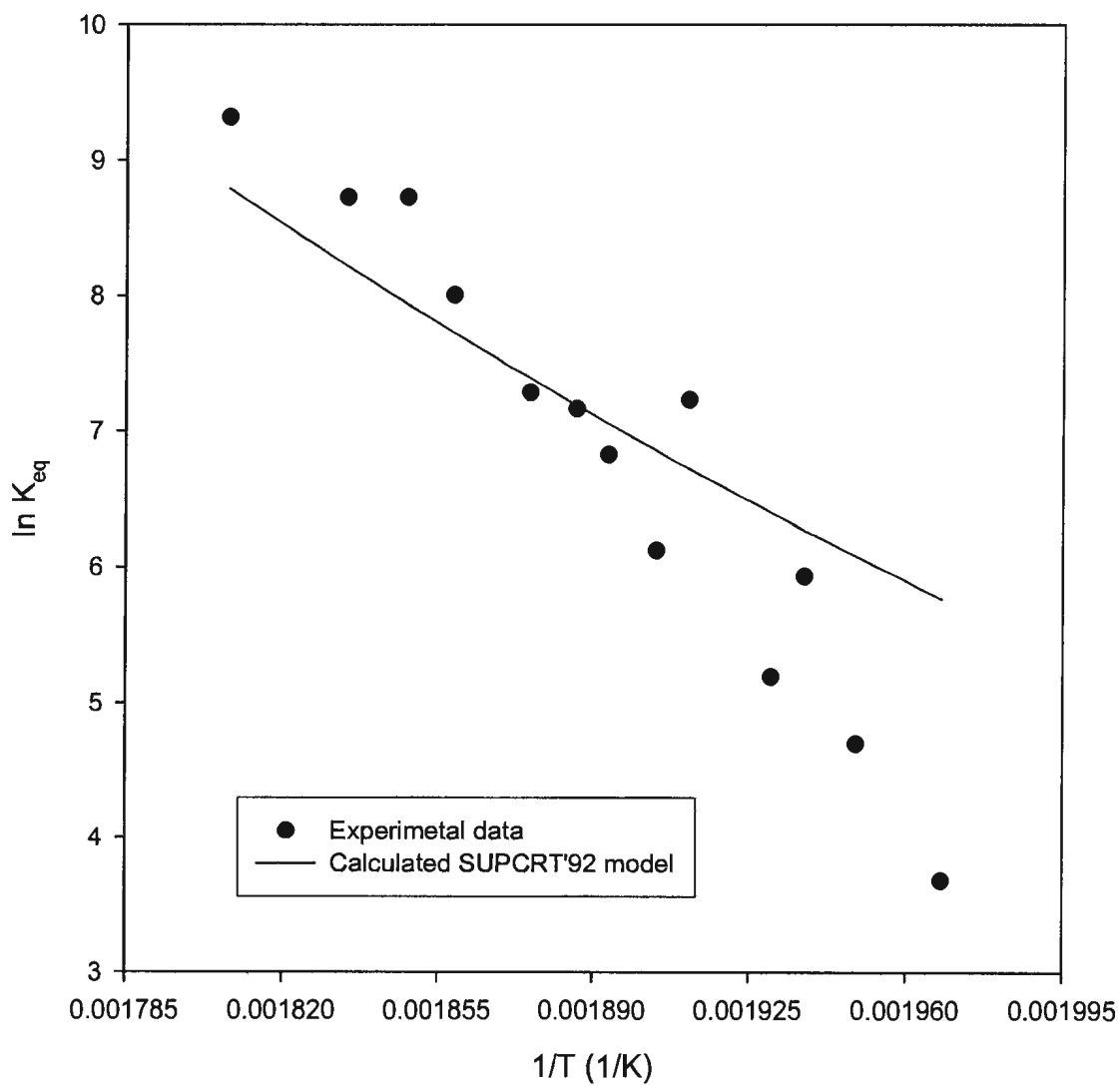


Figure 4.8: Comparison of experimental data and values calculated from SUPCRT'92 for the SNHP formation reaction

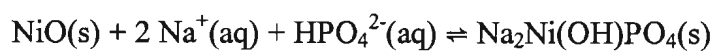
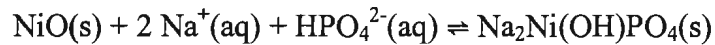


Table 4.10 Standard state properties of the SNHP formation reaction



t °C	p bars	d _{H₂O} g·cm ⁻³	log K	Δ _r G ^o cal·mol ⁻¹	Δ _r H ^o cal·mol ⁻¹	Δ _r S ^o cal·mol ⁻¹ ·K ⁻¹	Δ _r V ^o cm ³ ·mol ⁻¹	Δ _r C _p ^o cal·mol ⁻¹ ·K ⁻¹
25.00	1.000	0.997	-3.228	4404	12656	27.8	-12.9	77.9
50.00	1.000	0.988	-2.460	3637	14362	33.3	-14.4	62.2
75.00	1.000	0.975	-1.725	2747	15873	37.8	-13.7	60.1
100.00	1.013	0.958	-1.024	1749	17417	42.1	-11.2	64.4
125.00	2.320	0.939	-0.353	642	19129	46.5	-6.8	73.5
150.00	4.757	0.917	0.300	-580	21121	51.4	-0.1	87.1
175.00	8.918	0.892	0.941	-1930	23502	56.8	9.6	106.1
200.00	15.536	0.865	1.582	-3426	26475	63.3	23.6	137.9
225.00	25.479	0.834	2.236	-5097	30458	71.4	44.7	193.0
250.00	39.736	0.799	2.921	-6992	36098	82.4	78.8	284.1
275.00	59.431	0.759	3.661	-9182	44319	97.7	136.5	432.8
300.00	85.838	0.712	4.485	-11762	56694	119.5	236.5	710.8

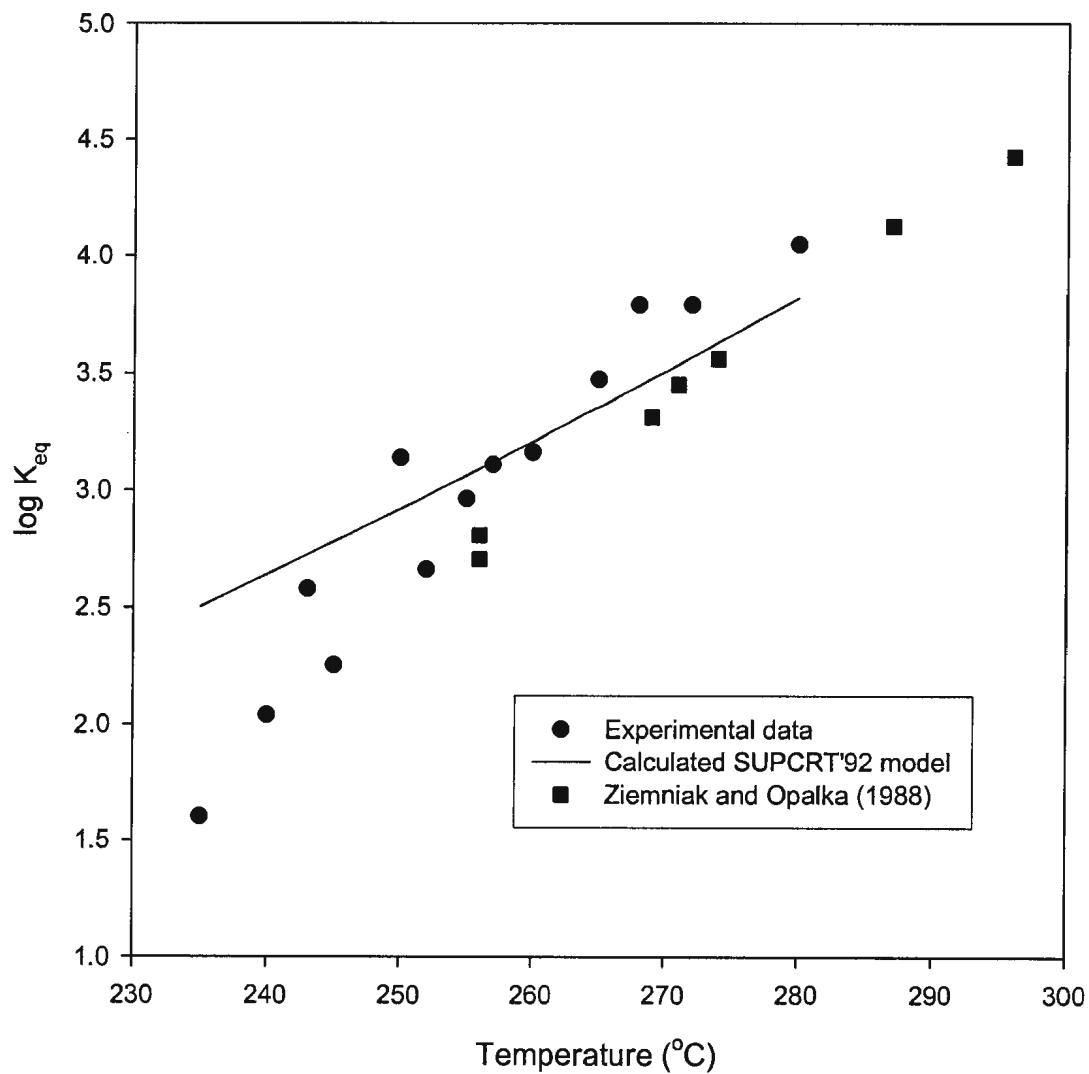
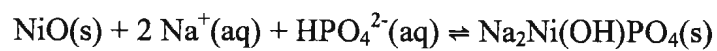


Figure 4.9: Comparison of experimental and equilibrium constants calculated from SUPCRT'92 model with those of Ziemniak and Opalka (1988) for the SNHP formation reaction



equilibrium constants obtained in this work with those of Ziemniak and Opalka (1988), and Figure 4.10 compares the Gibbs free energy of each. While the values at the highest temperatures compare well, those at lower temperature do not.

The Gibbs free energy and enthalpy of formation of $\text{Na}_2\text{Ni}(\text{OH})\text{PO}_4$ reported by Ziemniak and Opalka (1988) were $\Delta_f G_{298}^\circ = -415.7266$ and $\Delta_f H_{298}^\circ = -430.2103$ $\text{kcal}\cdot\text{mol}^{-1}$ respectively. Those obtained from this study were $\Delta_f G_{298}^\circ = -431.6615$ and $\Delta_f H_{298}^\circ = -468.3254$ $\text{kcal}\cdot\text{mol}^{-1}$. The discrepancy is undoubtedly due to lack of equilibration in this study and those of Ziemniak and Opalka (1988), at temperatures below 250 °C.

4.5 Future Work

The work presented in this study has provided reliable solubility data for the formation of SNHP under boiler conditions and from which thermodynamic data were calculated at 250 °C.

While the value of $\Delta_f G^\circ(\text{SNHP})$ and the equilibrium constant for Equation (4.1) have been accurately determined, our value of the enthalpy $\Delta_f H^\circ(\text{SNHP})$ contains more uncertainty. Further work should be done to obtain more accurate parameters for SNHP, by measuring solubility data over a wider range of temperatures or at more temperatures within the 235-280 °C range investigated in this study. Allowing at least ~75 hours for equilibrium to be reached at each sample temperature would give more reliable results,

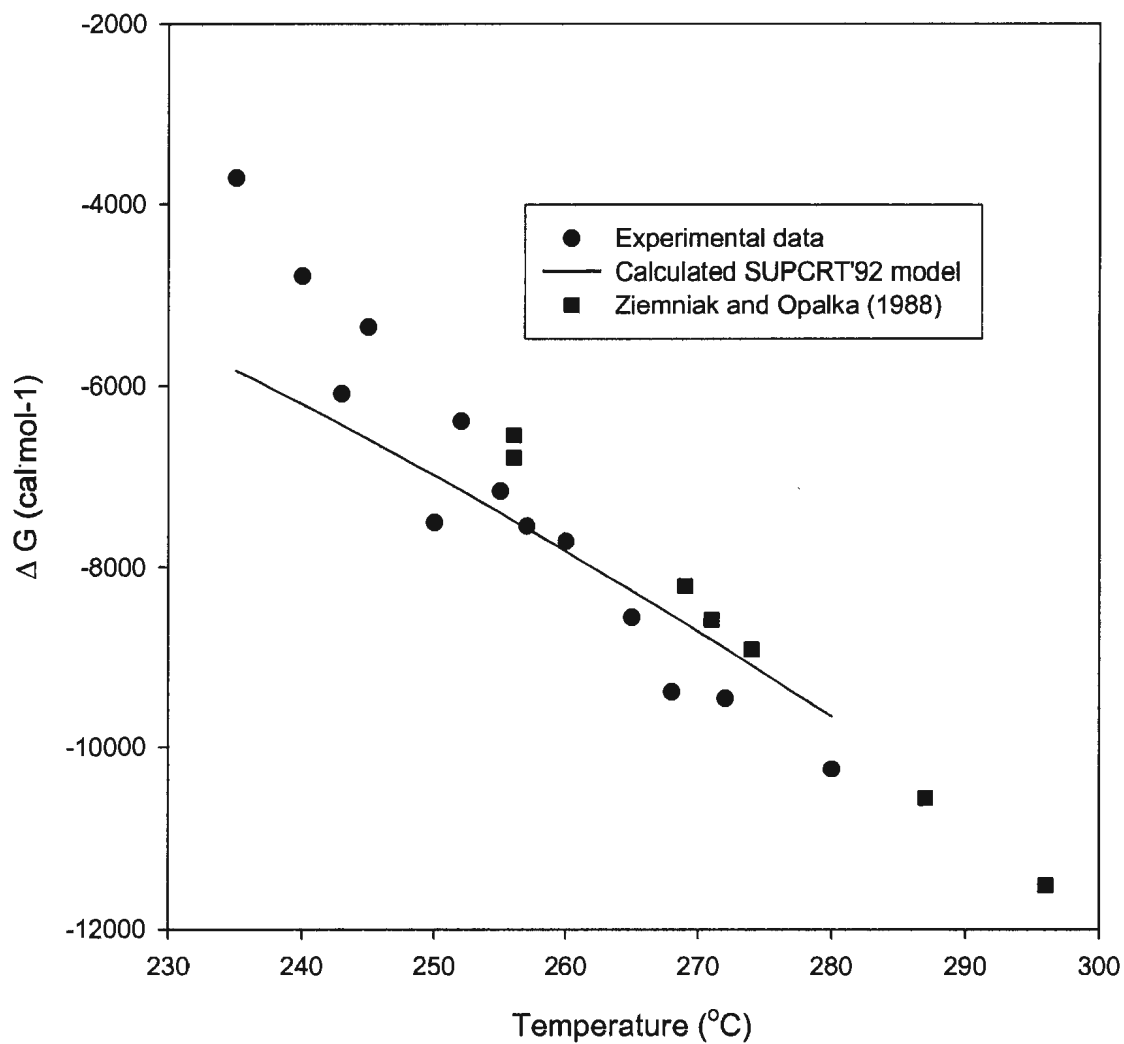
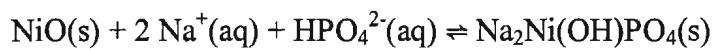


Figure 4.10: Comparison of experimental and Gibbs free energy data calculated from SUPCRT'92 model with those of Ziemniak and Opalka (1988) for the SNHP formation reaction



and a kinetic study should be carried out at temperatures below 250 °C since the reaction is slower at these temperatures.

In fitting a model to the experimental data, a fixed value was used for the heat capacity of the reaction based on the estimated value for that of SNHP. If a sufficiently pure sample of SNHP could be synthesized, an experimental value for $C_p(\text{SNHP})$ should be determined from calorimetric studies. This would improve the reliability of the fitted curve, and thus the thermodynamic parameters obtained from it.

5.0 CONCLUSIONS

The synthesis of maricite developed by Quinlan (1996) was shown to be reproducible and is a reliable hydrothermal means of synthesizing single crystals of maricite. SIHP crystals were also synthesized under conditions similar to the maricite synthesis but at a much higher sodium phosphate mole ratio than in the studies done by Quinlan (1996). Larger SIHP crystals were obtained from two different chelate decomposition reactions but future work on these reactions could include trying the synthesis at a higher Na/PO₄ mole ratio.

It can be concluded from this study that ammonium-iron-phosphate reaction products can form under boiler conditions. The synthesis of (NH₄)Fe^{II}Fe^{III}(PO₄)₂ by Boudin and Lii (1998) was repeated under conditions similar to those seen in boilers, and single crystals were synthesized, providing a new simpler synthesis for (NH₄)Fe^{II}Fe^{III}(PO₄)₂. Another ammonium iron phosphate hideout product that can indeed be formed at temperatures below 300 °C is (NH₄)Fe^{II}(PO₄)·H₂O. This is a new synthesis for this compound.

The sodium-nickel-phosphate hideout product originally reported by Ziemniak and Opalka (1988) was synthesized both from NiO and the decomposition of H⁺[NiNTA⁻] under boiler conditions. Although no pure samples of SNHP were obtained from either set of experiments, an alternative starting material to use in the future could be NaNiNTA. Since there is no H⁺ to neutralize, it may be used to synthesize SNHP at a

lower Na/PO₄ mole ratio than the reactions with H⁺[NiNTA⁻] in this study. Also, it provides another source of sodium for the reaction.

Equilibrium solubility data and kinetic data for the formation of Na₂Ni(OH)PO₄ have been obtained at boiler conditions from 235 to 280 °C. Ziemniak and Opalka (1988) also provided solubility and thermodynamic data for SNHP and the solubility work performed in this study has provided additional solubility data for the formation of SNHP under boiler conditions and a preliminary entry for the reaction product in the thermodynamic database. The thermodynamic model gives good agreement with the experimental data collected considering the limited amount of solubility data obtained in our study.

6.0 BIBLIOGRAPHY

Alexander J.H., and Luu L. (1989) MULTEQ: Equilibrium of an electrolyte solution with vapor-liquid partitioning and precipitation, Vol I. Users Manual, *EPRI Report NP-5561-CCM*.

Anderson G.M., and Crerar D.A. (1993) *Thermodynamics in Geochemistry- The Equilibrium Model*, Oxford University Press, New York, NY.

Ashoff A.F., Lee Y.H., Sopocy D.M., and Jonas O. (1986) Interim consensus guidelines on fossil cycle chemistry, *EPRI Report CS 4629*.

Atkins, P.W. (1993) *The Elements of Physical Chemistry*, W. H. Freeman and Company, New York.

Baes C.F., and Lindsay W.T. (1996) Modeling the formation of variable-composition liquid or solid phases in MULTEQ, *Proceedings of Conference on Improving the Understanding and Control of Corrosion on the Secondary Side Of Steam Generators*, Virginia R.W., Staehle W., Gorman J.A. and McIlree A.r. eds, NACE International, Houston, pp 577-600.

Balakrishnan P.V. (1977) A study of phosphate hide-out from boiling water, *Can. J. Chem. Eng.* **55**, 592-596.

Barrer, R.M. (1948) Syntheses and reactions of mordenite, *J. Chem. Soc.*, 2158.

Bell, C.F. (1977) *Principles and Applications of Metal Chelation*, Clarendon Press, Oxford.

Benson S.W. (1968) *Thermochemical Kinetics*, Wiley, New York, NY.

Blesa M.A., Morando P.J., and Regazzoni, A.E. (1994) *Chemical Dissolution of Metal Oxides*, CRC Press, Boca Raton, FL.

Booy M., and Swaddle T.W. (1978) Hydrothermal preparation of magnetite from iron chelates, *Can. J. Chem.* **56**, 402-403.

Boudin S., and Lii K.H. (1998) Ammonium iron(II,III) phosphate: Hydrothermal synthesis and characterization of $\text{NH}_4\text{Fe}_2(\text{PO}_4)_2$, *Inorg. Chem.* **37**, 799-803.

Bridson J.N., Quinlan S., and Tremaine P.R. (1998) Synthesis and crystal structure of maricite and sodium iron(III) hydroxyl phosphate, *Chem. Materials* **10**, 763-768.

Broadbent D., Lewis G.G., and Wetton E.A.M. (1977) Phase equilibria in aqueous sodium phosphate solution at elevated temperatures, *J.Chem. Soc. Dalton Trans.* **5**, 564-468.

Broadbent D., Lewis G.G., and Wetton E.A.M. (1978) High-temperature phosphate chemistry, Part IV Corrosion of mild steel in sodium phosphate solutions at 250, 300, and 350°C, *CEGB Research Reoprt NW/SD/RR/67/78*.

Broadbent D., Lewis G.G., and Wetton E.A.M. (1978) The chemistry of high temperature phosphate solutions in relation to steam generation, *Proc. BNES Conf. Water Chem. Nuclear Reactor Systems* (London) pp. 53-62.

Bursik L. (2002) Once-through boiler as an autoclave for testing and organic cycle treatment chemical, *PowerPlant Chemistry* **4(2)**, 81-85.

Byrappa K. (1994) Hydrothermal growth of crystals, *Handbook of Crystal Growth*, Hurle, D.T.J., ed, Elsevier Science B.V., England, pp. 465-562.

Byrappa K., and Yoshimura M. (2001) *Handbook of Hydrothermal Technology*, William Andrew Publishing, New York, NY.

Chang, H.C., Healy, T.W., and Matijevic, E. (1983) Interactions of Metal Hydrous Oxides with Chelating Agents: III. Adsorption on Spherical Colloidal Hematite Particles, *J. Colloid Interface Sci.*, **92**, 469-478.

Chang, H.C., and Matijevic, E. (1983) Interactions of Metal Hydrous Oxides with Chelating Agents: IV. Dissolution of Hematite, *J. Colloid Interface Sci.*, **92**, 479-488.

Connor W.M., and Panson A.J. (1983) Investigation of phosphate-sludge interactions, *EPRI Report NP-2963*.

Daidouh A., Martinez J.L., Pico C., and Veiga M.L. (1999) Structure characterization and magnetic behaviour of $\text{NaNi}_4(\text{PO}_4)_3$ and $\text{KMn}_4(\text{PO}_4)_3$, *J. Solid State Chem.* **144**, 169-174.

Dooley R.B., and McNaughton W. (1996) Boiler tube failures, theory and practice, *EPRI Technical Report TR 105261*, Vol 2, Chapter 16.

Dooley R.B., Goodstine S., Jonas O., Pocock F., Rice J., and Stodola J. (1994) Cycle chemistry guidelines for fossil plants: phosphate treatment for drum units, *EPRI Report TR-103655*, Electric Power Research Institute, Palo Alto, Ca.

Dooley R.B., and Paterson S. (1994) Phosphate treatment: boiler tube failures lead to optimum treatment, *Proc. 55th Int. Water Conf. (Pittsburgh, P.A.)* Paper IWC-94-50.

Economy G., Panson A.J., Liu Chia-tsun, Esposito J.N., and Lindsay W.T. Jr. (1975) Sodium phosphate solutions at boiler conditions: Solubility, phase equilibria and interactions with magnetite, *Proc. 36th Int. Water Conf.* (Pittsburgh, PA.) pp.161-173.

Goranson R.W., (1931) Solubility of water in granite magmas, *Amer. J. Sci.* **22**, 481-502.

Greeden J.E., Reubenbauer K. Birchall T., Ehlert M., Corbin D.R., and Subramanian M.A. (1988) A magnetic and mössbauer study of the layered compound $(\text{NH}_4)\text{Fe}(\text{PO}_4) \cdot \text{H}_2\text{O}$, *J. Solid State Chem.* **77**, 376-388.

Greenburg J.P., and Moller N. (1989) The prediction of mineral solubilities in natural waters: A chemical equilibrium model for the Na-K-Ca-SO₄-H₂O systems to high concentration from 0 to 250°C, *Geochim. Cosmochim. Acta.*, **53**, 2503-2518.

Haar L., Gallagher J.S., and Kell G.S. (1984) *NBS/NRC Steam Tables. Thermodynamic and Transport Properties and Computer Programs for Vapour and Liquid States of Water in SI Units*, Hemisphere Publishing, New York.

Habashi F. (1994) Recent advances in pressure leaching technology, *Proc. 1st Int. Conf. Solvothermal Reactions 13-16* (Takamatsu, Japan).

Harada K., Arai T., Shimada M., Kawai N., and Kurosawa T. (1978) Corrosion of Inconel 600 in high temperature water. Part I: Design and construction of high temperature experimental apparatus under boiling heat transfer condition and corrosion behaviour in sodium triphosphate solution, *Central Research Institute of Electric Power Industry (Japan), Report EEL-E277010*.

Helgeson H.C., Delaney J.M., and Nesbitt H.W., and Bird D.K. (1978) Summary and critique of the thermodynamic properties of rock-forming minerals, *Am., J. Sci.* **278A**, 1-229.

Helgeson H.C., and Kirkham D.H. (1976) Theoretical prediction of the thermodynamic properties of aqueous electrolytes at high pressures and temperatures: III. Equation of state for aqueous species at infinite dilution, *Am J. Sci.* **276**, 97-240.

Helgeson H.C., and Kirkham D.H. (1981) Theoretical prediction of the thermodynamic properties of aqueous electrolytes at high pressures and temperatures: IV. Calculation of activity coefficients, osmotic coefficients, and apparent molal and standard and relative molal properties to 600°C and 5kb, *Am. J. Sci.* **281**, 1249-1493.

Ivanov Y.A., Egorov-Tismenko Y.K., Simonov M.A., and Belov N.V. (1974) Crystal structure of cadmium ammonium phosphate, $(\text{NH}_4)\text{Cd}[\text{PO}_3\text{OH}](\text{OH})$, *Sov. Phys. Crystallogr.* **19(5)**, 665-666.

Ivanov Y.A., Simonov M.A., and Belov N.V. (1976) The crystal structure of a second modification of cadmium ammonium phosphate $(\text{NH}_4)\text{Cd}[\text{PO}_3\text{OH}](\text{OH})$, *Sov. Phys. Crystallogr.* **21**(1), 109-110.

JCPDS (1991) Powder Diffraction File, *JCPDS Int. Center for Diffraction Data Swarthmore, P.A.*

Johnson J.W., Oelkers E.H., and Helgeson H.C. (1992) SUPCRT'92: A software package for calculation the standard molal thermodynamic properties of minerals, gases, aqueous species and reactions from 1 to 5000 bar and 0 to 1000°C, *Computers and Geoscience* **18**(7), 899-947.

Jonas O., Blood F., Connick B., Lehner K., and Homan W.R. (1987) Water, steam, and turbine deposit chemistries in phosphate-treated drum boiler units, *EPRI Report CS-5275, Project No. 1986-9.*

Jonas O., and Layton K.F. (1988) Phosphate boiler water treatment for high pressure boilers, *Proc. Second EPRI Fossil Plant Cycle Chemistry Conf.* (Seattle, WA).

Kirsh H. (1964) Phosphate containing deposits in high pressure steam generators. *Mitteilung, VGB* **89**, 80-88.

LePage, Y.; Donnay, G. *Can. Mineral.* **1977**, 15,518-521.

Lindsay W.T. Jr. (1989) Computer modeling of aqueous systems in power cycles, in *Properties of Water and Steam*, M. Pichal and O. Sifner, eds., Hemisphere Publishing, New York, NY. pp. 29-38.

Lindsay W.T. (1990) Chemistry of steam cycle solutions: principles, in *The ASME Handbook on Water Technology for Thermal Power Systems*, Cohen, P. ed., Amer. Soc. Mech. Engineers, New York, NY. Chapter 7, 341-544.

Lobachev, A.N. (1971) *Hydrothermal Synthesis of Crystals*, Consultants Bureau, NewYork-London.

Maier C.G., and Kelley K.K. (1932) An equation for the representation of high temperature heat content data, *J. Am. Chem. Soc.* **54**, 3243-3246.

Marcy V.M., and Halstead S.L. (1964) Improved basis for coordinated phosphate-pH control of boiler water, *Combustion Jan.*, 45-47.

Marshall W.L. (1985) Aqueous inorganic phase equilibria at high temperatures: Some experimental, theoretical, and applied aspects, *Pure and Appli. Chem.* **57**, 283-301.

- Marshall W.L. (1982) Two-liquid-phase boundaries and critical phenomena at 275-400°C for high-temperature aqueous potassium phosphate and sodium phosphate solutions. Potential applications for steam generators, *J. Chem. Eng. Data* **27**, 175-180.
- Marshall W.L., and Begun G.M. (1989) Raman spectroscopy of aqueous phosphate solutions at temperatures up to 450°C, *J. Chem. Soc., Faraday Trans. 2*, **85**, 1963-1978.
- Martell, A.E., and Calvin, M. (1956) *Chemistry of the Metal Chelate compounds*, Prentice-Hall, Inc., New Jersey.
- Martell, A.E., Motekaitis, R.J., Fried, A.R., Wilson, J.S., and MacMillan, D.T. (1975) Thermal Decomposition of EDTA, NTA, and Nitrilotrimethylene Phosphonic Acid in Aqueous Solutions, *Can. J. Chem.*, **53**, 3471-3476.
- Mesmer, R.E., and Baes, C.F. Jr. (1974) Phosphoric acid dissociation equilibria in aqueous solutions to 300°C, *J. Solution Chem.* **3**, 307-322.
- Morey G.W. (1953) The system H₂O-NaPO₃, *J. Amer. Chem. Soc.* **75**, 5794-5797.
- Nacken, R. (1946) Artificial quartz crystals, etc., *U.S. Office Of Technical Services Report, PB-18-748*, 28-897.
- Nordmann F., Dijoux M., and Stutzmann A., (2001) *PowerPlant Chemistry* **3(4)**, 209.
- Panson A.J., Economy G., Liu Chia-tsun, Bulischeck T.S., and Lindsay W.T. Jr. (1975) Sodium phosphate solubility and phase relations basis for invariant point chemistry control, *J. Electrochem. Soc.* **122**, 915-918.
- Partridge E.P., and Hall R.E. (1939) Attack on steel in high-capacity boilers as a result of overheating due to steam blanketing, *Trans. ASME*, **10**, 597-627.
- Pessall N., Dunlop A.B., and Feldman D.W. (1977) The corrosion resistance of Inconel Alloy 600 in high temperature phosphate solutions, *Corrosion* **33(4)**, 130-144.
- Pitzer K.S., and Simonson J.M. (1986) Thermodynamics of multicomponent, miscible, ionic systems: Theory and equations, *J. Phys. Chem.* **90**, 3005-3009.
- Pitzer K.S. (1991) *Activity Coefficients in Electrolyte Solutions*, 2nd ed, CRC Press, Boca Raton, Fl.
- Pollard A.J., and Edwards A.J. (1963) An investigation of the effects of alkaline phosphate solutions at elevated temperature on compounds prepared at room temperature, *U.S. Naval Research Laboratory Report NRL 5865*.

Quinlan S. (1996) Thermochemistry of aqueous sodium phosphate interactions with metal oxides in high temperature water, *M.Sc. Thesis, Memorial University of Newfoundland*.

Qui, L., and White, M.A. (2001) The constituent additivity method to estimate heat capacities of complex inorganic solids, *J. Chemical Education* **78(8)**, 1076-1079.

Ravich M.I., and Scherbakova L.A. (1955) Nature of the solid phase which crystallizes from aqueous solutions of trisodium orthophosphate at high temperatures, *Izvest. Sektora Fiz. Khim. Anal., Inst. Obshchei Neorg. Khim. Akad. Nauk SSSR* **26**, 248-258.

Sanz F., Parada C., Rojo J.M., and Ruiz-Valero C. (1999) Crystal structure, magnetic properties, and ionic conductivity of a new mixed-anion phosphate $\text{Na}_4\text{Ni}_5(\text{PO}_4)_2(\text{P}_2\text{O}_7)_2$, *Chem. Mater.* **11**, 2673-2679.

Schroeder W.C., Berk A.A., and Gabriel A. (1937) Solubility of equilibria of sodium sulfate at temperatures from 150 to 350°C. III. Effect of sodium hydroxide and sodium phosphate, *J. Amer. Chem. Soc.* **59**, 1783-1790.

Shock H.L., and Helgeson H.C. (1988), Calculation of the thermodynamic and transport properties of aqueous species at high pressures and temperatures: Correlation algorithms for ionic species and equation of state predictions to 5kbar and 1000°C, *Geochim. Cosmochim. Acta*, **52**, 2009.

Shock E.L., Oelkers E.H., Johnson J.W., Swerjensky D.A., and Helgeson H.C. (1992) Calculation of the thermodynamic properties of aqueous species at high pressures and temperatures: Effective electrostatic radii, dissociation constants and standard partial molar properties to 1000°C and 5kbar, *J. Chem. Soc. Faraday Trans.* **88**, 803-826.

Sir Roderick Murchison (1840's), (cited by S. Somiya)

Straub F.G. (1950) Hideout of sodium phosphate in high-pressure boilers, *Trans. ASME* **72**, 479-489.

Stodola J. (1985) Phosphate and other hide-out, *Proc. Fossil Plant Water Chemistry Symposium, EPRI Report CS-4950*.

Stodola J. (1986) Review of boiler water alkalinity control, *Proc. 47th Int. Water. Conf. (Pittsburgh, PA.)* pp. 1-9.

Stumm W., and Morgan J.J. (1970) *Aquatic Chemistry*, Wiley-Interscience, New York, NY.

Sweeton F.H., Mesmer R.E., and Baes C.F. (1974) Acidity measurements at elevated temperature VII. Dissolution of water, *J. Solution Chem.* **3**, 191-214.

Tanger J.C., and Helgeson H.C. (1988) Calculation of the thermodynamic and transport properties of aqueous species at high temperatures and pressures: Revised equation of state for the standard partial molar properties of ions and electrolytes. *Am. J. Sci.* **288**, 19-98.

Taylor P., Tremaine P.R., and Bailey M.G. (1979) Sodium oxide-phosphorus (V) oxide-water phase diagram near 300°C: equilibrium solid phases, *Inorganic Chem.* **11**, 2947-2953.

Tremaine P.R., Gray L.G.S., Wiwchar B., Stodola J., and Taylor P (1992) Sodium phosphate chemistry under high pressure utility drum boiler condition, *Can. Electrical Assoc. R&D Agreement 913G730, Final Report* Vol I, 104pp; Vol II, 196pp; Vol III, 183pp.

Tremaine P.R., Gray L.G.S., Wiwchar B., Stodola J., and Taylor P (1993) Phosphate interactions with metal oxides under high-pressure boiler hideout conditions, *Proc. 54th Int. Water Conf.* Paper IWC-93-35.

Tremaine P.R., Quinlan S., Bridson J., and Stodola J (1996) Solubility and thermodynamics of sodium phosphate reaction products under hideout conditions in high-pressure boilers, *Proc. 57th Int. Water Conference, (Pittsburg, October, 1996) Paper IWC-96-21.*

Tremaine P., Schvedov D., Trevani L., and Xiao C. (1998) Sodium phosphate hideout mechanisms: Data and models for the solubility and redox behaviour of Iron(II) and Iron(III) sodium-phosphate hideout reaction products, *EPRI Research Project WO 2712-18-Final Report.*

Tremaine et al., *personal communication*, 2002.

Ulmer G.C., and Barnes H.L. (1983) *Hydrothermal Experimental Techniques*, Wiley-Interscience, N.Y.

Van Wazer J.R. (1958) *Phosphorus and Its Compounds*, Interscience, N.Y.

Wendrow B. and Kobe K.A. (1955) The system sodium oxide-phosphorus pentoxide-water, *Ind. Eng. Chem.* **44**, 1439-1448.

Wetton E.A.M. (1980) High-temperature phosphate chemistry in relation to the phosphate treatment of boilers, *Central Electricity Generating Board Report No. NW/SSD/RM/58/80.*

Wetton E.A.M. (1981) Phase equilibria in aqueous sodium phosphate solutions at 350°C, *Power Industry Research* **1**, 151-158.

Ziemniak S.E., Jones M.E., and Combs K.E.S. (1989) Solubility and phase behaviour of nickel oxide in aqueous sodium phosphate solutions at elevated temperatures, *J. Solution. Chem.* **18**, 1132-1152.

Ziemniak S.E. and Opalka E.P. (1988) Nickel oxide stability in aqueous sodium phosphate solutions at elevated temperatures, *Proc. Int. Symp. on Environmental Degradation of materials in Nuclear Power Systems-Water Reactors*, Theus. G.J., and Weeks, J.R., eds. Pp. 153-156.

Ziemniak S.E., and Opalka E.P. (1992) Magnetite stability in aqueous sodium phosphate solution at elevated temperatures, *Knolls Atomic Power Lab Report KAPL-4735*.

Ziemniak S.E., and Opalka E.P. (1993) *Proc. Sixth Int. Symposium on Environmental Degradation of Materials in Nuclear Power Systems-Water Reactors*, Gold R.E., and Simonen E.P., eds. (Warrendale, PA.) pp. 929-935.

Ziemniak S.E., Stalnaker N.D., Jones M.E., and Grossman B. (1981) Chemical interactions between high temperature aqueous solutions of sodium phosphate and magnetite, *EPRI Workshop* (Minneapolis., MN, June 1981) Abstract.

APPENDICES

APPENDIX I: Powder X-ray Diffraction Results

TABLE A.I.1: X-Ray Diffraction Results for Maricite

Product RGH05		Quinlan (1996), synthesized from FeNTA		Quinlan (1996), synthesized from Fe powder		JCPDS database Maricite	
d_{obs}	I/I_{100}	d_{obs}	I/I_{100}	d_{obs}	I/I_{100}	d_{obs}	I/I_{100}
4.4944	33.9	4.514	45	4.512	49	4.500	5
4.3969	13.4	4.417	31	4.409	53	4.400	20
		3.768	13	3.775	54	3.757	10
3.6995	13.0	3.714	18	3.721	63	3.705	40
3.3550	6.6						
2.7220	70.0	2.730	28	2.728	84	2.729	90
		2.710	36	2.713	85	2.707	80
2.5751	100	2.582	100	2.579	100	2.574	100
2.5216	11.8	2.527	17	2.522	43	2.525	30
2.4282	7.5	2.432	23	2.431	30	2.431	15
2.3991	6.5			2.401	28	2.401	10
2.2466	10.6			2.254	22	2.244	1
		2.203	8				
2.0934	8.9	2.098	10	2.096	30	2.096	10
		2.062	6			2.062	2
				2.027	49		
1.8798	22.7	1.883	15	1.880	41	1.881	30
1.8518	16.0	1.854	21	1.852	35	1.853	60
1.7158	6.9	1.717	13	1.717	23	1.714	15
1.6934	7.9	1.697	10	1.690	22	1.696	1
				1.681	21		
		1.654	7	1.653	21		
1.5183	18.0			1.520	28	1.519	10
1.5073	11.6			1.509	27	1.508	15
1.4982	21.3					1.490	15
1.4282	11.0					1.429	5
1.2880	13.8					1.288	5

TABLE A.I.2: X-Ray Diffraction Results for SIHP from FeNTA Decomposition

Product RGH32B		Quinlan(1996) SIHP From FePO ₄		JCPDS Database Magnetite		JCPDS Database Maricite		JCPDS Database Na ₃ PO ₄	
d _{obs}	I/I ₁₀₀	d _{obs}	I/I ₁₀₀	d _{obs}	I/I ₁₀₀	d _{obs}	I/I ₁₀₀	d _{obs}	I/I ₁₀₀
7.7812	18.3	7.769	78						
7.3562	15.2	7.367	73						
								7.160	30
5.3421	27.9	5.343	32						
4.8540	31.8			4.8520	8				
						4.500	5		
						4.400	20		
								4.180	90
						3.757	10		
						3.705	40	3.700	50
3.6345	29.2	3.637	7						
								3.580	60
3.4285	17.9	3.432	15						
3.3190	10.9	3.323	19						
2.9658	10.5			2.9670	30				
						2.729	90		
						2.707	80		
2.6661	100	2.668	100						
2.6205	41.2	2.624	6						
								2.582	100
2.5571	29.4	2.557	8			2.574	100		
2.5494	18.1			2.5320	100			2.531	70
						2.525	30		
								2.478	40
		2.450	13	2.4243	8	2.431	15	2.433	70
						2.401	10	2.389	50
								2.279	40
						2.244	1		
2.1335	8.4	2.116	5						
				2.0993	20	2.096	10		
2.0723	7.1	2.081	8			2.062	2		
								1.995	30
1.9390	37.9	1.940	60					1.955	30

TABLE A.I.2 (continued)

Product RGH32B		Quinlan(1996) SIHP From FePO ₄		JCPDS Database Magnetite		JCPDS Database Maricite		JCPDS Database Na ₃ PO ₄	
d _{obs}	I/I ₁₀₀	d _{obs}	I/I ₁₀₀	d _{obs}	I/I ₁₀₀	d _{obs}	I/I ₁₀₀	d _{obs}	I/I ₁₀₀
		1.935	34					1.916	30
		1.876	4			1.881	30		
						1.853	60	1.854	40
1.8353	13.7	1.837	38						
		1.832	23						
1.7771	11.3	1.779	4					1.792	50
				1.7146	10	1.714	15		
						1.696	1		
				1.6158	30				
1.5438	22.7	1.546	5					1.550	20
						1.519	10		
1.5035	21.8	1.505	4	1.4845	40	1.508	15	1.498	40
						1.490	15	1.472	70
				1.4192	2	1.429	5		
								1.383	20
		1.334	5	1.3277	4				
				1.2807	10	1.288	5	1.291	30
				1.2659	4				
				1.2119	2				

TABLE A.I.3: X-Ray Diffraction Results for SIHP from FeNTA Decomposition

Product RGH59B		Quinlan (1996) SIHP		JCPDS Database Magnetite		JCPDS Database Hematite		JCPDS Database Maricite		JCPDS Database Na ₃ PO ₄	
d _{obs}	I/I ₁₀₀	d _{obs}	I/I ₁₀₀	d _{obs}	I/I ₁₀₀	d _{obs}	I/I ₁₀₀	d _{obs}	I/I ₁₀₀	d _{obs}	I/I ₁₀₀
7.7610	21.8	7.769	78								
7.3373	19.7	7.367	73								
										7.160	30
5.3326	25.7	5.343	32								
4.8524	14.8			4.8520	8						
								4.500	5		
								4.400	20		
										4.180	90
								3.757	10		
						3.6840	30	3.705	40	3.700	50
3.6309	19.8	3.637	7								
										3.580	60
3.4245	19.4	3.432	15								
3.3154	14.6	3.323	19								
				2.9670	30						
2.7211	26.0							2.729	90		
								2.707	80		
						2.7000	100				
2.6638	100	2.668	100								
2.6202	24.6	2.624	6								
2.5806	15.0									2.582	100
2.5706	11.0	2.557	8					2.574	100		
				2.5320	100					2.531	70
						2.5190	70	2.525	30		
										2.478	40
2.4425	6.4	2.450	13	2.4243	8			2.431	15	2.433	70
								2.401	10	2.389	50
						2.2920	3			2.279	40
								2.244	1		
						2.2070	20				
		2.116	5								
				2.0993	20			2.096	10		
2.0683	8.7	2.081	8			2.0779	3	2.062	2		
										1.995	30
1.9377	38.4	1.940	60							1.955	30
		1.935	34							1.916	30

TABLE A.I.3 (continued)

Product RGH59B		Quinlan (1996) SIHP		JCPDS Database Magnetite		JCPDS Database Hematite		JCPDS Database Maricite		JCPDS Database Na ₃ PO ₄	
d _{obs}	I/I ₁₀₀	d _{obs}	I/I ₁₀₀	d _{obs}	I/I ₁₀₀	d _{obs}	I/I ₁₀₀	d _{obs}	I/I ₁₀₀	d _{obs}	I/I ₁₀₀
1.8755	12.2	1.876	4					1.881	30		
1.8518	10.6					1.8406	40	1.853	60	1.854	40
1.8343	16.7	1.837	38								
		1.832	23								
		1.779	4							1.792	50
				1.7146	10			1.714	15		
						1.6941	45	1.696	1		
						1.6367	1				
				1.6158	30	1.6033	5				
						1.5992	10				
1.5436	14.3	1.546	5							1.550	20
								1.519	10		
1.5029	22.6	1.505	4	1.4845	40	1.4859	30	1.508	15	1.498	40
								1.490	15	1.472	70
						1.4538	30				
				1.4192	2	1.4138	1	1.429	5		
										1.383	20
		1.334	5	1.3277	4	1.3497	3				
						1.3115	10				
				1.2807	10	1.3064	6	1.288	5	1.291	30
				1.2659	4	1.2592	8				
						1.2272	4				
				1.2119	2	1.2141	2				

TABLE A.I.4: X-Ray Diffraction Results for SIHP from FeNTA Decomposition

Product RGH60A		Quinlan (1996) SIHP from FePO ₄		JCPDS database Na ₃ PO ₄		JCPDS database Fe ₂ PO ₅	
d _{obs}	I/I ₁₀₀	d _{obs}	I/I ₁₀₀	d _{obs}	I/I ₁₀₀	d _{obs}	I/I ₁₀₀
13.9757	21.0						
7.7593	19.2	7.769	78				
7.3563	19.9	7.367	73				
5.3410	28.3	5.343	32				
						5.2500	20
4.8533	29.9					4.8800	20
				4.3350	40		
4.2830	11.9			4.2750	50		
				3.6900	20		
3.6346	29.7	3.637	7				
3.4260	14.4	3.432	15				
3.3223	13.1	3.323	19				
						3.3200	100
						3.2200	20
						2.9520	19
						2.7440	70
2.6685	100.0	2.668	100	2.6550	30		
2.6183	72.6	2.624	6	2.6250	100	2.6220	25
2.5528	52.2	2.557	8				
		2.450	13			2.4300	28
						2.3570	19
						2.3170	50
				2.2510	20		
2.2376	11.2			2.2290	15		
2.1336	9.1	2.116	5	2.1390	10		
		2.081	8			2.0620	25
				1.9940	3		
1.9415	18.9	1.940	60				
		1.935	34				
		1.876	4	1.8530	30	1.8640	19
1.8373	13.3	1.837	38				
		1.832	23				
1.7731	11.7	1.779	4				
				1.7180	1		
				1.7080	1		
				1.6580	5	1.6530	25

TABLE A.I.4 (continued)

Product RGH60A		Quinlan (1996) SIHP from FePO ₄		JCPDS database Na ₃ PO ₄		JCPDS database Fe ₂ PO ₅	
d _{obs}	I/I ₁₀₀	d _{obs}	I/I ₁₀₀	d _{obs}	I/I ₁₀₀	d _{obs}	I/I ₁₀₀
						1.6090	55
						1.5760	14
1.5456	20.3	1.546	5			1.5380	30
1.5042	20.8	1.505	4	1.5150	20		
1.4770	8.8					1.4770	12
				1.4260	10	1.4470	18
		1.334	5			1.3310	20
						1.3150	18

TABLE A.I.5: X-Ray Diffraction Results for SIHP from $\text{Fe}_2(\text{C}_4\text{H}_4\text{O}_6)_3$ Decomposition

Product RGH29A		Quinlan (1996) SIHP From FePO_4		JCPDS Database Maricite		JCPDS Database Na_3PO_4		JCPDS Database Sodium Tartrate Hydrate		JCPDS Database $\text{H}_3\text{PO}_4 \cdot 0.5$ H_2O	
d_{obs}	I/I_{100}	d_{obs}	I/I_{100}	d_{obs}	I/I_{100}	d_{obs}	I/I_{100}	d_{obs}	I/I_{100}	d_{obs}	I/I_{100}
9.0172	27.4							9.031	100		
7.7786	14.8	7.769	78								
7.3730	9.8	7.367	73								
						7.160	30				
										7.020	40
								5.730	29		
5.3419	24.0	5.343	32								
4.8488	9.8									4.890	46
								4.698	25		
4.4826	22.2			4.500	5			4.498	41		
				4.400	20						
						4.180	90				
										3.880	46
				3.757	10						
3.7062	6.6			3.705	40	3.700	50			3.720	52
										3.680	15
3.6348	14.0	3.637	7					3.633	42	3.650	100
						3.580	60				
3.5566	13.3									3.560	44
										3.510	12
								3.482	25		
3.4213	13.8	3.432	15								
										3.390	11
3.3125	36.0	3.323	19					3.339	17		
								3.332	18		
										3.250	68
										3.210	44
2.9943	15.9									2.980	3
								2.964	22		
										2.910	26
								2.865	21		
2.8518	9.8							2.856	21	2.840	14

TABLE A.I.5 (continued)

Product RGH29A		Quinlan (1996) SIHP From FePO ₄		JCPDS Database Maricite		JCPDS Database Na ₃ PO ₄		JCPDS Database Sodium Tartrate Hydrate		JCPDS Database H ₃ PO ₄ ·0.5 H ₂ O	
d _{obs}	I/I ₁₀₀	d _{obs}	I/I ₁₀₀	d _{obs}	I/I ₁₀₀	d _{obs}	I/I ₁₀₀	d _{obs}	I/I ₁₀₀	d _{obs}	I/I ₁₀₀
2.8021	8.1							2.797	59	2.830	15
2.7148	16.4			2.729	90					2.810	4
				2.707	80						
2.6614	100	2.668	100					2.669	10		
		2.624	6					2.622	22		
2.5828	21.8					2.582	100			2.592	6
2.5684	12.8	2.557	8	2.574	100						
						2.531	70				
				2.525	30						
						2.478	40	2.481	34		
		2.450	13	2.431	15	2.433	70	2.466	18	2.446	14
										2.438	12
2.3986	9.2			2.401	10	2.389	50				
								2.311	28		
						2.279	40				
2.2396	8.1			2.244	1			2.249	10	2.254	8
2.1109	6.8	2.116	5								
				2.096	10						
		2.081	8	2.062	2			2.063	27		
						1.995	30				
1.9378	16.9	1.940	60			1.955	30				
		1.935	34			1.916	30				
		1.876	4	1.881	30						
1.8551	19.3			1.853	60	1.854	40	1.860	10		
1.8310	9.4	1.837	38								
		1.832	23								
		1.779	4			1.792	50				
				1.714	15						
				1.696	1						
1.5436	5.0	1.546	5			1.550	20				

TABLE A.I.5 (continued)

Product		Quinlan (1996) SIHP From FePO ₄		JCPDS Database Maricite		JCPDS Database Na ₃ PO ₄		JCPDS Database Sodium Tartrate Hydrate		JCPDS Database H ₃ PO ₄ ·0.5 H ₂ O	
d _{obs}	I/I ₁₀₀	d _{obs}	I/I ₁₀₀	d _{obs}	I/I ₁₀₀	d _{obs}	I/I ₁₀₀	d _{obs}	I/I ₁₀₀	d _{obs}	I/I ₁₀₀
1.5008	5.0	1.505	4	1.519	10	1.498	40				
				1.490	15	1.472	70				
				1.429	5			1.383	20		
		1.334	5			1.291	30				
				1.288	5						

TABLE A.I.6: X-Ray Diffraction Results for SIHP from $\text{Fe}_2(\text{C}_2\text{O}_4)_3 \cdot 5\text{H}_2\text{O}$
Decomposition

Product RGH78B		Quinlan (1996) SIHP From FePO_4		JCPDS Database Fe_2PO_5		JCPDS Database Na_3PO_4	
d_{obs}	I/I_{100}	d_{obs}	I/I_{100}	d_{obs}	I/I_{100}	d_{obs}	I/I_{100}
7.9709	14.4						
7.8460	47.6						
		7.769	78				
7.3952	11.3	7.367	73				
						7.160	30
5.3712	27.2	5.343	32				
				5.2500	20		
4.8939	16.0			4.8800	20		
						4.180	90
						3.700	50
3.6525	24.8	3.637	7				
						3.580	60
3.4474	13.4	3.432	15				
3.4400	14.7						
3.3333	8.0	3.323	19	3.3200	100		
3.3261	12.8						
				3.2200	20		
				2.9520	19		
				2.7440	70		
2.6727	100	2.668	100				
2.6359	28.1	2.624	6	2.6220	25		
2.5637	22.0	2.557	8			2.582	100
						2.531	70
						2.478	40
		2.450	13	2.4300	28	2.433	70
						2.389	50
				2.3570	19		
				2.3170	50		
						2.279	40
2.1369	6.7	2.116	5				
2.1168	7.9						

TABLE A.I.6 (continued)

Product RGH78B		Quinlan (1996) SIHP From FePO ₄		JCPDS Database Fe ₂ PO ₅		JCPDS Database Na ₃ PO ₄	
d _{obs}	I/I ₁₀₀	d _{obs}	I/I ₁₀₀	d _{obs}	I/I ₁₀₀	d _{obs}	I/I ₁₀₀
		2.081	8	2.0620	25		
1.9412	48.2	1.940	60			1.995	30
		1.935	34			1.955	30
		1.876	4			1.916	30
1.8341	10.8			1.8640	19	1.854	40
		1.837	38				
		1.832	23				
1.7876	6.5	1.779	4			1.792	50
				1.6530	25		
				1.6090	55		
				1.5760	14		
1.5458	16.7	1.546	5	1.5380	30	1.550	20
1.5029	13.4	1.505	4			1.498	40
				1.4770	12	1.472	70
				1.4470	18		
						1.383	20
		1.334	5	1.3310	20		
				1.3150	18		
						1.291	30

TABLE A.I.7: X-Ray Diffraction Results for $(\text{NH}_4)\text{Fe}_2(\text{PO}_4)_2$ from $\text{Fe}_2(\text{C}_4\text{H}_4\text{O}_6)_3$ Decomposition

Product RGH51A		Boudin and Lii (1998) $(\text{NH}_4)\text{Fe}_2$ $(\text{PO}_4)_2$		JCPDS database Hematite		JCPDS database $\text{Fe}(\text{PO}_4)$ $\cdot 2\text{H}_2\text{O}$		JCPDS database $(\text{NH}_4)\text{H}_5(\text{PO}_4)_2$ $\cdot \text{H}_2\text{O}$	
d_{obs}	I/I_{100}	d_{obs}	I/I_{100}	d_{obs}	I/I_{100}	d_{obs}	I/I_{100}	d_{obs}	I/I_{100}
		8.2854	43.73					6.5200	50
6.2014	63.2							6.0300	10
		5.9792	15.57					5.5600	10
5.6685	15.1	5.6508	56.41						
						5.5090	60	5.4500	50
5.4645	9.3					4.9540	30		
						4.3830	85		
4.1315	9.9	4.1446	11.79			3.9960	45		
								3.9200	15
								3.8700	10
								3.8300	70
						3.7190	25		
				3.6840	30			3.6000	10
								3.5700	100
3.5033	15.8								
		3.3975	8.68						
3.1172	16.3					3.1140	100		
3.1039	12.0								
		3.0562	6.96						
		3.0188	14.45			3.0020	45		
2.9836	100.0	2.9894	100.0						
								2.9600	35
						2.9490	45		
2.7299	64.6	2.7360	7.51						
2.6890	51.3			2.7000	100	2.6900	5		
2.6156	8.7					2.6310	11		
2.5341	12.9	2.5264	15.19			2.5460	50		

TABLE A.I.7 (continued)

Product RGH51A		Boudin and Lii (1998) (NH ₄)Fe ₂ (PO ₄) ₂		JCPDS database Hematite		JCPDS database Fe(PO ₄) ·2H ₂ O		JCPDS database (NH ₄)H ₅ (PO ₄) ₂ ·H ₂ O	
d _{obs}	I/I ₁₀₀	d _{obs}	I/I ₁₀₀	d _{obs}	I/I ₁₀₀	d _{obs}	I/I ₁₀₀	d _{obs}	I/I ₁₀₀
						2.5310	35		
2.4994	21.8	2.5007	13.8	2.5190	70			2.4700	5
2.4938	15.4							2.4600	10
		2.4424	6.22			2.4440	25		
				2.2920	3				
				2.2070	20			2.2130	15
2.1545	9.5	2.1785	3.05					2.1530	10
						2.1320	35		
				2.0779	3				
						2.0030	20		
1.9773	10.4	1.9712	2.88			1.9580	20	1.9750	5
1.9225	9.2							1.9280	5
		1.8836	8.22						
		1.8540	9.37	1.8406	40				
1.8076	7.3	1.8248	9.56			1.8058	16	1.8210	5
								1.7940	5
1.6858	10.5	1.6905	11.71	1.6941	45			1.6950	5
				1.6367	1			1.6390	15
				1.6033	5				
				1.5992	10				
		1.5335	9.58			1.5557	20		
1.4868	8.8	1.4886	4.12	1.4859	30	1.4789	19	1.4950	5
						1.4746	11		
				1.4538	30				
				1.4138	1				
				1.3497	3				
				1.3115	10				
				1.3064	6				
				1.2592	8				
				1.2276	4				
				1.2141	2				

TABLE A.I.8: X-Ray Diffraction Results for $(\text{NH}_4)\text{Fe}_2(\text{PO}_4)_2$ from $\text{Fe}_2(\text{C}_4\text{H}_4\text{O}_6)_3$ Decomposition

Product RGH62A		Boudin and Lii (1998) $(\text{NH}_4)\text{Fe}_2(\text{PO}_4)_2$		JCPDS Database Hematite		JCPDS Database $(\text{NH}_4)\text{H}_2\text{PO}_4$	
d_{obs}	I/I_{100}	d_{obs}	I/I_{100}	d_{obs}	I/I_{100}	d_{obs}	I/I_{100}
		8.2854	43.73				
6.3203	41.0						
6.2460	57.0						
		5.9792	15.57				
		5.6508	56.41				
		4.1446	11.79			5.3243	64
3.7511	15.6					3.7507	50
				3.6840	30		
		3.3975	8.68				
3.1237	14.3						
3.0884	14.5					3.0779	94
3.0678	8.0	3.0562	6.96			3.0673	100
		3.0188	14.45				
2.9838	100	2.9894	100				
2.7257	51.6	2.7360	7.51				
2.6914	47.6			2.7000	100		
2.6804	13.2					2.6604	25
						2.6525	25
2.5430	16.0	2.5264	15.19				
2.4970	28.1	2.5007	13.8	2.5190	70		
2.4940	34.2						
		2.4424	6.22				
						2.3877	14
						2.3725	13
				2.2920	3		
				2.2070	20		
2.1542	18.3	2.1785	3.05				
2.1166	9.5						
2.0901	15.5			2.0779	3		
						2.0146	59
						2.0091	67
1.9792	18.3	1.9712	2.88				
		1.8836	8.22				

TABLE A.I.8 (continued)

Product RGH62A		Boudin and Lii (1998) (NH ₄)Fe ₂ (PO ₄) ₂		JCPDS Database Hematite		JCPDS Database (NH ₄)H ₂ PO ₄	
d _{obs}	I/I ₁₀₀	d _{obs}	I/I ₁₀₀	d _{obs}	I/I ₁₀₀	d _{obs}	I/I ₁₀₀
		1.8540	9.37	1.8406	40		
1.8225	26.3	1.8248	9.56			1.7748	11
1.7400	8.9						
		1.6905	11.71	1.6941	45	1.6871	8
						1.6776	10
				1.6367	1		
				1.6033	5	1.6036	21
				1.5992	10	1.6010	21
1.5147	17.8	1.5335	9.58				
		1.4886	4.12	1.4859	30	1.4771	9
						1.4716	11
				1.4538	30		
				1.4138	1		
						1.3711	15
				1.3497	3	1.3312	12
				1.3115	10		
				1.3064	6		
				1.2592	8	1.2541	13
				1.2276	4		
				1.2141	2		

TABLE A.I.9: X-Ray Diffraction Results for $(\text{NH}_4)\text{Fe}(\text{PO}_4)\cdot\text{H}_2\text{O}$ from FeNTA Decomposition

Product RGH18B		Generated Pattern for $(\text{NH}_4)\text{Fe}(\text{PO}_4)\cdot\text{H}_2\text{O}$		JCPDS database Hematite	
d_{obs}	I/I_{100}	d_{obs}	I/I_{100}	d_{obs}	I/I_{100}
8.7734	100.0	8.7985	100		
4.7532	2.1	4.7643	10.51		
4.3843	3.6				
4.2223	1.9	4.2360	11.48		
		3.7300	3.16	3.6840	30
		3.5996	7.09		
		3.3929	2.83		
3.1082	1.8	3.1157	11.73		
2.9263	2.6				
2.8173	10.5	2.8335	17.93		
		2.8214	33.61		
				2.7000	100
2.5379	3.1	2.5426	9.71		
2.5021	3.0	2.5073	5.10	2.5190	70
		2.4165	4.86		
2.2894	1.2	2.2929	3.67	2.2920	3
		2.2563	5.35		
				2.2070	20
2.0715	2.0	2.0753	4.07	2.0779	3
2.0472	2.5				
1.8846	1.8				
		1.8287	6.12	1.8406	40
1.7571	4.0	1.7542	3.61		
1.7362	2.2				
1.6782	4.2			1.6941	45
		1.6336	4.27	1.6367	1
				1.6033	5
				1.5992	10
1.5174	1.1				
1.4930	2.3	1.4949	3.26	1.4859	30
1.4647	1.4			1.4538	30
		1.4174	3.77	1.4138	1
				1.3497	3

TABLE A.I.9 (continued)

Product RGH18B		Generated Pattern for (NH ₄)Fe(PO ₄)·H ₂ O		JCPDS database Hematite	
d _{obs}	I/I ₁₀₀	d _{obs}	I/I ₁₀₀	d _{obs}	I/I ₁₀₀
1.3014	1.7			1.3115	10
				1.3064	6
				1.2592	8
				1.2276	4
				1.2141	2

TABLE A.I.10: X-Ray Diffraction Results for Na₂Ni(OH)PO₄ from NiO Reaction

Product RGH92A		Ziemniak and Opalka (1988) Na ₂ Ni(OH)PO ₄		JCPDS Database Na ₄ Ni(PO ₄) ₂		JCPDS Database NiO		JCPDS Database Na ₃ PO ₄	
d _{obs}	I/I ₁₀₀	d _{obs}	I/I ₁₀₀	d _{obs}	I/I ₁₀₀	d _{obs}	I/I ₁₀₀	d _{obs}	I/I ₁₀₀
		10.780	29						
				8.120	17				
7.4855	7.2	7.510	53						
7.4134	12.9								
				6.500	8				
		6.160	27						
6.0997	6.7								
				5.900	5				
				5.780	8				
				5.090	3				
				4.770	16				
				4.458	5				
4.2650	6.1							4.2800	70
4.2167	5.1	4.200	52	4.235	70				
4.1817	20.0								
				3.924	25				
				3.873	8				
								3.7100	20
		3.550	12						
		3.400	13	3.381	6				
3.2235	7.8	3.210	20	3.250	6				
				3.151	5				
				3.108	6				
		2.940	9	2.932	5				
				2.829	18				
				2.771	4				
				2.701	25				
2.6226	6.8							2.6210	100
2.6071	18.3								
2.5851	48.5	2.590	100	2.592	100				
2.5322	16.1	2.520	32	2.540	8				
				2.511	4				
				2.453	5				
2.4062	57.3			2.401	14	2.4120	60		
		2.370	4						

TABLE A.I.10 (continued)

Product RGH92A		Ziemniak and Opalka (1988) Na ₂ Ni(OH)PO ₄		JCPDS Database Na ₄ Ni(PO ₄) ₂		JCPDS Database NiO		JCPDS Database Na ₃ PO ₄	
d _{obs}	I/I ₁₀₀	d _{obs}	I/I ₁₀₀	d _{obs}	I/I ₁₀₀	d _{obs}	I/I ₁₀₀	d _{obs}	I/I ₁₀₀
				2.293	6				
		2.270	5	2.226	6				
		2.180	6	2.201	12				
		2.150	8					2.1400	20
2.0970	8.1	2.100	7	2.117	8				
2.0834	100					2.0880	100		
		2.050	9	2.042	4				
		1.974	5	1.962	5				
				1.925	4				
				1.909	6				
1.8668	6.1	1.875	7					1.8530	20
		1.865	5						
		1.830	19	1.831	15				
1.7925	7.0	1.790	12	1.7742	3				
		1.782	8						
		1.654	5	1.6658	4				
				1.6353	5				
		1.601	3						
		1.557	3						
1.5048	4.9	1.508	11					1.5130	30
1.4745	55.4	1.472	12	1.4955	12	1.4770	35		
						1.4760	35		
								1.4260	40
1.2582	18.3					1.2600	18		
						1.2586	12		
1.2051	10.1					1.2064	16		

TABLE A.I.11: X-Ray Diffraction Results for Na₂Ni(OH)PO₄ from H⁺[NiNTA⁻] Decomposition

Product RGH89A		Ziemniak and Opalka (1988) Na ₂ Ni(OH)PO ₄		JCPDS Database Ni(OH) ₂		JCPDS Database Na ₄ Ni(PO ₄) ₂		JCPDS Database Na ₂ HPO ₄	
d _{obs}	I/I ₁₀₀	d _{obs}	I/I ₁₀₀	d _{obs}	I/I ₁₀₀	d _{obs}	I/I ₁₀₀	d _{obs}	I/I ₁₀₀
		10.780	29						
						8.120	17		
		7.510	53						
7.0426	16.6								
6.8782	24.8								
6.8155	19.8								
6.5451	16.5								
						6.500	8		
		6.160	27			5.900	5		
						5.780	8		
						5.090	3		
								4.900	10
4.7767	25.6					4.770	16		
				4.605	100				
4.4967	12.4								
						4.458	5		
						4.235	70		
		4.200	52						
3.9611	14.6							3.980	45
3.9036	11.8					3.924	25		
3.8887	34.4					3.873	8		
								3.840	55
3.7523	16.0								
3.7433	27.1								
3.7111	50.5								
3.5661	14.1	3.550	12						
		3.400	13					3.420	20
						3.381	6		
		3.210	20						
3.2936	11.0								
						3.250	6		
3.1997	14.3								
						3.151	5		

TABLE A.I.11 (continued)

Product RGH89A		Ziemniak and Opalka (1988) Na ₂ Ni(OH)PO ₄		JCPDS Database Ni(OH) ₂		JCPDS Database Na ₄ Ni(PO ₄) ₂		JCPDS Database Na ₂ HPO ₄	
d _{obs}	I/I ₁₀₀	d _{obs}	I/I ₁₀₀	d _{obs}	I/I ₁₀₀	d _{obs}	I/I ₁₀₀	d _{obs}	I/I ₁₀₀
						3.108	6		
		2.940	9			2.932	5		
								2.880	40
2.7846	79.0					2.829	18	2.805	100
						2.771	4		
2.7154	73.0							2.730	50
								2.720	25
2.7034	100.0			2.707	45	2.701	25		
2.6988	63.0								
								2.655	20
2.5960	76.8	2.590	100			2.592	100		
2.5640	66.3								
2.5216	16.6	2.520	32			2.540	8	2.537	8
						2.511	4		
						2.453	5	2.453	18
						2.401	14		
		2.370	4						
				2.334	100				
				2.302	2			2.309	8
						2.293	6		
		2.270	5						
						2.226	6		
		2.180	6			2.201	12	2.197	10
		2.150	8						
2.0943	10.4	2.100	7			2.117	8		
		2.050	9			2.042	4	2.047	8
2.0222	10.6								
								1.994	16
		1.974	5			1.962	5		
1.9423	13.9					1.925	4	1.921	18
						1.909	6		
		1.875	7						
1.8582	18.6	1.865	5						
		1.830	19			1.831	15		

TABLE A.I.11 (continued)

Product RGH89A		Ziemniak and Opalka (1988) Na ₂ Ni(OH)PO ₄		JCPDS Database Ni(OH) ₂		JCPDS Database Na ₄ Ni(PO ₄) ₂		JCPDS Database Na ₂ HPO ₄	
d _{obs}	I/I ₁₀₀	d _{obs}	I/I ₁₀₀	d _{obs}	I/I ₁₀₀	d _{obs}	I/I ₁₀₀	d _{obs}	I/I ₁₀₀
		1.790	12					1.812	8
		1.782	8			1.774	3		
1.7128	10.3			1.754	35			1.751	18
								1.712	16
		1.654	5			1.6658	4		
						1.6353	5		
		1.601	3					1.595	14
1.5472	10.9	1.557	3	1.563	25				
				1.535	1				
		1.508	11						
		1.472	12	1.480	16	1.4955	12		
				1.354	4				
				1.335	8				
				1.299	10				
				1.293	2				
				1.167	8				

TABLE A.I.12: X-Ray Diffraction Results for $\text{Na}_2\text{Ni}(\text{OH})\text{PO}_4$ from $\text{H}^+[\text{NiNTA}]$ Decomposition

Product RGH66A		Ziemniak and Opalka (1988) $\text{Na}_2\text{Ni}(\text{OH})\text{PO}_4$		JCPDS Database $\text{Ni}(\text{OH})_2$		JCPDS Database $\text{Na}_4\text{Ni}(\text{PO}_4)_2$	
d_{obs}	I/I_{100}	d_{obs}	I/I_{100}	d_{obs}	I/I_{100}	d_{obs}	I/I_{100}
10.9222	4.4	10.780	29			8.120	17
7.4861	18.8	7.510	53			6.500	8
6.1475	13.6	6.160	27			5.900	5
						5.780	8
						5.090	3
						4.770	16
4.6071	8.0			4.605	100	4.458	5
						4.235	70
4.2041	40.6	4.200	52			3.924	25
						3.873	8
		3.550	12				
3.5286	6.1						
3.4089	11.3	3.400	13			3.381	6
3.2374	16.4					3.250	6
		3.210	20				
						3.151	5
						3.108	6
		2.940	9			2.932	5
						2.829	18
						2.771	4
				2.707	45	2.701	25
2.5895	100.0	2.590	100			2.592	100
2.5406	38.4	2.520	32			2.540	8
						2.511	4
						2.453	5
						2.401	14
		2.370	4				
2.3324	10.8			2.334	100		

TABLE A.I.12 (continued)

Product RGH66A		Ziemniak and Opalka (1988) $\text{Na}_2\text{Ni}(\text{OH})\text{PO}_4$		JCPDS Database $\text{Ni}(\text{OH})_2$		JCPDS Database $\text{Na}_4\text{Ni}(\text{PO}_4)_2$	
d_{obs}	I/I_{100}	d_{obs}	I/I_{100}	d_{obs}	I/I_{100}	d_{obs}	I/I_{100}
				2.302	2	2.293	6
2.2693	7.9	2.270	5			2.226	6
2.1843	5.1	2.180	6			2.201	12
2.1545	6.8	2.150	8				
2.1001	9.8	2.100	7			2.117	8
2.0468	5.4	2.050	9			2.042	4
		1.974	5			1.962	5
						1.925	4
						1.909	6
		1.875	7				
1.8678	14.8	1.865	5				
		1.830	19			1.831	15
1.7966	17.4	1.790	12				
		1.782	8			1.774	3
				1.754	35		
		1.654	5			1.6658	4
						1.6353	5
		1.601	3				
		1.557	3	1.563	25		
				1.535	1		
1.5048	14.2	1.508	11				
1.4764	16.5	1.472	12	1.480	16	1.4955	12
				1.354	4		
				1.335	8		
				1.299	10		
				1.293	2		
				1.167	8		

TABLE A.I.13: X-Ray Diffraction Results for $\text{Na}_2\text{Ni}(\text{OH})\text{PO}_4$ from $\text{H}^+[\text{NiNTA}^-]$ Decomposition

Product RGH73A		Ziemniak and Opalka (1988) $\text{Na}_2\text{Ni}(\text{OH})\text{PO}_4$		JCPDS Database $\text{Na}_4\text{Ni}(\text{PO}_4)_2$		JCPDS Database Na_3PO_4		JCPDS Database Na_2HPO_4	
d_{obs}	I/I_{100}	d_{obs}	I/I_{100}	d_{obs}	I/I_{100}	d_{obs}	I/I_{100}	d_{obs}	I/I_{100}
10.9590	8.1								
		10.780	29	8.120	17				
7.7002	8.1								
7.5840	18.3								
		7.510	53	6.500	8				
6.2272	16.2								
6.2028	9.2								
		6.160	27	5.900	5				
				5.780	8				
				5.090	3			4.900	10
				4.770	16				
				4.458	5				
4.3078	13.9					4.280	70		
4.2290	48.9	4.200	52	4.235	70				
4.0243	8.8								
								3.980	45
				3.924	25				
				3.873	8				
						3.710	20	3.840	55
		3.550	12						
3.4243	10.5	3.400	13					3.420	20
				3.381	6				
3.2546	20.8			3.250	6				
		3.210	20						
				3.151	5				
				3.108	6				
		2.940	9	2.932	5				
								2.880	40
				2.829	18			2.805	100

TABLE A.I.13 (continued)

Product RGH73A		Ziemniak and Opalka (1988) Na ₂ Ni(OH)PO ₄		JCPDS Database Na ₄ Ni(PO ₄) ₂		JCPDS Database Na ₃ PO ₄		JCPDS Database Na ₂ HPO ₄	
d _{obs}	I/I ₁₀₀	d _{obs}	I/I ₁₀₀	d _{obs}	I/I ₁₀₀	d _{obs}	I/I ₁₀₀	d _{obs}	I/I ₁₀₀
				2.771	4				
								2.730	50
				2.701	25			2.720	25
2.6635	17.2							2.655	20
2.6360	9.9								
2.6227	20.0					2.621	100		
2.6006	100.0	2.590	100	2.592	100				
2.5467	32.2	2.520	32	2.540	8			2.537	8
				2.511	4				
				2.453	5			2.453	18
				2.401	14				
		2.370	4						
				2.293	6			2.309	8
		2.270	5						
				2.226	6				
		2.180	6	2.201	12			2.197	10
		2.150	8			2.140	20		
		2.100	7	2.117	8				
2.0417	23.3	2.050	9	2.042	4			2.047	8
								1.994	16
		1.974	5	1.962	5				
				1.925	4			1.921	18
				1.909	6				
1.8777	8.4	1.875	7						
		1.865	5			1.853	20		
		1.830	19	1.831	15			1.812	8
1.7985	9.3	1.790	12						
		1.782	8	1.774	3				
								1.751	18
								1.712	16
		1.654	5	1.6658	4				
				1.6353	5				
		1.601	3					1.595	14
		1.557	3						
1.5101	8.4					1.513	30		

TABLE A.I.13 (continued)

Product		Ziemniak and Opalka (1988)		JCPDS Database		JCPDS Database		JCPDS Database	
RGH73A		Na ₂ Ni(OH)PO ₄		Na ₄ Ni(PO ₄) ₂		Na ₃ PO ₄		Na ₂ HPO ₄	
d _{obs}	I/I ₁₀₀	d _{obs}	I/I ₁₀₀	d _{obs}	I/I ₁₀₀	d _{obs}	I/I ₁₀₀	d _{obs}	I/I ₁₀₀
1.5088	9.0	<i>1.508</i>	<i>11</i>	<i>1.4955</i>	<i>12</i>				
1.4763	10.9	<i>1.472</i>	<i>12</i>						
						1.426	40		

APPENDIX II: X-ray Crystal Structure of $(\text{NH}_4)\text{Fe}^{\text{II}}(\text{PO}_4)\cdot\text{H}_2\text{O}$

X-ray Structure Report

For
Dr. P. Tremaine

Prepared by
David O. Miller

May 31, 2001

Introduction

Collection, solution and refinement all proceeded normally. Hydrogen atoms were introduced in calculated or difference map positions with isotropic thermal parameters set twenty percent greater than those of their bonding partners at the time of their inclusion. Some were optimized by positional refinement but all were fixed for the final round of refinement.

Experimental

Data Collection

A colorless irreg.plate crystal of $\text{H}_7\text{O}_5\text{FePN}$ having approximate dimensions of $0.40 \times 0.35 \times 0.15$ mm was mounted on a glass fiber. All measurements were made on a Rigaku AFC6S diffractometer with graphite monochromated Mo- $K\alpha$ radiation.

Cell constants and an orientation matrix for data collection, obtained from a least-squares refinement using the setting angles of 23 carefully centered reflections in the range $47.53 < 2\theta < 49.34^\circ$ corresponded to a primitive orthorhombic cell with dimensions:

$$\begin{aligned}a &= 17.597(2) \text{ \AA} \\b &= 5.667(2) \text{ \AA} \\c &= 4.833(2) \text{ \AA} \\V &= 481.9(2) \text{ \AA}^3\end{aligned}$$

For $Z = 4$ and F.W. = 187.88, the calculated density is 2.59 g/cm^3 . Based on the systematic absences of:

$$\begin{aligned}0kl: k+l \pm 2n \\hk0: h \pm 2n\end{aligned}$$

packing considerations, a statistical analysis of intensity distribution, and the successful solution and refinement of the structure, the space group was determined to be:

$$\text{Pnma (\#62)}$$

The data were collected at a temperature of $26 \pm 1^\circ\text{C}$ using the ω - 2θ scan technique to a maximum 2θ value of 55.1° . Omega scans of several intense reflections, made prior to data collection, had an average width at half-height of 0.43° with a take-off angle of 6.0° . Scans of $(1.84 + 0.35 \tan \theta)^\circ$ were made at a speed of $4.0^\circ/\text{min}$ (in ω). The weak reflections ($I < 10.0\sigma(I)$) were rescanned (maximum of 8 scans) and the counts were accumulated to ensure good counting statistics. Stationary background counts were recorded on each side of the reflection. The ratio of peak counting time to background counting time was 2:1. The diameter of the incident beam collimator was 1.0 mm, the crystal to detector distance was 400 mm, and the detector aperture was 6.0×6.0 mm (horizontal x vertical).

Data Reduction

A total of 707 reflections was collected. The intensities of three representative reflections were measured after every 150 reflections. No decay correction was applied.

The linear absorption coefficient, μ , for Mo-K α radiation is 33.9 cm⁻¹. An empirical absorption correction based on azimuthal scans of several reflections was applied which resulted in transmission factors ranging from 0.68 to 1.00. The data were corrected for Lorentz and polarization effects. A correction for secondary extinction was applied (coefficient = 2.54394e-006).

Structure Solution and Refinement

The structure was solved by direct methods¹ and expanded using Fourier techniques². The non-hydrogen atoms were refined anisotropically. Hydrogen atoms were included but not refined. The final cycle of full-matrix least-squares refinement³ on F was based on 587 observed reflections ($I > 2.00\sigma(I)$) and 47 variable parameters and converged (largest parameter shift was 0.00 times its esd) with unweighted and weighted agreement factors of:

$$R = \sum ||F_o| - |F_c|| / \sum |F_o| = 0.061$$

$$R_w = [\sum w (|F_o| - |F_c|)^2 / \sum w F_o^2]^{1/2} = 0.078$$

The standard deviation of an observation of unit weight⁴ was 7.57. The weighting scheme was based on counting statistics and included a factor ($p = 0.010$) to downweight the intense reflections. Plots of $\sum w (|F_o| - |F_c|)^2$ versus $|F_o|$, reflection order in data collection, $\sin \theta/\lambda$ and various classes of indices showed no unusual trends. The maximum and minimum peaks on the final difference Fourier map corresponded to 2.27 and -1.01 e⁻/Å³, respectively.

Neutral atom scattering factors were taken from Cromer and Waber⁵. The values for the mass attenuation coefficients are those of Creagh and Hubbell⁶. All calculations were performed using the teXsan⁷ crystallographic software package of Molecular Structure Corporation.

References

(1) SIR92: Altomare, A., Cascarano, M., Giacovazzo, C., Guagliardi, A. (1994). J. Appl. Cryst., 26, 343.

(2) DIRDIF94: Beurskens, P.T., Admiraal, G., Beurskens, G., Bosman, W.P., de Gelder, R., Israel, R. and Smits, J.M.M.(1994). The DIRDIF-94 program system, Technical Report of the Crystallography Laboratory, University of Nijmegen, The Netherlands.

(3) Least Squares function minimized:

$$\Sigma w(|F_o| - |F_c|)^2 \text{ where}$$

$$w = 1/[\sigma^2(F_o)] = [\sigma_c^2(F_o) + p^2 F_o^2/4]^{-1}$$

$\sigma_c(F_o)$ = e.s.d. based on counting statistics
 p = p-factor

(4) Standard deviation of an observation of unit weight:

$$[\Sigma w(|F_o| - |F_c|)^2 / (N_o - N_v)]^{1/2}$$

where: N_o = number of observations

N_v = number of variables

(5) Cromer, D. T. & Waber, J. T.; "International Tables for X-ray Crystallography", Vol. IV, The Kynoch Press, Birmingham, England, Table 2.2 A (1974).

(6) Creagh, D. C. & Hubbell, J.H.; "International Tables for Crystallography", Vol C, (A.J.C. Wilson, ed.), Kluwer Academic Publishers, Boston, Table 4.2.4.3, pages 200-206 (1992).

(7) teXsan for Windows version 1.06: Crystal Structure Analysis Package, Molecular Structure Corporation (1997-9).

EXPERIMENTAL DETAILS

A. Crystal Data

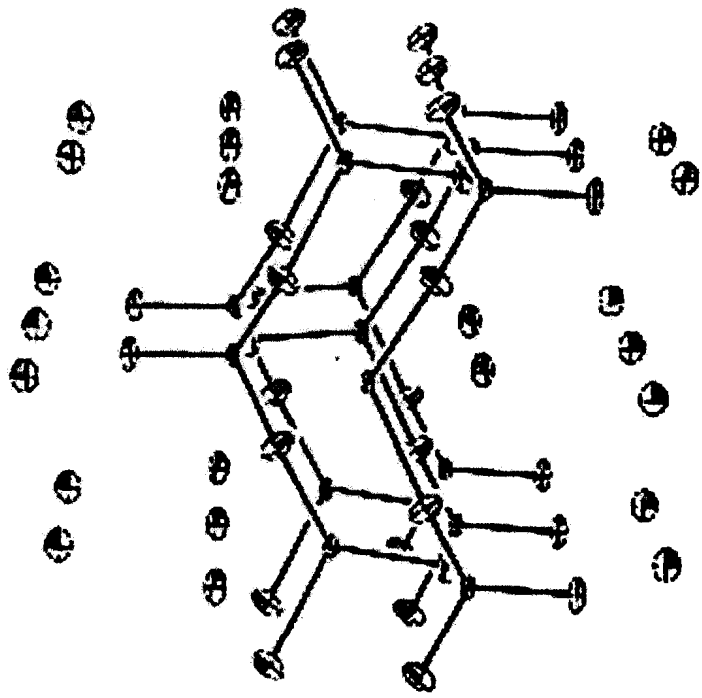
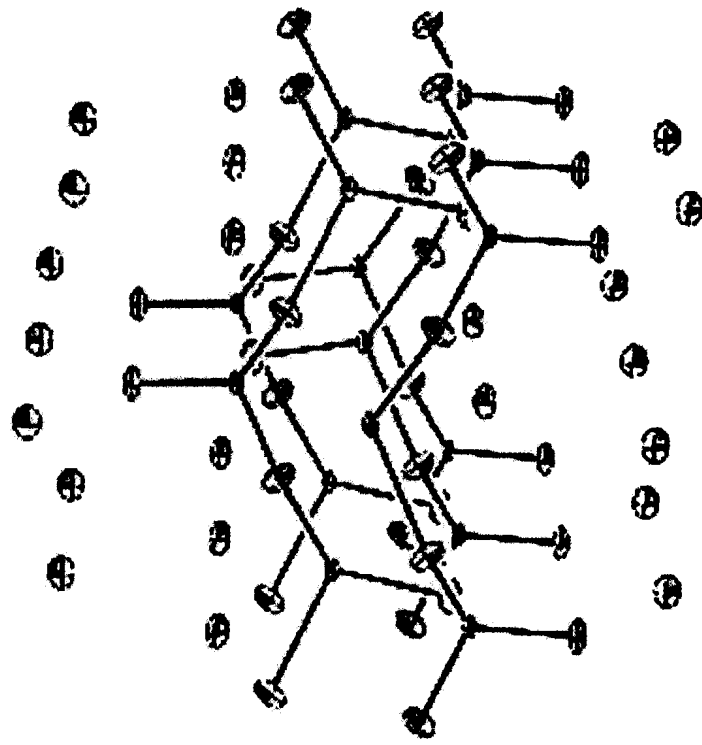
Empirical Formula	H ₇ O ₅ FePN
Formula Weight	187.88
Crystal Color, Habit	colorless, irreg.plate
Crystal Dimensions	0.40 X 0.35 X 0.15 mm
Crystal System	orthorhombic
Lattice Type	Primitive
No. of Reflections Used for Unit Cell Determination (2 θ range)	23 (47.5 - 49.3 $^{\circ}$)
Omega Scan Peak Width at Half-height	0.43 $^{\circ}$
Lattice Parameters	a = 17.597(2) Å b = 5.667(2) Å c = 4.833(2) Å V = 481.9(2) Å ³
Space Group	Pnma (#62)
Z value	4
D _{calc}	2.589 g/cm ³
F ₀₀₀	380.00
μ (MoK α)	33.88 cm ⁻¹

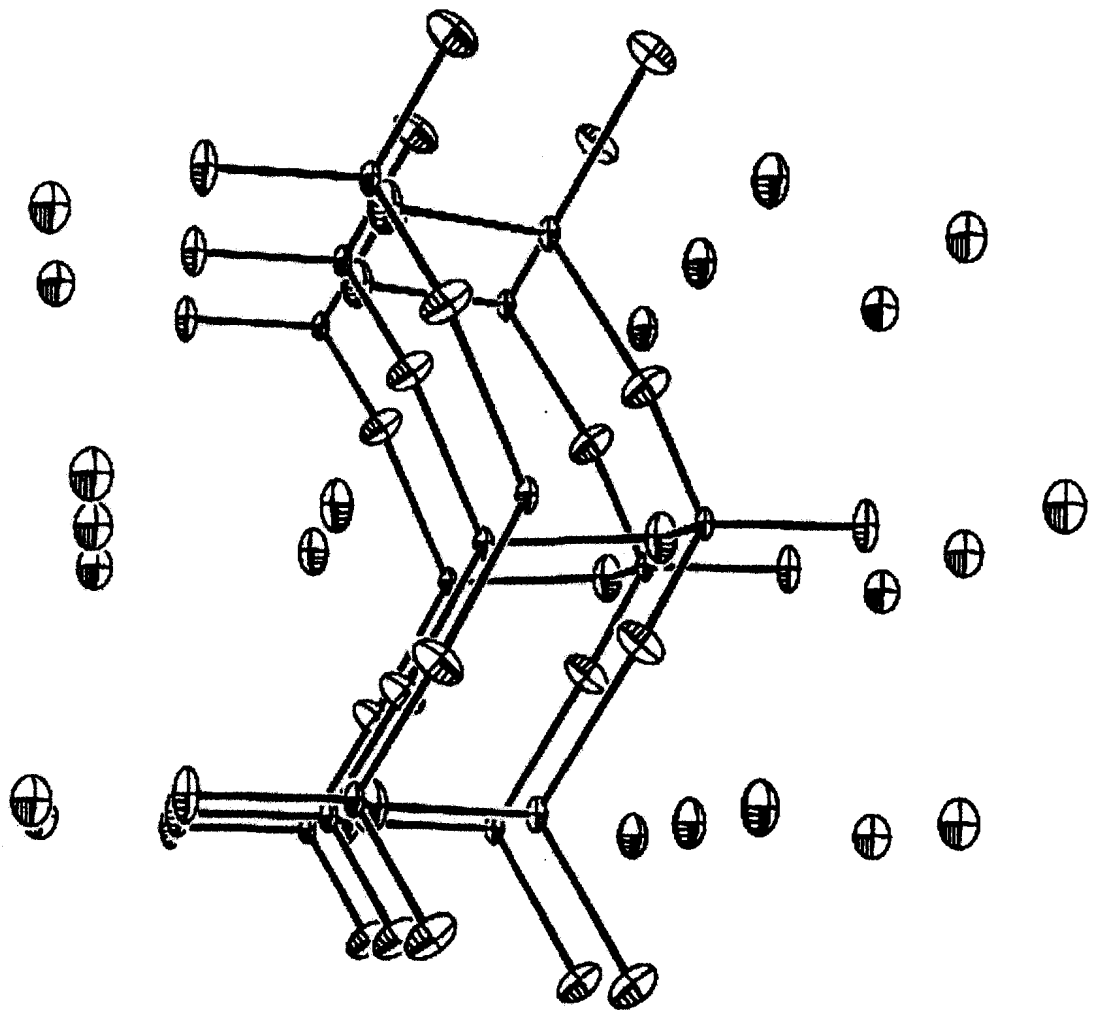
B. Intensity Measurements

Diffractometer	Rigaku AFC6S
Radiation	MoK α ($\lambda = 0.71069 \text{ \AA}$) graphite monochromated
Take-off Angle	6.0 $^\circ$
Detector Aperture	6.0 mm horizontal 6.0 mm vertical
Crystal to Detector Distance	400 mm
Voltage, Current	50kV, 27.5mA
Temperature	26.0 $^\circ$ C
Scan Type	ω -2 θ
Scan Rate	4.0 $^\circ$ /min (in ω) (up to 8 scans)
Scan Width	(1.84 + 0.35 tan θ) $^\circ$
2 θ_{max}	55.1 $^\circ$
No. of Reflections Measured	Total: 707
Corrections	Lorentz-polarization Absorption (trans. factors: 0.6751 - 1.0000) Secondary Extinction (coefficient: 2.54394e-006)

C. Structure Solution and Refinement

Structure Solution	Direct Methods (SIR92)
Refinement	Full-matrix least-squares on F
Function Minimized	$\Sigma w (F_o - F_c)^2$
Least Squares Weights	$1/\sigma^2(F_o) = 4F_o^2/\sigma^2(F_o^2)$
p-factor	0.0100
No. Observations ($I > 2.00\sigma(I)$)	587
No. Variables	47
Reflection/Parameter Ratio	12.49
Residuals: R; R _w	0.061 ; 0.078
Goodness of Fit Indicator	7.57
Max Shift/Error in Final Cycle	0.00
Maximum peak in Final Diff. Map	$2.27 \text{ e}^-/\text{\AA}^3$
Minimum peak in Final Diff. Map	$-1.01 \text{ e}^-/\text{\AA}^3$





**APPENDIX III: Kinetic and Solubility Data for $\text{Na}_2\text{Ni}(\text{OH})\text{PO}_4$ Formation
Equilibria with Nickel Oxide**

TABLE A.III.1: Summary of ICP ES Results for Standard Solutions

run name	stock sol'n	m(P)total mol·kg ⁻¹	% dev	m(Na ⁺) mol·kg ⁻¹	% dev
Prec. 1	Standard 1	1.5028	0.19	3.8848	3.59
		1.4941	0.39	3.8839	3.57
	Standard 2	0.9448	5.52	2.8596	14.4
		0.9370	6.30	2.7865	11.5
	Standard 3	0.7070	1.00	2.3034	17.5
		0.6910	1.29	2.2103	12.8
Prec. 2	Standard 1	1.4642	2.39	3.8585	2.89
		1.4639	2.40	3.8451	2.54
	Standard 2	1.0094	0.94	2.7187	8.75
		1.0137	1.37	2.6184	4.73
	Standard 3	0.7017	0.24	2.0057	2.33
		0.7076	1.09	2.0946	6.87
	Standard 4	0.5042	0.83	1.3497	7.98
		0.4976	0.48	1.3031	4.25
Rediss. 1	Standard 1	1.5035	0.24	3.9589	5.57
		1.5145	0.96	3.9929	6.48
	Standard 2	1.0222	2.22	2.6856	7.42
		1.0171	1.71	2.6663	6.65
	Standard 3	0.6994	0.09	2.0222	3.18
		0.6930	1.01	2.0135	2.73
	Standard 4	0.5043	0.85	1.3340	7.17
		0.5072	1.44	1.3889	11.1
Rediss. 2	Standard 1	1.5171	1.14	3.9880	6.35
		1.5026	0.18	3.8987	3.97
	Standard 2	1.0116	1.16	2.6468	5.87
		1.0238	2.38	2.6825	7.30
	Standard 3	0.6945	0.79	1.9651	0.26
		0.7067	0.95	2.0203	3.08
Solubility 1	Standard 1	1.5592	3.95	3.9237	4.63
		1.5606	4.04	3.8955	3.88
	Standard 3	0.7251	3.58	2.0303	3.59
		0.7260	3.70	2.0023	2.16
	Standard 4	0.5256	5.12	1.3340	6.72
		0.5210	4.21	1.3109	4.87

TABLE A.III.1 (continued)

run name	stock sol'n	m(P)total mol·kg ⁻¹	% dev	m(Na ⁺) mol·kg ⁻¹	% dev
Solubility 2	Standard 2	1.0256	2.56	2.5678	2.71
		1.0346	3.46	2.6724	6.90
	Standard 3	0.7268	3.83	2.1043	7.36
		0.7146	2.09	1.9930	1.68
	Standard 4	0.5176	3.52	1.3402	7.21
		0.5173	3.46	1.3203	5.63

TABLE A.III.2: Kinetic Data

Time hr	$m(\text{Na}^+)$ $\text{mol}\cdot\text{kg}^{-1}$	$m(\text{P})_{\text{total}}$ $\text{mol}\cdot\text{kg}^{-1}$	$m(\text{HPO}_4^{2-})$ $\text{mol}\cdot\text{kg}^{-1}$
Precipitation at 250 °C			
0.8	2.520	0.9389	0.5054
0.8	2.414	0.9163	0.5216
0.82	2.154	0.8282	0.4998
0.82	2.160	0.8363	0.5117
5.78	2.060	0.7700	0.4440
5.78	2.060	0.7653	0.4361
5.85	1.987	0.7383	0.4256
5.85	2.049	0.7443	0.4055
18.68	1.821	0.6405	0.3443
18.68	1.829	0.6421	0.3433
18.73	1.713	0.5889	0.3125
18.73	1.742	0.5956	0.3111
22.28	1.633	0.5528	0.2930
22.28	1.680	0.5610	0.2873
22.33	1.630	0.5467	0.2863
22.33	1.652	0.5540	0.2881
2.61	1.606	0.5368	0.2814

TABLE A.III.2 (continued)

Time hr	$m(\text{Na}^+)$ $\text{mol}\cdot\text{kg}^{-1}$	$m(\text{P})_{\text{total}}$ $\text{mol}\cdot\text{kg}^{-1}$	$m(\text{HPO}_4^{2-})$ $\text{mol}\cdot\text{kg}^{-1}$
Precipitation at 250 °C			
26.1	1.552	0.5360	0.3002
26.12	1.669	0.5481	0.2743
26.12	1.645	0.5360	0.2671
42.8	1.502	0.4818	0.2469
42.8	1.513	0.4817	0.2436
42.83	1.449	0.4744	0.2551
42.83	1.440	0.4719	0.2545
46.75	1.435	0.4681	0.2515
46.75	1.448	0.4729	0.2533
46.78	1.450	0.4741	0.2543
46.78	1.412	0.4697	0.2613
50.17	1.419	0.4674	0.2559
50.17	1.376	0.4555	0.2550
50.22	1.438	0.4647	0.2465
50.22	1.441	0.4682	0.2499
67.15	1.407	0.4655	0.2573
67.15	1.416	0.4687	0.2584

TABLE A.III.2 (continued)

Time hr	$m(\text{Na}^+)$ $\text{mol}\cdot\text{kg}^{-1}$	$m(\text{P})_{\text{total}}$ $\text{mol}\cdot\text{kg}^{-1}$	$m(\text{HPO}_4^{2-})$ $\text{mol}\cdot\text{kg}^{-1}$
Precipitation at 250 °C			
67.17	1.436	0.4690	0.2525
67.17	1.413	0.4675	0.2580
73.58	1.396	0.4573	0.2506
73.58	1.394	0.4604	0.2552
73.62	1.436	0.4684	0.2517
73.62	1.419	0.4716	0.2611
90.83	1.420	0.4606	0.2472
90.83	1.366	0.4560	0.2592
90.85	1.390	0.4577	0.2531
90.85	1.377	0.4553	0.2546
114.73	1.421	0.4629	0.2496
114.73	1.382	0.4517	0.2484
114.78	1.442	0.4769	0.2603
114.78	1.472	0.4798	0.2541
138.9	1.391	0.4517	0.2454
138.9	1.410	0.4576	0.2466
138.95	1.377	0.4494	0.2470
138.95	1.381	0.4524	0.2493

TABLE A.III.2 (continued)

Time hr	m(Na ⁺) mol·kg ⁻¹	m(P)total mol·kg ⁻¹	m(HPO ₄ ²⁻) mol·kg ⁻¹
Precipitation at 250 °C			
162.82	1.332	0.4397	0.2493
162.82	1.322	0.4434	0.2575
162.87	1.319	0.4418	0.2561
162.87	1.311	0.4398	0.2565
186.95	1.278	0.4157	0.2367
186.95	1.288	0.4152	0.2331
186.98	1.205	0.3993	0.291
186.98	1.235	0.3907	0.2198
Redissolution at 275-250 °C			
3.37	0.8653	0.2717	0.1823
3.37	0.8562	0.2707	0.1834
3.37	0.9444	0.3130	0.2100
3.37	0.9401	0.3153	0.2140
5.08	1.085	0.3667	0.2354
5.08	1.039	0.3628	0.2450
5.08	1.062	0.3731	0.2513
5.08	1.092	0.3689	0.2358
8.92	1.189	0.3759	0.2157

TABLE A.III.2 (continued)

Time hr	$m(\text{Na}^+)$ $\text{mol}\cdot\text{kg}^{-1}$	$m(\text{P})_{\text{total}}$ $\text{mol}\cdot\text{kg}^{-1}$	$m(\text{HPO}_4^{2-})$ $\text{mol}\cdot\text{kg}^{-1}$
Redissolution at 275-250 °C			
8.92	1.099	0.3713	0.2369
8.92	1.091	0.3781	0.2483
8.92	1.107	0.3796	0.2451
12.77	1.173	0.3903	0.2376
12.77	1.147	0.3826	0.2361
12.77	1.145	0.3818	0.2358
12.77	1.151	0.3853	0.2384
23.19	1.212	0.3991	0.2369
23.19	1.206	0.3999	0.2396
23.19	1.219	0.3921	0.2261
23.19	1.207	0.3987	0.2377
28.75	1.224	0.4000	0.2341
28.75	1.204	0.3948	0.2337
28.75	1.180	0.3891	0.2341
28.75	1.152	0.3863	0.2395
47.78	1.209	0.3924	0.2293
47.78	1.178	0.3885	0.2339
47.78	1.169	0.3896	0.2383

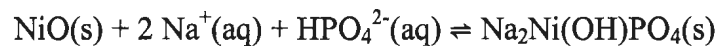
TABLE A.III.2 (continued)

Time hr	m(Na ⁺) mol·kg ⁻¹	m(P)total mol·kg ⁻¹	m(HPO ₄ ²⁻) mol·kg ⁻¹
Redissolution at 275-250 °C			
47.78	1.126	0.3776	0.1976
58.27	1.241	0.4000	0.2289
58.27	1.189	0.3932	0.2366
58.27	1.234	0.3967	0.2271
58.27	1.196	0.3886	0.2287
76.82	1.196	0.3921	0.2331
76.82	1.178	0.3925	0.2391
76.82	1.176	0.3871	0.2330
76.82	1.150	0.3827	0.2353
120.57	1.220	0.3978	0.2327
120.57	1.215	0.3944	0.2299
120.57	1.188	0.3803	0.2212
120.57	1.173	0.3755	0.2198
143.92	1.199	0.3837	0.2220
143.92	1.188	0.3847	0.2264
143.92	1.151	0.3708	0.2206
143.92	1.146	0.3703	0.2214
168.57	1.157	0.3697	0.2176

TABLE A.III.2 (continued)

Time hr	m(Na ⁺) mol·kg ⁻¹	m(P)total mol·kg ⁻¹	m(HPO ₄ ²⁻) mol·kg ⁻¹
Redissolution at 275-250 °C			
168.57	1.136	0.3701	0.2242
168.57	1.090	0.3507	0.2143
168.57	1.073	0.3500	0.2183
240.73	1.108	0.3449	0.2025
240.73	1.169	0.3565	0.1992
240.73	1.041	0.3271	0.2003
240.73	1.019	0.3262	0.2051

TABLE A.III.3: Experimental Data for the Reaction



t °C	m(PO ₄) _{Total} mol·kg ⁻¹	m(HPO ₄ ²⁻) mol·kg ⁻¹	m(Na ⁺) mol·kg ⁻¹	Equil. time (hrs)	Average ln Q	Average ln K	Average K
Na/P = 2.5, run 1							
240	1.183	0.6609	3.111				
240	1.163	0.7148	2.949	50	-1.8436	4.6995	1.099·10 ²
240	1.165	0.7537	2.892				
255	0.6199	0.3801	1.648				
255	0.6226	0.3907	1.643	53	-0.0286	6.8289	9.242·10 ²
255	0.6104	0.3964	1.589				
265	0.4033	0.2310	1.207				
265	0.3977	0.2435	1.151				
265	0.3449	0.2241	1.004	75	1.2889	8.0048	2.995·10 ³
265	0.3470	0.2300	0.9951				
272	0.2684	0.1783	0.8288				
272	0.2696	0.1771	0.8381				
272	0.2501	0.1699	0.7815	62	2.1755	8.7277	6.172·10 ³
272	0.2509	0.1702	0.7841				
280	0.2010	0.1383	0.6729				
280	0.1974	0.1403	0.6468	95	2.8026	9.3196	1.116·10 ⁴

TABLE A.III.3 (continued)

t °C	m(PO ₄) _{Total} mol·kg ⁻¹	m(HPO ₄ ²⁻) mol·kg ⁻¹	m(Na ⁺) mol·kg ⁻¹	Equil. time (hrs)	Average ln Q	Average ln K	Average K
Na/P = 2.5, run 2							
235	1.5019	0.9095	3.807				
235	1.4836	0.9552	3.669	60	-2.5841	3.6788	3.960·10 ¹
235	1.5238	0.9020	3.896				
245	1.0667	0.7034	2.629				
245	1.0602	0.7183	2.584	69	-1.5748	5.1918	1.798·10 ²
252	0.8175	0.5154	2.086				
252	0.8289	0.5326	2.094	52	0.83341	6.1264	4.578·10 ²
252	0.8282	0.5268	2.102				
260	0.5337	0.3537	1.395				
260	0.5357	0.3589	1.391				
260	0.5478	0.3658	1.420	68	0.3307	7.2840	1.457·10 ³
260	0.5523	0.3779	1.412				
268	0.2659	0.200	0.6815				
268	0.2661	0.2153	0.6982	53	2.2674	8.7273	6.169·10 ³

TABLE A.III.3 (continued)

t °C	m(PO ₄) _{Total} mol·kg ⁻¹	m(HPO ₄ ²⁻) mol·kg ⁻¹	m(Na ⁺) mol·kg ⁻¹	Equil. time (hrs)	Average ln Q	Average ln K	Average K
Na/P = 2.5, run 2							
257	0.5173	0.3024	1.459				
257	0.5568	0.4250	1.341	50	0.3123	7.1632	1.291·10 ³
257	0.5565	0.4259	1.338				
243	0.7505	0.4937	1.913				
243	0.7538	0.4857	1.940	65	-0.5919	5.9345	3.779·10 ²
243	0.7475	0.4915	1.907				

